2012

Probabilistic Earthquake Structural Damage Assessment of Steel Special CBF and Steel Self-Centering CBF Buildings

Gulce Akbas
Lehigh University

Probabilistic Earthquake Structural Damage Assessment of Steel Special CBF and Steel Self-Centering CBF Buildings

by

Gulce Akbas

A Thesis
Presented to the Graduate and Research Committee
of Lehigh University
in Candidacy for the Degree of
Master of Science

in

Structural Engineering

Lehigh University

September 2012

This thesis is accepted and approved in partial fulfillment of the requirements for the Master of Science.

_____
Date

_____
Dr. Richard Sause
Thesis Advisor

_____
Dr. James M. Ricles
Thesis Advisor

_____
Dr. Sibel Pamukcu
Department of Civil and Environmental Engineering

ACKNOWLEDGEMENTS

The work presented in this thesis was conducted at the Advanced Technology for Large Structural Systems (ATLSS) Engineering Research Center, Department of Civil and Environmental Engineering, Lehigh University, Bethlehem, Pennsylvania. During the study, the chairmanship of the department was held by Dr. Sibel Pamukcu.

I would like to thank my thesis advisors, Dr. Richard Sause and Dr. James M. Ricles for their guidance, direction, patience, and advice. I believe, without doubt, that this work wouldn't have been completed without their guidance. Their efforts were invaluable towards my academic progress and becoming a skillful engineer.

I would like to thank to all my professors at Lehigh, especially to Dr. John L. Wilson and Dr. Shamim N. Pakzad. I learned a great deal from them. The computer technical support provided by Peter Bryan is much appreciated. Thanks are extended to my fellow graduate students, especially Brent Chancellor and Ebrahim Tahmasebi, for their assistance with many technical and nontechnical challenges throughout my studies. I would like to thank Duygu Saydam, he was always very helpful, friendly and willing to lend a hand. I also thank Ms. Prisca Vidanage, and Ms. Betty MacAdam for their kindness and administrative assistance.

Another special thanks to my undergraduate advisor and a Lehigh alum, Dr. Cetin Yilmaz for guiding and inspiring me to come to Lehigh University.

Many thanks to my Issa Abi, Issa Omar, who is a great structural engineer, for his help and support.

I would like to thank all my friends, especially to Okan Ilhan and Kayla M. Hampe, for their company and support which made me feel at home, here in Bethlehem.

My dearest friend Nihal Karagoz is also thanked for always being there and being a great friend.

I am thankful to my deary Bora Baloglu, for all his love, patience and never-ending support. He was the one who made life easier when nothing was easy.

Lastly but not the least, I would like to thank my family for their love, continuous encouragement and believing in me despite the miles between us. I am grateful to my mother, Gulsun Akbas, for her endless compassion and encouragement in every decision I made in my life. I am indebted to my father, Halit Levent Akbas, for his care and love; he has been my role model as a successful structural engineer. I can't wait for the projects that we succeed together with him as colleagues. Heartfelt thanks and love to my little sister, Tugce Akbas, for being my family, my best friend, my roommate, my classmate and my colleague at the same time. This past year in Lehigh wouldn't have been the same without her. To my family this thesis is dedicated.

.

TABLE OF CONTENTS

LIST OF TABLES

LIST OF FIGURES

ABSTRACT

Steel special concentrically braced frames (SCBFs) are effective, economic and stiff lateral force resisting systems for steel structures. However, they have limited ductility capacity because of brace buckling. Steel self-centering concentrically braced frames (SC-CBFs) have been developed to have the effectiveness, economy and stiffness of SCBFs with increased lateral drift capacity and reduced residual lateral drift.

A probabilistic structural damage assessment of SCBF and SC-CBF buildings is presented in this thesis. The assessment shows the differences between the earthquake performance of SCBFs and SC-CBFs, and verifies the expected earthquake performance of SC-CBFs.

Structural damage assessment is an essential part of performance based earthquake engineering (PBEE). In an earthquake structural damage assessment, the earthquake response of the structure is related to physical damage states observed in the structure after the earthquake. In this research, structural damage is considered as a combination of building damage (collapse/non-collapse and demolition/no demolition events) and damage of the braces of an SCBF or SC-CBF (repair actions corresponding to the damage).

Four model buildings (4- and 9-story SCBF and SC-CBF buildings) are used in the assessment and their earthquake performance is assessed under the design level

earthquake (DBE) and maximum considered earthquake (MCE). Structural response data (EDPs) are obtained from nonlinear dynamic analysis. The peak story drift (θ_m), the peak residual story drift (θ_r) and the residual out-of-plane displacement of the braces, Δ_{or}, are the EDPs used in this study. EDP limit values, that are defined to be the minimum value of the EDP corresponding to a related damage state, are established for each damage state. When the EDP value obtained from the dynamic analysis equals or exceeds the EDP limit, the building is considered to be in the related damage state. The EDP limit values are treated as random variables. Fragility functions providing the probability that a building reaches or exceeds a level of damage are obtained for each specified damage state.

Damage scenarios are described as sequences of the individual building and brace damage events, and shown schematically using an event tree (ET) model. The probability of each damage scenario is obtained using a multi-event analysis for each model building under the DBE and MCE.

Results of this study show that the SC-CBF buildings have better earthquake performance than the SCBF buildings both under the DBE and MCE, as a result of the low probability of structural damage. Both systems achieved low collapse probabilities. SC-CBFs have lower probability of post-earthquake demolition, since the residual drift is nearly eliminated. The probability of brace damage is lower in the SC-CBF buildings than in the SCBF buildings.

CHAPTER 1

INTRODUCTION

1.1 Overview

Special concentrically braced frames (SCBFs) are effective, economical and frequently-used earthquake lateral force resisting systems for steel structures. The braces provide large lateral strength and stiffness, and are the critical components of an SCBF. Deterioration and fracture of the braces under earthquake loading limits the capability of SCBFs to undergo large inelastic deformations. This limited deformation capacity is associated with significant damage to the braces leading to permanent lateral deformation (such as residual lateral drift) in the system.

Self-centering concentrically braced frames (SC-CBFs) have been developed to maintain the effectiveness, economy and stiffness of SCBFs, and to have increased lateral drift capacity before damage and reduced residual lateral drift (Roke et al., 2006). An SC-CBF is designed to rock on its foundation, and the rocking action increases the lateral drift capacity of the system. An SC-CBF has vertically-oriented PT bars that provide restoring forces to self-center the frame during the earthquake (Roke et al., 2010). The main structural components are designed to remain undamaged under the design earthquake to permit the system to self-center. The controlled rocking action and the self-centering behavior of SC-CBFs enable the structural damage to be concentrated into a few replaceable elements and to eliminate significant residual drift.

SCBFs are designed to prevent collapse under severe earthquakes, although damage occurs. SC-CBFs are also designed to prevent collapse, however damage is expected to be minimal under the design level earthquake.

The main difference between SCBFs and SC-CBFs is expected to be in the damage to the braces and in the residual drift. The probability of structural damage and residual drift of an SC-CBF is expected to be very low under the design level earthquake. To verify the expected earthquake performance of SC-CBFs, compared to the earthquake performance of SCBFs, and to show the differences between the two systems, an earthquake structural damage assessment for these two systems is performed in this study.

Structural damage assessment is an essential part of the performance based earthquake engineering (PBEE). In an earthquake structural damage assessment, the earthquake response of the structures is related to physical damage states observed in the structure after the earthquake. Necessary repair actions are determined for the corresponding damage states. The relationship between the structural response and the damage is expressed as the probability of being in a specific damage state.

Four model buildings are used in the earthquake damage assessment in this study. 4- and 9-story SCBF building are designed for earthquake loading according to current building codes. The earthquake performance of these SCBF buildings is compared to that of previously designed 4- and 9-story SC-CBF buildings (Chancellor, 2013). These buildings are office-type buildings designed for a site in Southern California. Two different building heights were selected to see the effect of building height on the

earthquake performance of SCBFs and SC-CBFs. Nonlinear dynamic earthquake response analyses of the model buildings which were performed for two ground motion intensity levels, namely the design level earthquake (DBE) and the maximum considered earthquake (MCE) (Tahmasebi, 2014). The results of these analyses are used for the damage assessment. Damage criteria are developed for the buildings and the braces. A probabilistic methodology is developed and used for the damage assessment. The assessment results for the model buildings are compared with each other.

1.2 Research Objectives

The overall objective of this research is to develop a better understanding of the earthquake performance of SC-CBFs by comparing this performance with the earthquake performance of SCBFs. The specific objectives necessary to achieve the overall objective are as follows:

1. To design model SCBF buildings for the purpose of comparing their performance with that of previously designed SC-CBF buildings (Chancellor, 2013).
2. To obtain the structural response of the model buildings from nonlinear dynamic earthquake response analysis performed by Chancellor (2013) for the SC-CBF buildings and by Tahmasebi (2014) for the SCBF buildings.
3. To define critical earthquake damage states for the buildings and the braces.
4. To establish limit values for structural response parameters corresponding to each damage state.
5. To develop damage fragility functions for each damage state.

6. To perform probabilistic earthquake structural damage assessment for the model buildings.
7. To compare the damage assessment results for the model buildings.

1.3 Report Scope

To achieve the research objectives, the following work was completed. Two SCBF model buildings with different building heights were designed according to the seismic design procedures given in ASCE 7-10 (ASCE, 2010). These SCBF model buildings are used to make comparisons with SC-CBF model buildings designed previously (Chancellor, 2013) using the design procedure developed by Roke et al. (2010). The nonlinear dynamic earthquake response analysis of the SCBF and SC-CBF model buildings were performed by Tahmasebi (2014) and by Chancellor (2013); the results of these analyses are used in this study to obtain the structural response parameters of the model buildings under earthquake loading. Building damage criteria are established for collapse and demolition conditions. Brace damage criteria are established from a previous experimental study. A probabilistic methodology is developed and used to relate structural response parameters to specified damage criteria.

1.4 Organization of Thesis

The remaining chapters of this thesis are organized as follows:

- Chapter 2 presents background information about Performance Based Earthquake Engineering (PBEE) methodology, and the earthquake performance of SCBFs and SC-CBFs.

- Chapter 3 describes the seismic design procedures used for the SCBF and SC-CBF model buildings. The nonlinear numerical models created for nonlinear dynamic earthquake response history analyses are also explained, and results of the dynamic analyses are given.
- Chapter 4 discusses the building earthquake damage assessment considering building collapse and building demolition. Collapse and demolition criteria are established in terms of related structural response parameters. Collapse/non-collapse and demolition/no demolition fragility functions are presented. Building damage is assessed as the probability of collapse and the probability of demolition.
- Chapter 5 discusses the damage assessment of the braces. Damage states are established based on a previous experimental study and on the potential for the damage state to be established in a post-earthquake inspection. Brace damage fragility functions for each damage state are presented. The brace damage assessment is expressed as probability of needing the repair action corresponding to each damage state.
- Chapter 6 presents a probabilistic earthquake structural damage assessment that combines the building damage assessment discussed in Chapter 4 and the damage assessment of the braces discussed in Chapter 5. Possible damage scenarios for the model buildings are described. An event tree is formed to illustrate the damage scenarios. The method for estimating the probability of each damage scenario occurrence is described. Assessment results are presented and compared.

- Chapter 7 summarizes the research work, and presents conclusions and recommendations for future work.

CHAPTER 2

BACKGROUND

2.1 General

Several research studies have been conducted on damage to buildings (i.e., on "building losses") from earthquakes. The present research focuses on the potential for self-centering systems to reduce earthquake losses. Probabilistic earthquake structural damage assessments will be conducted to compare the earthquake performance of SC-CBF and SCBF systems.

The Pacific Earthquake Engineering Research Center (PEER) developed a performance-based earthquake engineering (PBEE) framework based on loss estimates, using conditional probability concepts and the total probability theorem (Moehle and Deierlein, 2004). An enhanced building-specific loss estimation procedure was developed by Miranda (2010) that considers building losses associated with collapse, repair of damage, and demolition. The Applied Technology Council (ATC) developed guidelines for performance assessment based on losses in the ATC-58-1 project "Seismic Performance Assessment of Buildings".

Other previous research has examined the performance-based design of SCBFs and SC-CBFs. This chapter summarizes the concepts and results of recent research related to the PBEE methodology, and performance assessment of SCBFs and SC-CBFs.

2.2 PEER Performance-Based Earthquake Engineering (PBEE)

The first generation PBEE approaches (e.g., FEMA 273, 350 and 351) tried to relate structural response parameters to performance objectives such as Immediate Occupancy (IO), Life safety (LS) and Collapse Prevention (CP). The design of a structure is considered to satisfy the performance objectives if deformations or forces in each component do not exceed the specified limits (Porter, 2003). Whittaker et al. (2003) listed the key shortcomings of the first generation PBEE approaches as follows:

- The structural response and demand are evaluated for the whole structure, whereas the performance assessment is done on the basis of damage of individual components (and most of the time, the weakest component's performance controls the structural performance)
- Most criteria for the performance of structures in building codes are based on judgment instead of reliable data
- Most structural engineers presume that code-specified performance objectives are too conservative with respect to prescriptive criteria
- Specified performance levels do not consider the concerns of the stakeholders such as economic losses (in terms of repair costs), occupancy losses in damaged buildings, casualties, etc.

These shortcomings led to the development of an improved methodology that correlates structural response parameters to performance measures.

In the PEER PBEE methodology, earthquake performance risks are estimated on a design-specific basis. Risks are expressed in terms of specific losses (e.g., repair cost of a damaged facility, casualties and downtime) instead of through code-specified performance objectives (Moehle and Deierlein, 2004).

The PEER PBEE methodology involves four types of parameters. The ground motion intensity (seismic hazard) is expressed by ground motion Intensity Measures (IMs). Non-linear analyses are performed to determine the response of the structure to earthquake ground motions and the response is defined in terms of Engineering Demand Parameters (EDPs). EDPs are linked to damage observed in a building, which is expressed in terms of Damage Measures (DMs). Finally, Decision Variables (DVs), which depend on DMs, are obtained. Thereby, the damage is translated into decision making quantities.

These four parameters are obtained in four stages that are summarized by Deierlein et al. (2003), Moehle and Deierlein (2004) and Porter (2003) as follows:

Hazard Analysis: Intensity Measures (IMs) are obtained by seismic hazard analysis. The analysis considers the seismic environment of the structure. A seismic hazard function is obtained that expresses the rate of exceedance of ground motion intensity that is specific to the location and design. The hazard function considers potential earthquakes from all nearby sources. The parameter that is used to define the intensity of the ground motion is the IM. An IM is useful if it is compatible with the structural analysis that gives the structural response and is well-correlated with structural response. The most commonly used IM in the PEER methodology is the spectral acceleration at the fundamental period

of the structure, $Sa(T_1)$. In addition to determining the IM, input ground motion records which are appropriate for the site should be selected for nonlinear dynamic earthquake response analysis.

Structural Analysis: For the given IMs and input ground motions, nonlinear dynamic earthquake response analysis of the building are carried out to estimate the structural response in terms of Engineering Demand Parameters (EDPs). The EDPs can be story drift ratios, component deformations or internal member forces. The Incremental Dynamic Analysis (IDA) procedure is used to establish the relationship between the EDP and IMs. Deierlein et al. (2003) defined IDA as;

> *"IDA is a strategy for conducting nonlinear time history analyses where a structure is subjected to multiple analyses for a given ground record, which has been scaled to various intensities".*

In an IDA, the input ground motion intensities are scaled, such that all have the same IM. The analysis is repeated several times at increasing levels of the IM.

Damage Analysis: Using the EDPs, a damage analysis is performed to estimate the relationship between the EDPs and Damage Measures (DMs). In the probabilistic PBEE methodology, damage is modeled using fragility functions. A fragility function gives the probability of a level of damage as functions of one (or more) EDPs (Porter et al. 2007). Damage is defined in terms of the repair actions required to return the building to an undamaged state.

Loss analysis: Losses are associated with the DMs. Losses are expressed in terms of Decision Variables (DVs). DVs indicate the seismic performance of the building according to the interests of the stakeholders. DVs can be dollar losses, deaths, or downtime. The relationship of DVs to DMs is given in terms of loss functions. Loss functions provide information on the probability of exceeding a certain level of repair/replacement cost at a specified damage state.

The PEER PBEE methodology is illustrated schematically in Figure 2.1. This methodology considers the inherent uncertainties of earthquake performance assessment with a consistent framework.

To account for these uncertainties, PEER developed a framework equation by using conditional probability concepts and total probability theory (Moehle and Deierlein, 2004). The DVs are the seismic performance measures. Various sources of uncertainty that cause uncertainty in the DVs are combined. Three sources of uncertainties should be taken into account: uncertainty in the DVs for a certain level of structural response (expressed by EDPs), uncertainty in the structural response at a certain level of ground motion intensity (expressed by IMs), and uncertainty in the ground motion intensity. These uncertainties are accounted for by corresponding random variables. The consideration of uncertainties in the PEER framework is explained as follows by Aslani and Miranda (2005):

> *"The uncertainty in estimating the seismic hazard at the site has been modeled by considering a ground motion intensity measure (IM) as a random variable and estimating the mean annual frequency of exceedance*

of the seismic hazard at the site, v(IM > im), by performing a Probabilistic Seismic Hazard Analysis (PSHA). The uncertainty in estimating the intensity of the structural response is incorporated by considering a vector of engineering demand parameters (EDPs) and estimating the conditional probability of an EDP exceeding a certain intensity, edp, at different levels of ground motion intensity, P(EDP > edp | IM=im). The uncertainty in estimating the decision variables, DVs, is incorporated using the conditional probabilities of exceeding a certain level of dv at a level of edp, P(DV > dv| EDP=edp)."

The first version of the PEER framework equation estimated the mean annual frequency of exceedance of a DV as follows (Cornell and Krawinkler, 2000):

$$\nu_{DV}(DV > dv) = \iint P(DV > dv \mid EDP = edp) \left| dP(EDP > edp \mid IM = im) \right| \left| d\nu(IM > im) \right| \quad (2.1)$$

However later work showed that a more realistic estimation of DV can be obtained by estimating the DV as a function of the level of damage by introducing random variables to quantify damage, the DMs.

A recent version of the PEER framework equation is as follows (Krawinkler and Miranda, 2004):

$$\nu_{DV}(DV > dv) = \iiint P(DV > dv \mid DM = dm) \left| dP(DM > dm \mid EDP = edp) \right| \left| dP(EDP > edp \mid IM = im) \right| \left| d\nu(IM > im) \right| \quad (2.2)$$

In Equation 2.2, DMs are assumed to be continuous random variables. However, while expressing the seismic performance in terms of economic losses, it is better to assume the

DMs to be discrete random variables, because repair work is a discrete action. In this manner, Equation 2.2 was modified as follows (Krawinkler and Miranda, 2004):

$$\nu_{DV}(DV > d\nu) = \sum_i \iint P(DV > d\nu \mid DM = dm) \left|\Delta P(DM_i > dm \mid EDP = edp)\right| \left|dP(EDP > edp \mid IM = im)\right| \left|d\nu(IM > im)\right| \quad (2.3)$$

As it is seen from Equation 2.3, one of the integrals in Equation 2.2 is replaced with a summation to consider discrete damage states of building components; i.e., dP(DM>dm|EDP=edp) in Equation 2.2 is replaced by ΔP(DM>dm|EDP=edp) to consider damage states as discrete random variables (Miranda and Aslani, 2003).

2.3 Response Assessment for Building-Specific Loss Estimation

Miranda et al. (2004) proposed a performance-based approach that estimates the total loss in the building from damage as a summation of individual losses of building components. Analyses were done with an existing non-ductile seven story reinforced concrete building. It was stated that the total loss is the sum of losses associated with non-collapse and losses associated with collapse. In this approach, collapse (C) and non-collapse (NC) damage states are considered as mutually exclusive.

The probability of collapse was estimated for two conditions: sidesway collapse and collapse as a result of loss of vertical carrying capacity. The analysis results showed that the second type of collapse is more critical for non-ductile structures (Aslani and Miranda, 2005).

The expected total loss in the building given that collapse does not occur at a ground motion intensity IM, $E[L_T \mid NC,IM]$, is obtained as the sum of the losses of individual components of the building as follows:

$$E[L_T \mid NC, IM] = E\left[\sum_{i=1}^{N}(a_i \cdot L_i \mid NC, IM)\right] = \sum_{i=1}^{N} a_i \cdot E[L_i \mid NC, IM] \qquad (2.4)$$

where,

$E[L_i \mid NC, IM]$= the expected normalized loss in the i^{th} component of building conditioned on the building non-collapse (NC) and a ground motion intensity (IM)

a_i = the replacement cost of component i

L_i = the normalized loss in the ith component defined as the cost of repair or replacement in the component normalized by a_i

Economic losses are estimated by combining uncertainties in seismic hazard, structural response, component fragility, and costs of repair actions associated with the damage. The damage in the system is estimated by relating structural response parameters (EDPs) with component fragility functions. Economic losses are interpreted as expected annual loss or as the probability of experiencing an economic loss larger than a given amount.

In the proposed approach by Miranda and Aslani (2003) the annual expected loss was estimated as follows for a single component:

- Estimation of component expected loss as a function of the EDPs by summation over all damage states
- Estimation of component expected loss as a function of the IMs by integration over a range of EDPs
- Estimation of component annual expected loss by integration over the various levels of IM

Finally, the annual expected loss of the building can be estimated with a summation of all component losses (structural components and nonstructural components). These steps can be shown in a single formula as follows:

$$E[L_j] = \sum_{i=1}^{m} \int_0^{\infty} \int_0^{\infty} E[L_j \mid DS = ds_i] P(DS = ds_i \mid EDP_j = edp) P(EDP_j > edp \mid IM = im) \left| \frac{d\nu(IM)}{dIM} \right| dEDP \; dIM \tag{2.5}$$

where,

$\frac{d\nu(IM)}{dIM}$ = the derivative of the hazard curve as a function of IM at the site

$P(EDP_j>edp|IM=im)$ = the probability of EDP for component j exceeding a certain limit, edp, for a given level of intensity

$P(DS=ds_i|EDP_j=edp)$ = the probability of being at damage state i, DS_i, for a given level of deformation

$E[L_j|DS=ds_i]$ = the expected loss in the component j for a given damage state i

In another study, Zareian and Krawinkler (2006) developed a simplified PBEE approach. This simple procedure contains three domains: Hazard Domain, Structural System Domain, and Loss Domain. Building-specific economic losses are represented in a semi-graphical way. The Structural System Domain and Loss Domain consider both non-collapse and collapse cases as separate sub-domains. This approach recommends to group building components into subsystems (at the story level or building level). By this way, components in the same subsystem can be related to a single response parameter. A comprehensive structural response database was established within the scope of this study. This database includes EDPs for various reinforced concrete moment-resisting frames and shear walls. This approach gives only the mean values of performance not a full probabilistic performance assessment.

Mitrani-Reiser (2007) developed another performance assessment methodology that estimates economic losses in terms of repair costs, building downtime and human fatalities. An event-tree-based virtual inspection procedure was used to check the safety of buildings according to the current code-based guidelines. An analytical methodology was presented in the form of a toolbox (MatLab Damage and Loss Analysis) for damage and loss estimation. A new reinforced concrete moment frame office building was analyzed in this study. Mean losses as a function of ground motion intensity level and expected total annual loss were estimated for different structural design approaches. For the components with available fragility functions, non-collapse losses were estimated in a component basis. The expected annual loss results indicated that the non-code conforming design had the worst performance. Additionally, an event-tree-based fatality

model was created to evaluate factors affecting human injuries and deaths. The fatality estimation results showed that there is no life safety risk in code-conforming building designs at all hazard levels.

In the seismic performance assessment approach of Ramirez and Miranda (2009), a story-based loss estimation is used. This approach estimates damage by directly relating structural response to loss of each story of a building through EDP-DV functions. There is no need to estimate component damage in this approach, because it is included in the building story losses. With this alternative approach, the performance assessment can be obtained in a more efficient manner. The total loss estimation was also modified to consider the losses associated with the demolition of a building that has not collapsed but cannot be repaired due to excessive residual deformations. Further information on this approach is given in Section 2.3.1 of this thesis.

2.3.1 Enhanced Building-Specific Seismic Performance Assessment

Miranda (2010) states that the total economic losses of a building after an earthquake are the sum of losses associated with the building collapse and losses associated with the non-collapse case of the building. The losses associated with non-collapse case are of two types: losses associated with reparable damage when the building does not collapse (i.e., non-collapse), and losses associated with building demolition when the building does not collapse (i.e., non-collapse). Residual drift is the EDP used to establish the reparability of the damage.

It is known that ductile lateral force resisting systems (without self-centering ability) are designed to resist large lateral displacements without collapse. For this reason, these systems experience residual deformations after intense ground motions (Miranda, 2010).

The expected value of the total loss in the building conditioned on ground motion intensity is formulated as follows:

$$E[L_T \mid IM] = L_R + L_D + L_C \tag{2.6}$$

where,

L_R= the losses associated with the case that collapse does not occur and the damage is reparable

L_D= the losses associated with the case that collapse does not occur, the damage is not reparable, and the building is demolished

L_C= the losses associated with the case that the building collapse occurs

Each of these losses can be obtained as follows:

$$L_R = E[L \mid NC \cap R, IM] \cdot P(NC \cap R \mid IM) \tag{2.7}$$

where,

E[L|NC∩R,IM]= expected building loss given the non-collapse case with reparable damage and conditioned on ground motion intensity

P[NC∩R|IM]= probability of the non-collapse case with reparable damage conditioned on ground motion intensity

$$L_D = E[L \mid NC \cap D, IM] \cdot P(NC \cap D \mid IM] \tag{2.8}$$

where,

E[L|NC∩D,IM]= expected building loss given the non-collapse case with building demolition due to non-reparable damage, and conditioned on ground motion intensity

P[NC∩D|IM]= probability of non-collapse case with building demolition conditioned on ground motion intensity

$$L_C = E[L \mid C] \cdot P(C \mid IM) \tag{2.9}$$

where,

E[L|C]= expected building loss given the collapse (C) case

P[C|IM]= probability of collapse conditioned on ground motion intensity

The following expression becomes valid by assuming repair and demolition, given the non-collapse case, are mutually exclusive events:

$$P(R \mid NC, IM) = 1 - P(D \mid NC, IM) \tag{2.10}$$

Similarly, collapse and non-collapse are also mutually exclusive as follows:

$$P(NC \mid IM) = 1 - P(C \mid IM) \tag{2.11}$$

Residual lateral deformation (residual lateral drift) in the system is treated as the main parameter controlling the demolition decision (Miranda, 2010). However, there is no specific residual drift value that represents demolition. It mainly depends on engineering judgment. Based on the limited information, it is assumed that the probability of having demolition at a certain residual drift value has a lognormal distribution with a median of 0.015 and a logarithmic standard deviation of 0.3 (Miranda, 2010). Residual drifts that cause demolition are in the range of 0.7 to 3%.

Within the scope of this research by Miranda (2010), several reinforced concrete buildings were analyzed in terms of their seismic performance with and without considering the demolition losses. According to the analysis results, the effect of demolition losses on the total loss is the largest at the MCE level of ground motion intensity. Although, both demolition and collapse contribute to the total loss of the building, the demolition losses are larger than the collapse losses. The reason for this difference is that the probability of demolition is much higher than the probability of collapse at the MCE.

A similar study was conducted by Ramirez and Miranda (2009) as well. It was observed that non-collapse reparable losses are larger than total losses due to collapse or demolition at lower intensities $S_a(T_1)$ less than 0.5g. In the intensity range of 0.6g and 1.7g, reparable losses are decreasing and non-collapse demolition losses are increasing. Finally, collapse losses are largest at intensities greater than 1.7g.

Ramirez and Miranda (2009) also studied different height buildings to see the effect of height on demolition losses. According to this study, the total losses appeared to be smaller for a high-rise building than for a low-rise building. However, the increase in the total loss after including the demolition losses is higher for the high-rise structure. This result indicates that high-rise buildings may have larger residual drifts so that the demolition probability is higher for them in the non-collapse case.

The results showed that previous earthquake performance assessment approaches underestimated the total loss, since L_D is appreciable. These underestimates seemed to be larger for ductile buildings than for non-ductile buildings; because ductile structures have more residual drift and less probability of collapse (Miranda, 2010).

The benefits of self-centering systems with reduced residual drifts can be seen more clearly with the application of the approach suggested by Miranda (2010). Although the initial cost of these systems is higher than the cost of conventional systems, their ability to minimize residual drifts reduces the probability of building demolition and economic losses associated with demolition.

2.4 Seismic Performance Assessment of Buildings (ATC-58 Project)

The ATC-58 project aims to establish guidelines to estimate the probable earthquake performance of both new and existing buildings (ATC, 2011). The PEER PBEE methodology was the basis of the ATC-58 project. An electronic database of component fragility specifications was developed. In the performance-based design process of ATC-58, the first step is for the project decision-makers to determine the performance

objectives. Then design professionals develop the design to meet the performance objectives. ATC-58 uses casualties (number of deaths), repair cost, repair time and "Unsafe Placards" (which deem the building to be unsafe for post-earthquake occupancy) as performance measures.

Factors affecting the building performance are as follows (ATC, 2011):

- The ground motion intensity and seismic hazard that the building experiences
- The building earthquake response
- The vulnerability of the building and its components to damage
- The number of people present and their location in the building when the earthquake occurs
- The results of post-earthquake inspections
- The details of the repair actions; the availability of labor and materials, the efficiency of contractors, etc.

Although it is impossible to predict these factors accurately, the performance measures can be assessed as probabilistic performance functions. The ATC-58 project provides procedures for obtaining these performance functions. The performance assessment can be done in three ways (ATC, 2011):

1. Intensity-Based Assessments: Probable performance assessment of the building when it is assumed that the building is subjected to a specific shaking intensity (e.g. from a 5% damped, elastic acceleration response spectra).

2. Scenario-Based Assessments: Probable performance assessment of the building when it is subjected to the effects of a specific magnitude earthquake.
3. Time-Based Assessments: Probable performance assessment of the building over a specific period of time, considering all earthquakes that may occur in that time period.

The ATC-58 process flow chart is illustrated in Figure 2.2. The process is similar to the PEER PBEE methodology that is explained in detail in Section 2.2.

A Performance Assessment Calculation Tool (PACT) was developed to make the necessary performance calculations using the damage database. PACT is an implementation of the PEER PBEE methodology. With input of the building information and a set of EDPs, PACT provides repair time and casualty models, "Unsafe Placard" probabilities, and structural collapse probabilities and consequences. It does intensity-based, scenario-based and time-based assessments. PACT is still under development, and is not appropriate for use in actual projects now.

2.5 Performance-Based Seismic Design and Analysis of Steel Braced-Frame Buildings

Performance-based seismic design (PBD) approach aims to achieve a predetermined performance objective under predetermined ground motion intensity. If the structure reaches a performance level at the specified intensity level, the performance objective is said to be achieved. A performance level is defined in terms of damage that is acceptable at that performance level. Damage is determined by the structural or non-structural limit

states that are reached or exceeded. Building performance levels and damage control for each performance level are defined broadly in ASCE-41-06 (2007) and can be seen in Table 2.1. Three seismic hazard levels (i.e., ground motion intensity level) are defined in FEMA 450 (FEMA, 2003) and can be seen in Table 2.2.

2.5.1 Performance-Based Earthquake Engineering Analysis of Multi Story Special Concentrically-Braced Steel Frame Structures (SCBFs)

PBD usually aims to meet multiple performance objectives. PBD enables structures to sustain their serviceability during small, frequent earthquakes with minor loss in their strength and stiffness. Similarly, PBD assures life safety and collapse prevention during large, infrequent earthquakes. A performance-based design strategy for SCBFs was proposed by Roeder et al. (2004) and is summarized in Table 2.3.

The performance of low- and mid-rise concentrically braced steel frames (SCBF), where the diagonal braces were hollow structural tube sections prone to low cycle fatigue and fracture, together with buckling-restrained braced frames (BRBF) was studied by Uriz and Mahin (2008). Improved brace models for the SCBFs were used to consider brace fracture due to low-cycle fatigue. Low-cycle fatigue leads to a sudden loss of strength and stiffness when the braces fracture. In many of the cases in the study by Uriz and Mahin (2008), collapse occurred where the brace fracture occurred. Nine frames were modeled including three- and six-story SCBFs and BRBFs (Uriz and Mahin, 2008). The SCBF models include out-of-plane buckling of the braces and columns, and consider low-cycle fatigue effects. SCBFs were also modeled in a way that considers column base

uplift. Additionally, two moment resisting frames (MRF) were studied for comparison. These models were subjected to several ground motions and their seismic responses were assessed.

When the analysis results for the low-rise frames were compared, the following findings were obtained:

- Damage in fixed based SCBFs concentrated in one story (most of the time in the lowest story), whereas rocking frames had a more uniform damage distribution throughout the height.
- Among all frame models, SCBFs with rocking bases had the least residual drift at the end of the earthquake motion.
- The interstory drift ratio observed at brace buckling is about 0.25%.
- Collapse occurred for only a few ground motions at the MCE level.
- Excessive lateral displacement of the lower story caused collapse of the fixed base SCBF model.
- Most of the time, when brace fracture occurred in the model, collapse also occurred. For the non-collapse case, no brace fracture was observed for more than half of the structures. Therefore, the collapse resistance depends on the fracture resistance of the braces.
- The yield drift for the SCBFs was 0.3%.
- Out-of-plane displacement can be used as an indicator of brace buckling in SCBFs. The median peak residual out-of-plane displacement of the braces was around 30 in. for MCE level ground motions and approximately 16 in. for DBE

level ground motions. Even for FOE level ground motions, the median peak out-of-plane residual displacement was more than 5 in. The rocking SCBF model had less buckling and hence had much less residual out-of-plane displacement compared to the fixed base model.

When the analysis results for the mid-rise frames were compared, following findings were obtained:

- Damage was concentrated in a single story, usually in the lower and upper stories which had large drift values. Drifts were much less than the low-rise structure drifts.
- The rocking model had a low natural frequency at rocking and a high frequency when contact with the ground occurred.
- The roof drift of the rocking model was slightly larger than the roof drift of the fixed base model, but the interstory drift was larger for the fixed base model.
- Collapse occurred for only a few ground motions at the MCE level for both the fixed base and rocking models. 30% of the ground motion records caused collapse for the fixed base SCBF. For the rocking SCBF, this value was reduced to 10%.
- Excessive lateral displacement of the lower and upper stories triggered collapse for the fixed base SCBF. The rocking SCBF collapsed because of an excessive overturning moment.

- Although the drift demand was less, more brace fractures were observed for the mid-rise frames compared to the low-rise frames. Longer periods and P-delta effects can cause this difference.
- The mid-rise frames have more brace damage.
- The residual drift values were almost the same for both the low-rise and mid-rise fixed base SCBF at the MCE level; however for smaller ground motion intensities, the mid-rise frame has larger residual drift.
- Residual out-of-plane displacements of the braces are larger for the mid-rise buildings.

This study points out the superiority of the rocking SCBF structure over the fixed-base SCBF structure. Some advantages are as follows: It has less damage to the braces, the damage is distributed uniformly throughout the height of the structure, and very little residual displacement is observed.

2.5.2 Performance-Based Seismic Design of Self-Centering Concentrically-Braced Frames (SC-CBFs)

Performance based design of the SC-CBF system was specified according to the performance levels identified in FEMA 450 (FEMA,2003) by Roke et al. (2010). Each performance level is related to a seismic hazard level and various limit states. Performance levels are determined according to the damage observed in the structure after the earthquake. The performance levels for the SC-CBF are as follows (Roke et al., 2010):

- Operational (O): This performance level represents no damage in the structure. Column decompression is expected to occur without causing any damage.
- Immediate Occupancy (IO): Slight structural damage has occurred at this level. The structure retains its pre-earthquake strength and stiffness. This level corresponds to the minimum damage to the system. Minor PT bar yielding is permitted.
- Life Safety (LS): Significant structural and non-structural damage has occurred at this level. The structure may lose stiffness, however there is still a significant collapse margin present in the system. For the SC-CBF system, column decompression, PT bar yielding, and member yielding are expected.
- Collapse Prevention (CP): The structure is almost collapsed. An extensive amount of damage is expected which includes column decompression, PT bar yielding, and member yielding.

In the PBD approach, these performance levels are associated with ground motion intensity levels to set the performance objectives. Roke et al. (2010) specified the performance objectives of an SC-CBF as: IO performance level under DBE level ground motions, and CP performance level under MCE level ground motions. Limited PT bar yielding is allowed under the DBE whereas significant yielding is allowed under the MCE. Frame members are designed to remain elastic under the DBE by using capacity design principles. Member yielding is allowed at the MCE level. Performance-based design objectives for SC-CBFs are summarized in Table 2.4. The probability of reaching (or exceeding) PT bar yielding under the DBE is 50%, while the probability of reaching

(or exceeding) member yielding is around 5%. Under the MCE, these probabilities are larger, as expected. The expected lateral force versus lateral roof drift behavior of an SC-CBF is illustrated by Roke et al. (2010) and can be seen in Figure 2.3.

For conventional systems (such as SCBFs), the usual performance objectives are LS performance level under DBE level ground motion and CP performance level under MCE level ground motion. From a comparison of the performance objectives for the two systems, it is seen that the performance of the SC-CBF is expected to be better than the conventional systems.

Roke et al. (2010) analyzed a four-story SC-CBF test structure by using nonlinear dynamic earthquake response analysis. This analysis results showed that system exceeded the specified performance objectives (i.e., there was less damage than specified). Under the DBE, the maximum story drifts are well below the code specified limit of 2% (ASCE, 2010), and the mean maximum story drifts under the MCE are also below 2%. In addition, Roke et al. (2010) stated that SC-CBF system has larger drift capacity prior to initiation of damage of the main structural members than a conventional CBF system.

2.6 Summary

SCBF systems are stiff and economical earthquake resistant systems. However, they have limited ductility capacity with a tendency to accumulate residual drift during an earthquake. Self-centering systems have been developed to increase the ductility and reduce the residual drift under seismic loading. The superiority of the SC-CBF system over conventional SCBF systems has been suggested, but should be shown in terms of

structural damage after an earthquake. The damage assessment procedure presented in this thesis can be used to show this advantage of SC-CBFs.

Table 2.1 – Building Performance Levels and Damage Control (ASCE 41-06)

	Target Building Performance Levels			
	Operational (O)	Immediate Occupancy (IO)	Life Safety (LS)	Collapse Prevention (CP)
Overall Damage	Very light	Light	Moderate	Severe
General	No permanent drift. Structure substantially retains original strength and stiffness. Minor cracking of facades, partitions, and ceilings as well as structural elements. All systems important to normal operation are functional.	No permanent drift. Structure substantially retains original strength and stiffness. Minor cracking of facades, partitions, and ceilings as well as structural elements. Fire protection operable.	Some residual strength and stiffness left in all stories. Gravity-load-bearing elements function. No out-of-plane failure of walls or tipping of parapets. Some permanent drift. Damage to partitions. Building may be beyond economical repair.	Little residual stiffness and strength, but load-bearing columns and walls function. Large permanent drifts. Some exits blocked. Infills and unbraced parapets failed or at incipient failure. Building is near collapse.
Nonstructural Components	Negligible damage occurs. Power and other utilities are available, possibly from standby sources.	Equipment and contents are generally secure, but may not operate due to mechanical failure or lack of utilities.	Falling hazards mitigated but architectural, mechanical, and electrical systems are damaged.	Extensive damage

Table 2.2 – Seismic Hazard Levels (FEMA 450)

Hazard level	Probability of exceedance in 50 years	Return period
MCE-Maximum Considered Earthquake	2%	2475 years
DBE-Design Basis Earthquake	2/3 of MCE	475 years
FOE-Frequently Occurring Earthquake	50%	72 years

Table 2.3 – Performance Based Design Strategy for SCBFs (Roeder et al., 2004)

Seismic Hazard Level	Performance Level	Limit States
FOE	Immediate Occupancy (IO)	• Brace buckling • Incipient Brace yielding
DBE	Life Safety (LS)	• Tension yielding of brace • Incipient yielding of gusset plate • Incipient elongation of bolt holes
MCE	Collapse Prevention (CP)	• Full brace yielding • Yielding of gusset plate • Elongation of bolt holes • Incipient brace fracture

Table 2.4 – Performance Based Design of SC-CBFs (Roke et al., 2010)

Seismic Hazard Level	Performance Level	Limit States
DBE	Immediate Occupancy (IO)	• Column decompression • Minor PT bar yielding
MCE	Collapse Prevention (CP)	• Column decompression • PT bar yielding • Member yielding

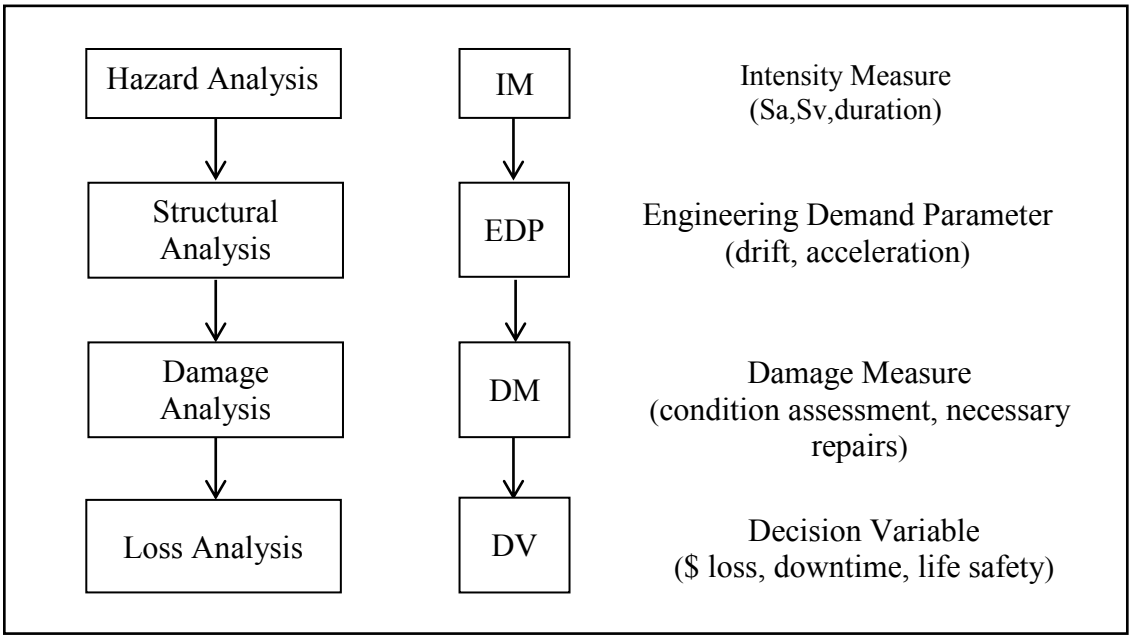

Figure 2.1 – Components of PEER's PBEE methodology

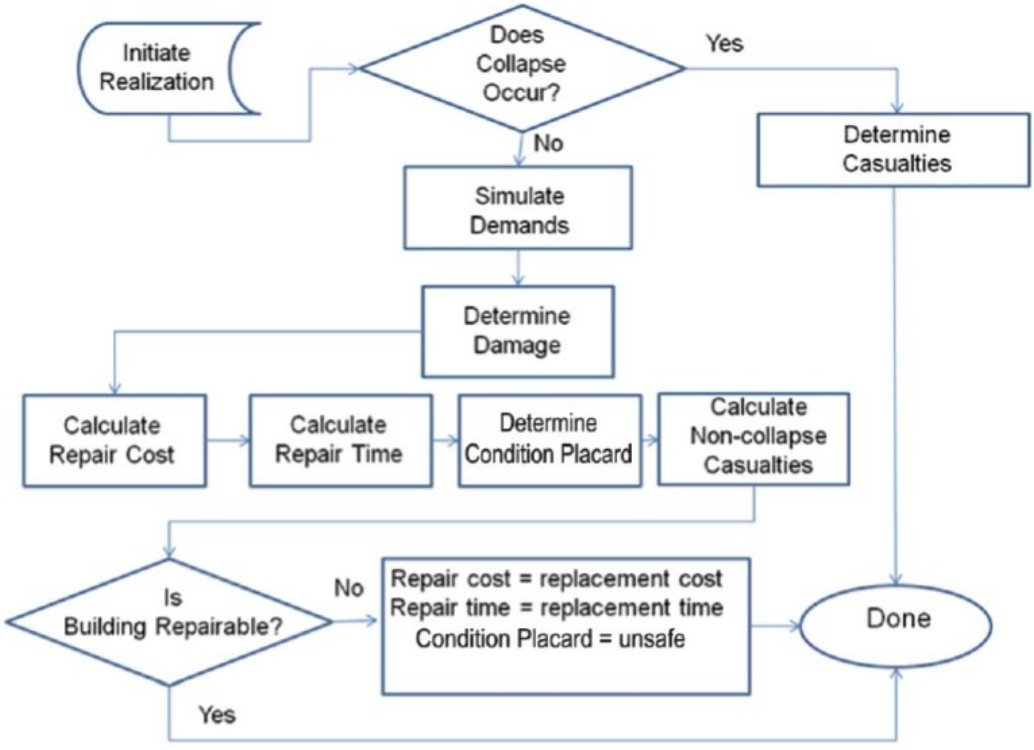

Figure 2.2 – ATC-58 process flow chart (ATC, 2011)

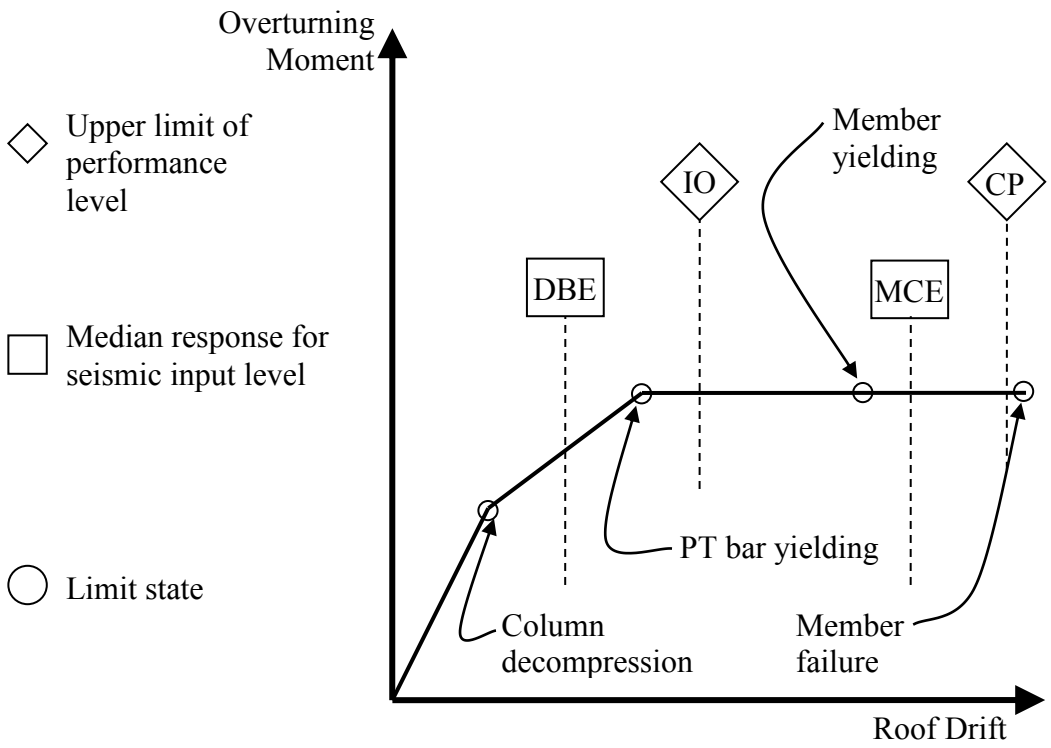

Figure 2.3 – Schematic illustration of PBD criteria of SC-CBF (Roke et al., 2010)

CHAPTER 3

SEISMIC DESIGN AND DYNAMIC ANALYSIS OF SCBFS AND SC-CBFS

3.1 General

In this study, the seismic performance of SCBFs and SC-CBFs is evaluated from a damage assessment and compared. As part of this study, engineering demand parameters (EDPs) such as story drift and component deformation are estimated by dynamic analysis. These EDPs are then related to damage states to quantify the necessary repair actions.

Four buildings are analyzed in this study: 4- and 9-story SCBF buildings (4SCBF and 9SCBF, respectively), and 4- and 9-story SC-CBF buildings (4SC-CBF and 9SC-CBF, respectively). These four model buildings are designed using design procedures described in this chapter. Analytical models of these four frames are created in OpenSees and the earthquake response of these models is determined from nonlinear dynamic earthquake response analysis.

The peak story drift (θ_m), the peak residual story drift (θ_r) and the normalized residual out-of-plane displacement of the braces (Δ_{or}) of the CBFs are the EDPs extracted from the dynamic analysis results. θ_m and θ_r are used for the collapse/non-collapse and demolition/no demolition damage assessment of the buildings presented in Chapter 4. Δ_{or} is used for the damage assessment of the brace components of the SCBFs and SC-CBFs

presented in Chapter 5. All three EDPs are used in a comprehensive damage assessment presented in Chapter 6.

This chapter describes the seismic design procedures for the SCBF and SC-CBF buildings used in this study. The nonlinear dynamic time history analyses of the buildings used to obtain the EDPs are also described. The nonlinear numerical models and ground motions used in dynamic analyses are described briefly. Finally, a brief discussion of the dynamic analysis results is given.

3.2 Earthquake Forces for Design

The earthquake design lateral forces are determined using two methods derived from ASCE 7-10 (ASCE, 2010).

3.2.1 Equivalent Lateral Force (ELF) Procedure

The equivalent lateral force (ELF) procedure starts by determining the approximate fundamental period (T_a) of the building. The equation to obtain the approximate period is as follows (ASCE, 2010):

$$T_a = C_t \cdot h_n^x \tag{3.1}$$

where,

$C_t = 0.02$

$x = 0.75$ (for both the SCBF and SC-CBF)

h_n = the total height of the structure (ft)

The seismic response coefficient, C_s, is determined as follows (ASCE, 2010):

$$C_s = \frac{S_{DS}}{\left(\frac{R}{I}\right)} \tag{3.2}$$

where,

R = the response modification factor (Table 12.2-1 in ASCE, 2010)

I = the occupancy importance factor (Table 11.5-1 in ASCE, 2010)

S_{DS} = the spectral response acceleration parameters for short periods (ASCE, 2010)

For the SCBF, R is equal to 6 and for the SC-CBF, R varies, but should not exceed 10. Detailed information about R in the design of SC-CBFs is given in Section 3.3.2.

Maximum and minimum values of C_s are (ASCE, 2010):

$$C_{S,\max} = \begin{Bmatrix} \dfrac{S_{D1}}{T \cdot \left(\frac{R}{I}\right)} & if\ T \le T_L \\ \dfrac{S_{D1} \cdot T_L}{T^2 \cdot \left(\frac{R}{I}\right)} & if\ T > T_L \end{Bmatrix} \tag{3.3}$$

$$C_{S,\min} = \begin{Bmatrix} 0.01 \\ 0.044 \cdot S_{DS} \cdot I \\ \dfrac{0.5 \cdot S_1}{\left(\dfrac{R}{I}\right)} \qquad if\ S_1 \geq 0.6g \end{Bmatrix} \tag{3.4}$$

where,

T = the fundamental period of the structure (sec)

S_{DS}, S_{D1} = the spectral response acceleration parameters for short periods and a period of 1 sec (ASCE, 2010)

T used in the above equations is determined as follows. The actual fundamental period, T_1 is estimated from an analysis of the structural model and corresponds to the first mode. T used in the above equations should be the smaller of T_1 and T_{max}, where T_{max} is calculated as follows.

$$T_{\max} = C_u \cdot T_a \tag{3.5}$$

where,

C_u = the coefficient for the upper limit on period (Table 12.8-1 ASCE, 2010)

Initially, T_a can be used as T for a preliminary design, and the ELFs are calculated using T_a. However, the ELFs should be recalculated after obtaining T_1 from a structural analysis and the design should be checked for the recalculated ELFs.

The design base shear is calculated (ASCE, 2010) as follows:

$$V = C_s \cdot W \tag{3.6}$$

where,

W = the total seismic weight of the building (kips)

$$W = DL + LL_{partition} \tag{3.7}$$

where,

DL = the total dead load of the building (kips)

$LL_{partition}$ = the portion of the live load of the building associated with the partitions (kips)

The dead and live loads used in the design of the SCBF and SC-CBF buildings are given in Tables 3.1 and 3.2.

Finally, the lateral earthquake forces (F_x) for each floor level are obtained as follows (ASCE, 2010):

$$F_x = C_{vx} \cdot V \tag{3.8}$$

$$C_{vx} = \frac{w_x h_x^k}{\sum_{i=1}^{n} w_i h_i^k} \tag{3.9}$$

where,

C_{vx} = the vertical distribution factor

w_i and w_x = the portion of total building weight (W) for level i or x (kips)

h_i and h_x = the building height from the base of the building to level i or x (ft)

$$k = \begin{Bmatrix} 1 & if\ T \le 0.5\,\text{sec} \\ 2 & if\ T \ge 2.5\,\text{sec} \\ 1 < k < 2 & if\ 0.5s < T < 2.5\,\text{sec} \end{Bmatrix} \tag{3.10}$$

Story drifts should be checked against the drift limits of ASCE7-10 (ASCE, 2010). The design story drift is determined as the difference between the center of mass deflections of two adjacent floors, modified as follows (ASCE, 2010):

$$\delta_x = \frac{C_d \delta_{xe}}{I} \tag{3.11}$$

where,

C_d = the deflection amplification factor (Table 12.2-1 in ASCE, 2010)

δ_{xe} = the story drift at level x determined by an elastic analysis

I = the occupancy importance factor (Table 11.5-1 in ASCE, 2010)

To obtain the elastic drifts (δ_{xe}), ELFs based on the estimated T_1 may be used without considering the period limit T_{max} in the structural analysis (ASCE, 2010).

3.2.2 Response Spectrum Analysis (RSA)

The earthquake lateral forces can be estimated from a modal response spectrum analysis (RSA). In this analysis, modal properties (modal shape, period, and other properties) of

the building are estimated. Then the earthquake response is estimated from the code-specified design response spectrum. The responses for the modes are then combined to obtain the total response of the building. The design response spectrum used in this analysis is defined in ASCE7-10 (ASCE, 2010) as follows:

$$S_a(T) = \begin{cases} S_{DS} \cdot \left(0.4 + 0.6\frac{T}{T_0}\right) & T \le T_0 \\ S_{DS} & T_0 < T \le T_S \\ \frac{S_{D1}}{T} & T_S < T \le T_L \\ \frac{S_{D1} \cdot T_L}{T^2} & T_L < T \end{cases} \quad (3.12)$$

where,

S_{DS}, S_{D1} = the spectral response acceleration parameters for short periods and a period of 1 sec

T_0, T_S, and T_L = the transition periods (sec)

T = the estimated period of a given vibration (sec) (ASCE, 2010)

The DBE-level design response spectrum determined from Equation 3.12 is shown in Figure 3.1. The MCE-level spectrum is obtained by multiplying the design response spectrum by 1.5 (ASCE, 2010).

To obtain modal response parameters (story drifts, reaction forces, individual member forces for each mode of response) for an RSA according to ASCE7-10, the design response spectrum (Equation 3.12) should be scaled down by dividing by the quantity of R/I as it is given in ASCE7-10 (ASCE, 2010). The response spectrum in Equation 3.12 is used in the design method for SC-CBFs proposed by Roke et al. (2010) without scaling down by R/I.

The modes to be included in the ASCE7-10 RSA are based on the combined modal mass participation ratio. At least 90% of the participating mass should be included in the RSA for each principal direction of the building.

The design response obtained for each mode is combined with the responses from other modes by using either the square root of the sum of the squares method (SRSS) or the complete quadratic combination (CQC) rule (ASCE, 2010).

The combined modal base shear (V_t) from the ASCE7-10 RSA should not be less than 85% of the calculated base design shear (V) from the ELF procedure. When V_t is less than 0.85V, the RSA results should be scaled up to that level using the following scale factor (ASCE, 2010):

$$S.F. = 0.85 \cdot \frac{V}{V_t} \tag{3.13}$$

Then the building design should be updated using the scaled results and V_t should be rechecked against the 85% limit. This design process is repeated until the 85% limitation in V_t is met.

For a structural design based on RSA, the design story drifts are checked against the story drift limit of ASCE 7-10. Modified story drifts are obtained from Equation 3.11. For the cases when the response is scaled up so V_t is greater than or equal to 0.85V, the story drifts need not be multiplied by the scale factor before they are compared against the drift limit (ASCE, 2010).

3.3 Structural Design

SCBF and SC-CBF frames were designed for both 4- and 9-story office buildings located in Southern California (near Los Angeles) on a stiff-soil site (Site Class D). The same floor plan is used for all buildings and is shown in Figure 3.2. The seismic design parameters are tabulated in Table 3.3 for both systems. The structural design of the two types of frames is explained in this section.

3.3.1 Design of SCBF

SCBFs consist of beams, columns, and diagonal bracing. The design of an SCBF starts with the determination of the base shear and the earthquake lateral forces. Member forces are then obtained from a structural analysis of the structure under the earthquake lateral forces. The brace design forces are taken from these analysis results. For the beams and columns, however, the design method for SCBFs from the AISC Seismic Provisions (AISC, 2010b) considers the *maximum expected* brace forces together with the gravity loads acting on the beams and columns (Powell, 2009).

2-dimensional SAP2000 models were used for the design of the 4- and 9-story SCBFs termed 4SCBF and 9SCBF, respectively. These SAP2000 models include only the main

structural members (beams, columns, and braces) and a lean-on column connected to the left-hand side of the SCBF. The lean-on column is modeled as weightless and connected to the SCBF with weightless rigid link elements. The tributary seismic mass for one frame (which is one quarter of the total building mass) is applied to the lean-on column. The lean-on column in the model considers the P-delta effects due to the total gravity load of the tributary area for one SCBF (corresponding to one quarter of the total floor area). Twenty five percent of the live load, as well as the full dead load, within the one quarter of the total floor area associated with one SCBF are applied to the lean-on column.

The connections between the beams and columns are modeled as full-moment connections without any moment release, but the brace connections are modeled as pin connections by releasing the moment at the ends of the braces. The columns are assumed to be fixed at the base and modeled accordingly.

3.3.1.1 Load Cases

The SCBFs are designed using the load combinations as follows (ASCE 2010):

$$1.4D \tag{3.14}$$

$$1.2D + 1.6L + 0.5L_r \tag{3.15}$$

$$1.2D + 1.6L_r + \gamma L \tag{3.16}$$

$$(1.2 + 0.2S_{DS})D + \rho Q_E + \gamma L \tag{3.17}$$

$$(0.9 - 0.2S_{DS})D + \rho Q_E \quad (3.18)$$

where,

D = the dead load

L = the live load

L_r = the roof live load

Q_E = the effects of earthquake lateral forces from the ELF procedure or RSA

ρ = the redundancy factor = 1.0 (Section 12.3.4.2 in ASCE, 2010)

γ = 0.5 when live load is less than or equal to 100 psf (ASCE, 2010)

Note, lateral earth pressure and snow load were omitted from the design.

The dead and live loads used in the design are given in Tables 3.1 and 3.2. Live load reduction is done in accordance with ASCE 7-10.

3.3.1.2 Member Selection

The 4- and 9-story SCBFs are designed for both ELF and RSA forces. The most economical design among the two is used for further analysis. Members are designed for the most critical load combination by using the SAP2000 Steel Design tool in accordance with the current AISC Design Specification.

The SCBFs with section sizes are given in Figure 3.3 through Figure 3.5. Figure 3.3 shows the 4SCBF. There is only one design for 4SCBF because both the ELF procedure

and RSA give the same design base shear and member section sizes for the 4SCBF. Figure 3.4 and Figure 3.5 show the 9SCBF designed using the ELF procedure and RSA, respectively. As seen from these figures, the ELF procedure and RSA give different designs.

The weights of the structural steel members, seismic weights, base shear values, base shear values normalized by seismic weight and fundamental periods of the 4- and 9-story SCBFs are given in Table 3.4. The 9SCBF designed using the RSA has lighter section sizes than the 9SCBF from the ELF procedure. The 9SCBF designed using the RSA is used in the remaining studies since it has the lightest weight.

3.3.2 Design of SC-CBF

3.3.2.1 System Behavior

The SC-CBF systems studied in this research were designed by Chancellor (2013). These SC-CBF systems consist of beams, columns and braces, as well as gravity columns adjacent to each SC-CBF (Figure 3.6). These gravity columns carry gravity loads; the SC-CBF columns do not carry gravity loads other than the weight of the SC-CBF. The SC-CBF columns are not rigidly connected to the foundation. Lateral load bearings are located between gravity columns and adjacent SC-CBF column at each floor. These bearings transfer the lateral forces from the floor diaphragm to the SC-CBF. Post-tensioning bars run vertically over the height of the SC-CBF. There is also a distribution strut in the top story that distributes the large concentrated force from the PT bars to the other stories (Chancellor et al., 2012).

As earthquake lateral forces are applied to the SC-CBF, the SC-CBF deforms elastically, similar to an SCBF. The initial overturning moment resistance is provided by the prestress force of the PT bars, the weight of SC-CBF, and the friction in the lateral load bearings. Once the applied overturning moment becomes greater than the initial overturning moment resistance of the system, one of the SC-CBF columns uplifts and the SC-CBF begins to rock on its foundation. When the earthquake lateral forces are reduced, system returns to its plumb position from the effect of the restoring overturning moment provided by the PT bars (Chancellor et al., 2012).

3.3.2.2 Design Procedure

A performance based design procedure was developed by Roke et al. (2010) for the SC-CBF system. As explained in Section 2.5.2, this design procedure targets performance objectives of Immediate Occupancy (IO) under the DBE and Collapse Prevention (CP) under the MCE. The design procedure limits the PT bar yielding under the DBE, but PT bar yielding is permitted under the MCE, along with some member yielding.

A modified version of the RSA procedure is used in the design of SC-CBFs. In a conventional RSA, to obtain the response of the structure for each mode, the design response spectrum is scaled down by R/I and the response is determined for each mode. The responses of the modes are combined with one of the modal combination methods (SRSS or CQC) to obtain the peak response. In the modified RSA for SC-CBFs, the response spectrum is scaled down for the first mode and scaled up for the higher modes.

The responses of the modes are combined by the CQC method with specially derived correlation coefficients.

The design procedure is summarized as follows (Chancellor et al., 2012):

1. Select the member sizes, number and area of PT bars, prestress ratio and the friction in the lateral load bearings
2. Determine the modal properties of the SC-CBF
3. Determine the decompression overturning moment (OM_D) and decompression roof drift (θ_D) (Roke et al., 2010)
4. Determine the overturning moment at PT bar yielding (OM_Y)
5. Calculate the response modification factor ($R_{A,D}$) which is similar to the R factor in ASCE7-10 (ASCE, 2010). $R_{A,D}$ is not a specified value, instead it is calculated as shown in Equation 3.19:

$$R_{A,D} = \frac{OM_{elastic,1}}{OM_D} \tag{3.19}$$

$$OM_{elastic,1} = \frac{M_1^*}{M_{total}} \cdot OM_{elastic} \tag{3.20}$$

where,

$OM_{elastic,1}$ = the elastic overturning moment using the first mode mass

$OM_{elastic}$ = the required elastic overturning moment from code-based ELF without scaling by R/I procedure

M_1^* = the effective modal mass for the first mode

M_{total} = the total mass

In the design of SC-CBFs, $R_{A,D}$ should not exceed 10.

6. Determine the first mode peak effective pseudo-acceleration. The first mode forces are limited by the SC-CBF rocking action and yielding of the PT bars. For this reason, the first mode pseudo-acceleration value ($\alpha_{y,1}$) is not obtained from the design spectrum. The equation for $\alpha_{1,y}$ is given as follows:

$$\alpha_{y,1} = \frac{OM_Y}{OM_1} \tag{3.21}$$

where,

OM_Y = the overturning moment at PT bar yielding

OM_1 = the overturning moment calculated from the first mode spatial distribution of mass (Roke et al., 2010)

$\alpha_{y,1}$ is then scaled up by a factor of 1.15 to consider the probability that the effective first mode pseudo-acceleration can exceed $\alpha_{y,1}$.

7. Determine the higher modes factored design pseudo-acceleration. In a conventional RSA, the entire spectrum is scaled down by R/I for all modes. However, in the design procedure by Roke et al. (2010), the pseudo-acceleration values for the higher modes are scaled up by a factor 2. In studies by Roke et al.

(2010), time history analysis results of SC-CBFs show these larger effective pseudo-acceleration responses for the higher modes. The factor of 2 is chosen to prevent member forces from the dynamic analysis from exceeding the member design forces, to prevent yielding under the DBE.

8. Determine the factored member force design demands from the combination of factored modal member forces. The CQC method is used to combine the modal forces. The correlation between the modes for the SC-CBF was studied by Roke et al. (2010), the suggested correlation coefficient is 0.25.
9. Calculate the energy dissipation ratio (β_E). The hysteretic energy dissipation ratio, β_E, is the ratio of the energy dissipated by the hysteresis loop of an SC system to the energy dissipated by a bilinear elasto-plastic system having the same strength as the SC system under cyclic loading (Seo and Sause, 2005). It is needed to estimate the peak roof drift under the DBE. The source of energy dissipation in the SC-CBF systems of this study is the lateral load bearings with friction. Equation 3.22 (Roke et al., 2010) is used to calculate β_E:

$$\beta_E = \mu \cdot \frac{b_{ED}}{h_1^*} \cdot \left(1 + \frac{\lambda}{2} \cdot \left(\frac{OM_Y}{OM_D} - 1\right)\right) \tag{3.22}$$

$$h_1^* = \frac{OM_1}{V_{b1}} = \frac{\{h\}^T \{F_1\}}{\{i\}^T \{F_1\}} \tag{3.23}$$

$$\lambda = \frac{OM_{\max} - OM_D}{OM_Y - OM_D} \tag{3.24}$$

where,

μ = the friction coefficient for the lateral load bearings

b_{ED} = the SC-CBF width + centerline distance between SC-CBF column and gravity column

h = the vector of the floor heights of the SC-CBF

i = the influence vector which has elements equal to 1

F_1 = the vector of the first mode forces

OM_{max} = the maximum overturning moment under DBE

OM_{max} depends on the estimated peak roof displacement under the DBE ($\theta_{R,DBE}$), and the calculation of $\theta_{R,DBE}$ depends on β_E. An iterative approach is used to calculate both $\theta_{R,DBE}$ and β_E. For the first iteration, OM_{max} is assumed to be equal to OM_Y as a starting point.

$\theta_{R,DBE}$ is obtained by multiplying θ_D (from Step-3) with μ (ductility). μ-R-T relationships from Seo (2005) are used to determine μ of the system under the DBE with known β_E, site soil condition, natural period (T_1), and $R_{A,D}$. In the design of SC-CBFs, PT bars should not yield under the DBE, and $\theta_{R,DBE}$ is taken as the design drift at which the PT bars should not yield.

According to Seo (2005), the maximum β_E value of SC systems is 0.5. Therefore, the design value of β_E should be less than 0.5 (Roke et al., 2010). For the design of 4SC-CBF, β_E is chosen as 0.5; and for the design of 9SC-CBF, β_E is chosen as 0.2.

10. Check the design parameters (β_E, $R_{A,D}$, PT bar yielding, member sizes) to see if further iterations are needed until all design criteria met.

4SC-CBF and 9SC-CBF are two of several SC-CBF buildings designed by Chancellor (2013) following the design procedure explained above. The member sizes of 4SC-CBF and 9SC-CBF are given in Figure 3.6 and 3.7. PT bars for the designed SC-CBFs are as follows: 4SC-CBF has 10 PT bars with 1.25" diameter; 9SC-CBF has 10 PT bars with 1.75"diameter.

3.3.3 Comparison of Designs

The 4- and 9-story SCBF and SC-CBFs are compared in terms of their weights of the structural steel members, seismic weights, base shear values, base shear values normalized by seismic weight and fundamental periods in Table 3.5.

Table 3.5 shows that the SC-CBFs are heavier than the SCBFs for both the 4- and 9-story buildings. Likewise, the design base shear values for the SC-CBFs are much larger than the design base shear values for the SCBFs. The base shear values normalized by seismic weight ($V_{base}/W_{seismic}$) for the SC-CBFs are about 13% and for the SCBFs are about 4%. The reason for this difference is the scaled up (by a factor of 2) rather than scaled down (by R/I) values of the pseudo acceleration for the higher modes in the SC-CBF design procedure.

The period values of the SCBF and SC-CBF designs are close since both systems have the same mass.

3.4 Nonlinear Dynamic Earthquake Response Analysis

Nonlinear dynamic earthquake response analyses of the model 4- and 9-story buildings were conducted to generate data for the damage assessment. Nonlinear dynamic earthquake response analyses are used to obtain the structural response in terms of EDPs. Peak story drift (θ_m), peak residual story drift (θ_r) and normalized residual out-of-plane (OOP) displacement of the braces (Δ_{or}) are the EDPs.

A nonlinear numerical model for each model building was developed in OpenSees by Tahmasebi (2014) and by Chancellor (2013). The Far-Field ground motion set specified in FEMA P695 (FEMA, 2009) was used in the analyses to perform the incremental dynamic analysis (IDA). Vamvatsikos and Cornell (2002) described IDA as a parametric analysis method to estimate structural performance under seismic loads. In an IDA, the structural model is subjected to scaled ground motions. A series of analyses are performed with the scale factor increased in each analysis, so that the intensity measure (IM) increases sequentially. An IDA curve is obtained for each ground motion. The curve is a plot of a response parameter (i.e., an EDP) vs. an IM (such as the first mode spectral acceleration, $Sa(T_1)$). This data is provided by Tahmasebi (2014) for the SCBF model buildings and by Chancellor (2013) for the SC-CBF model buildings. IDA is often used to determine the collapse capacity of a building. The use of IDA for building collapse analysis is discussed in detail in Chapter 4.

3.4.1 Nonlinear Numerical Models

As mentioned earlier, nonlinear numerical models for the 4- and 9-story SCBF and SC-CBF model buildings were created in OpenSees for the dynamic analyses by Tahmasebi (2014) and by Chancellor (2013).

The nonlinear numerical models for the SCBFs include the frame members (beams, columns, braces) and a lean-on column (Tahmasebi, 2014). Beam-column connections are modeled as rigid connections. The brace connections are modeled as moment-free pin connections. In a real building, buckling of the beams is restrained by the floor system and gravity load framing. The beams in the SCBF model are modeled without buckling to reflect this restraint. Column bases are modeled as fixed base.

The nonlinear numerical models for SC-CBFs include the frame members (beams, columns, and braces), two gravity columns adjacent to the SC-CBF columns, PT bars and a lean-on column (Chancellor, 2013). Beam-column connections are modeled as rigid connections. The brace connections are modeled as moment-free pin connections as in the SCBF model. Contact-gap elements are used to model gap opening and uplift at the base of the column. Friction-contact-gap elements are used to model the lateral load bearings between the SC-CBF columns and the adjacent gravity columns.

All of the SCBF and SC-CBF members are modeled with nonlinear beam-column elements.

Gravity loads are applied to the lean-on column according to the corresponding tributary area of both the SCBFs and SC-CBFs. The gravity loads for dynamic analysis are

different from the design gravity loads given in Section 3.3. The gravity loads used in the dynamic analysis are based on Equation 3.25 (FEMA, 2009):

$$1.05D + 0.25L \tag{3.25}$$

where,

D = the nominal dead load of the structure

L = the nominal live load

As stated in FEMA P695, the models should consider all seismic mass and P-delta effects associated with the gravity loads carried by the seismic-force-resisting system. The mass of the structure tributary to the modeled frame is put on the lean-on column. For both the SCBF and SC-CBF models, the lean-on column is connected to the frame with a rigid link by using the "equal DOF" feature of OpenSees which is assigned only in the horizontal direction (Tahmasebi, 2014 and Chancellor, 2013).

An initial imperfection is given to the braces in the models to create the potential for brace buckling in the model. The AISC Code of Standard Practice for Steel Buildings and Bridges (AISC, 2010a) specifies the maximum permissible out-of-straightness of brace members during fabrication as about L/1000. For this reason the initial imperfection of the braces was specified as L/1000 in the model. Since the diagonal braces in the model buildings are wide flange sections not prone to low-cycle fatigue and fracture (Powell, 2009), the braces are modeled without considering the effects of low-cycle fatigue and fracture.

3.4.2 Input Ground Motions

Nonlinear dynamic earthquake repsonse analyses were performed with the gravity loads from Equation 3.25 and the input Far-Field record set given in FEMA P695 (FEMA, 2009). The Far-Field record set consists of twenty-two ground motion pairs. These ground motion records are from sites located at least 10 km from a fault rupture (FEMA, 2009). The Far-Field record set includes records from earthquakes with magnitudes greater than 6.5. The records were selected from the PEER Next Generation Attenuation (NGA) database. The ground motions in the Far-Field record set are summarized in Table 3.6.

These 22 ground motion pairs (i.e., 44 ground motion records) are scaled to a specific intensity level according to the scaling methodology given in FEMA P695 (FEMA, 2009). This scaling methodology has two steps. The first step is the "normalization" step. In this normalization step, each individual record in the record set is normalized by its respective peak ground velocity. Normalization factors are given in FEMA P695. The normalization is intended to eliminate the variability due to the event magnitude, distance to source, source type and site conditions without the eliminating record-to-record variability (FEMA, 2009). The second step is to scale the normalized ground motion records to a specific ground motion intensity level. In this scaling, the median spectral acceleration of the record set coincides with a given spectral acceleration at the fundamental period of the building being studied (i.e., $Sa(T_1)$), which is treated as the IM in the present study.

The Far-Field record set ground motions were scaled to either the DBE or the MCE levels. Damage assessment was done using the dynamic analyses results at the DBE and MCE level. Figures 3.8, 3.9, 3.10 and 3.11 show the design spectrum (ASCE, 2010) and the pseudo-acceleration response spectrum for each of the scaled ground motions from the Far-Field record set used in this study. Since the fundamental periods of the 4SCBF and 4SC-CBF models (and similarly the 9SCBF and 9SC-CBF models) are very close, the same scaled ground motions are used for both systems.

The displacement response spectrum for each of the scaled ground motions are also shown in Figures 3.12 through 3.15.

3.4.3 Dynamic Analysis Results

Selected EDPs (θ_m, θ_r, Δ_{or}) are extracted from the results of the nonlinear dynamic analyses. The nonlinear numerical models for each model building were analyzed for each scaled ground motion record from the FEMA P695 Far-Field record set. Results are obtained for each of the 44 ground motion records. The statistical parameters, mean (μ) and standard deviation (σ) of θ_m, θ_r, and Δ_{or} from the 44 results from each model building are given in Table 3.7.

Table 3.7 shows the θ_m response of the SCBFs and SC-CBFs are similar with similar mean and standard deviation values. For both systems, θ_m increases with increasing building height.

The rocking action of SC-CBFs reduces the potential for residual drift; SC-CBFs are expected to have less θ_r than SCBFs. Table 3.7 shows the θ_r response of the SCBFs are

greater than the θ_r response of the SC-CBFs. θ_r values for 4SC-CBF are very small (close to zero). Therefore, 4SC-CBF has no significant residual drift under the DBE or MCE.

Δ_{or} results listed in Table 3.7 show that the braces of the 4SCBF and 9SCBF will be damaged more than the braces of the 4SC-CBF and 9SC-CBF. 4SC-CBF has very small Δ_{or} values. Damage to the braces increases with increasing building height, as the 9-story buildings have larger Δ_{or} values than the 4-story buildings. As expected, the structural response of the buildings to the MCE is larger than the response to the DBE. These θ_m, θ_r, and Δ_{or} values are used for the probabilistic structural damage assessments presented in the following chapters.

Table 3.1 – Dead loads

Item	(psf)
Floor / Roof Slabs	43
Floor / Roof Decks	3
Ceiling Material	5
Mechanical Weight per Floor	10
Mechanical Weight on Roof	25
Structural Steel – Floor	15
Structural Steel – Roof	10
Floor Finish	2
Steel Fireproofing	2
Vertical Projection of Exterior Wall	25
Roofing Material	10

Table 3.2 – Live loads

Item	(psf)
Office – Floor	50
Office – Roof	20
Partition	15

Table 3.3 – Seismic design parameters for SCBFs and SC-CBFs

Parameter	Notation	Value	
		SCBF	SC-CBF
Seismic design category		D	D
Occupancy importance factor	I	1.0	–
Site class	–	D (Firm soil)	D (Firm soil)
Site coefficients for site class	F_a	1.0	1.0
	F_v	1.5	1.5
Response modification factor	R	6	–
Deflection amplification factor	C_d	5	–
Deterministic MCE spectral acc. at short periods	S_s	1.5g	1.5g
Deterministic MCE spectral acc. at 1 sec period	S_1	0.6g	0.6g
Long-period transition period	T_L	8 sec	8 sec

Table 3.4 – Comparison of SCBF designs

SCBF	Steel Weight (W) (kips)	Seismic Weight ($W_{seismic}$) (kips)	Base Shear (V_{base}) (kips)	$\frac{V_{base}}{W_{seismic}}$	Fund. Period (T_1) (sec)
4-story	30.9	1.191E4	423.1	0.036	0.59
9-story ELF	97.3	2.847E4	987.6	0.035	1.52
9-story RSA	86.1	2.847E4	840.6	0.030	1.66

Table 3.5 – Comparison of designed buildings

Frame	Steel Weight (W) (kips)	Seismic Weight ($W_{seismic}$) (kips)	Base Shear (V_{base}) (kips)	$\frac{V_{base}}{W_{seismic}}$	Fund. Period (T_1) (sec)
4SCBF	30.9	1.191E4	423.1	0.036	0.55
4SC-CBF	56.7	1.191E4	1569.2	0.132	0.48
9SCBF	86.1	2.847E4	840.6	0.030	1.48
9SC-CBF	184.8	2.847E4	3866.8	0.136	1.32

Table 3.6 – Summary of Far-Field ground motion record set (FEMA, 2009)

ID No.	Earthquake			Recording Station
	M	Year	Name	
1	6.9	1995	Kobe, Japan	Nishi-Akashi
2	6.9	1995	Kobe, Japan	Shin-Osaka
3	7.5	1999	Kocaeli, Turkey	Arcelik
4	7.5	1999	Kocaeli, Turkey	Duzce
5	7.6	1999	Chi-Chi, Taiwan	CHY101
6	6.5	1976	Friuli, Italy	Tolmezzo
7	7.6	1999	Chi-Chi, Taiwan	TCU045
8	7.1	1999	Duzce, Turkey	Bolu
9	7.4	1990	Manji, Iran	Abbar
10	6.5	1979	Imperial Valley	Delta
11	6.5	1979	Imperial Valley	El Centro Array # 11
12	7.1	1999	Hector Mine	Hector
13	6.6	1971	San Fernando	LA-Hollywood Stor
14	6.5	1987	Superstition Hills	El Centro Imp. Co.
15	6.5	1987	Superstition Hills	Poe Road (temp)
16	6.9	1989	Loma Prieta	Capitola
17	6.9	1989	Loma Prieta	Gilroy Array # 3
18	7.0	1992	Cape Mendocino	Rio Dell Overpass
19	7.3	1992	Landers	Coolwater
20	7.3	1992	Landers	Yermo Fire Station
21	6.7	1994	Northridge	Beverly Hills-Mulhol
22	6.7	1994	Northridge	Canyon Country - WLC

Table 3.7 – Mean and standard deviation of buildings structural response quantities

Frame	Hazard	Peak story drift (θ_m)		Peak residual story drift (θ_r)		Largest normalized residual OOP displacement (Δ_{or})	
		μ	σ	μ	σ	μ	σ
4SCBF	DBE	0.011	0.005	8.34E-04	0.001	0.022	0.014
	MCE	0.019	0.009	0.003	0.003	0.038	0.022
4SC-CBF	DBE	0.010	0.004	1.24E-07	1.90E-07	1.74E-04	2.83E-05
	MCE	0.017	0.008	1.19E-04	7.81E-04	1.32E-04	6.78E-05
9SCBF	DBE	0.019	0.006	0.003	0.003	0.028	0.013
	MCE	0.026	0.008	0.008	0.007	0.044	0.023
9SC-CBF	DBE	0.016	0.008	0.001	0.001	0.006	0.01
	MCE	0.026	0.014	0.003	0.009	0.017	0.016

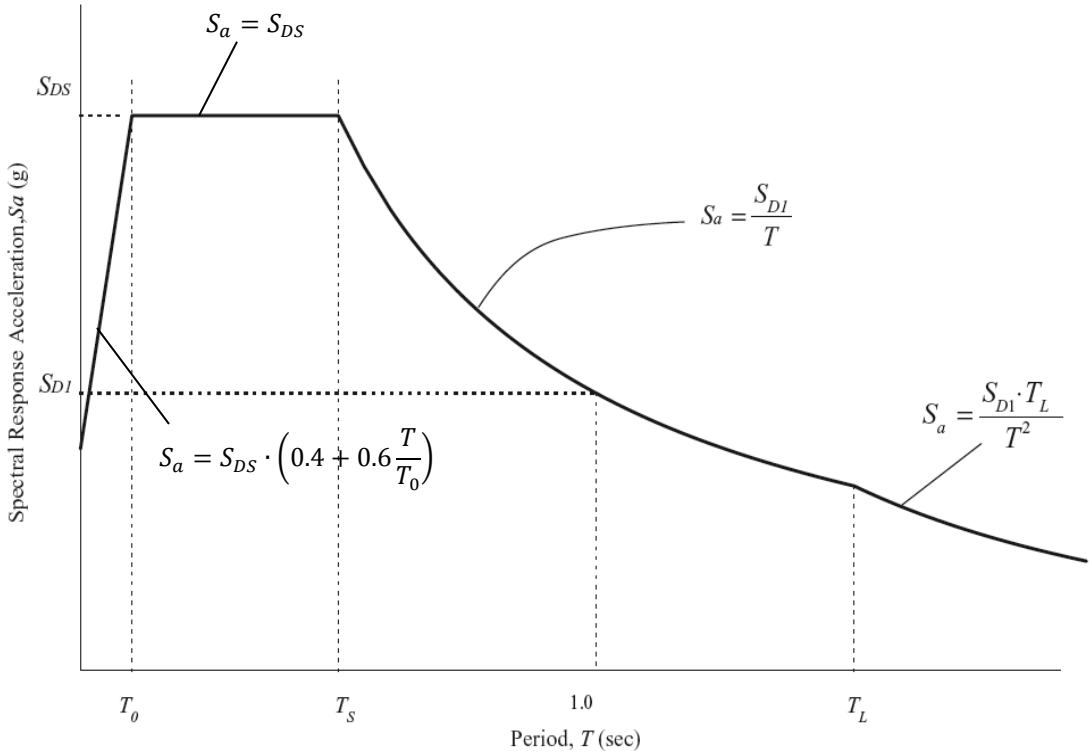

Figure 3.1 – General design response spectrum (ASCE 7-10)

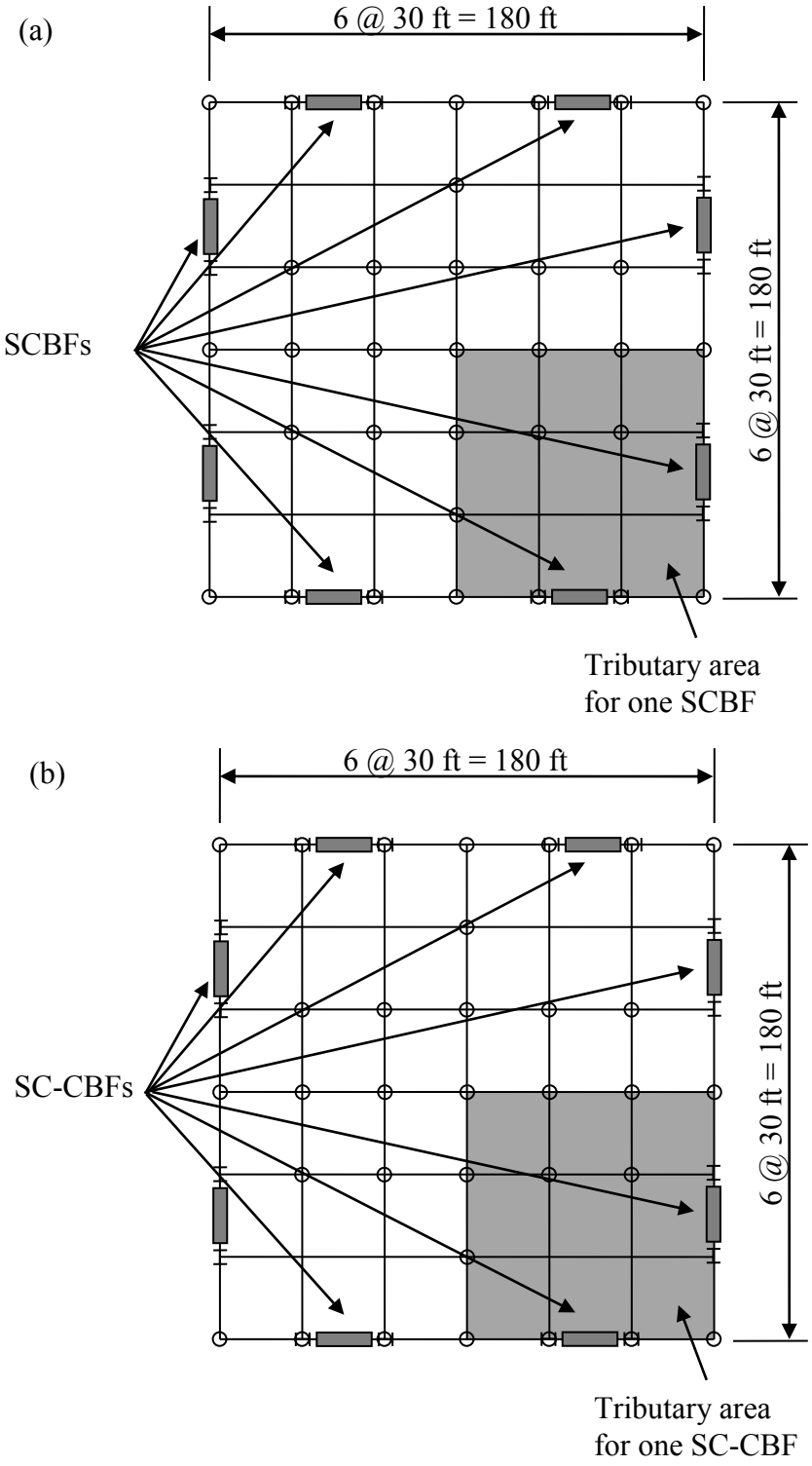

Figure 3.2 – Floor plan of building with (a) SCBFs, and (b) SC-CBFs

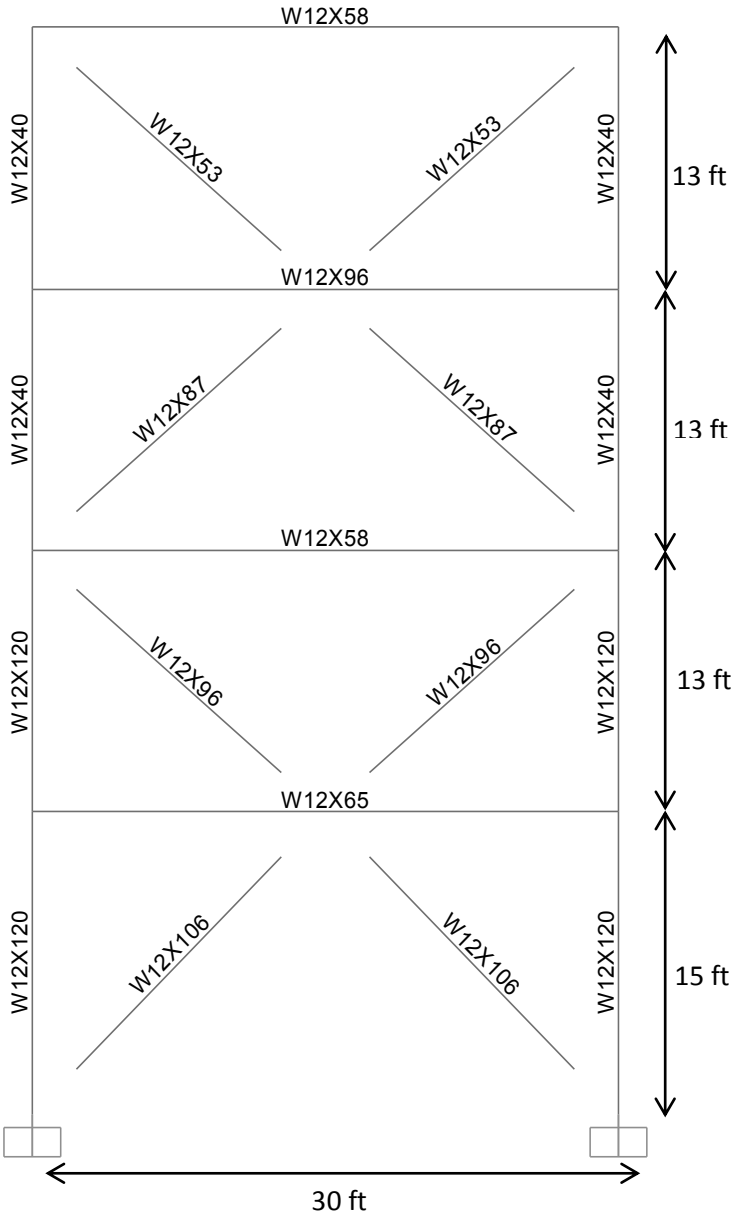

Figure 3.3 – 4SCBF with designed section sizes

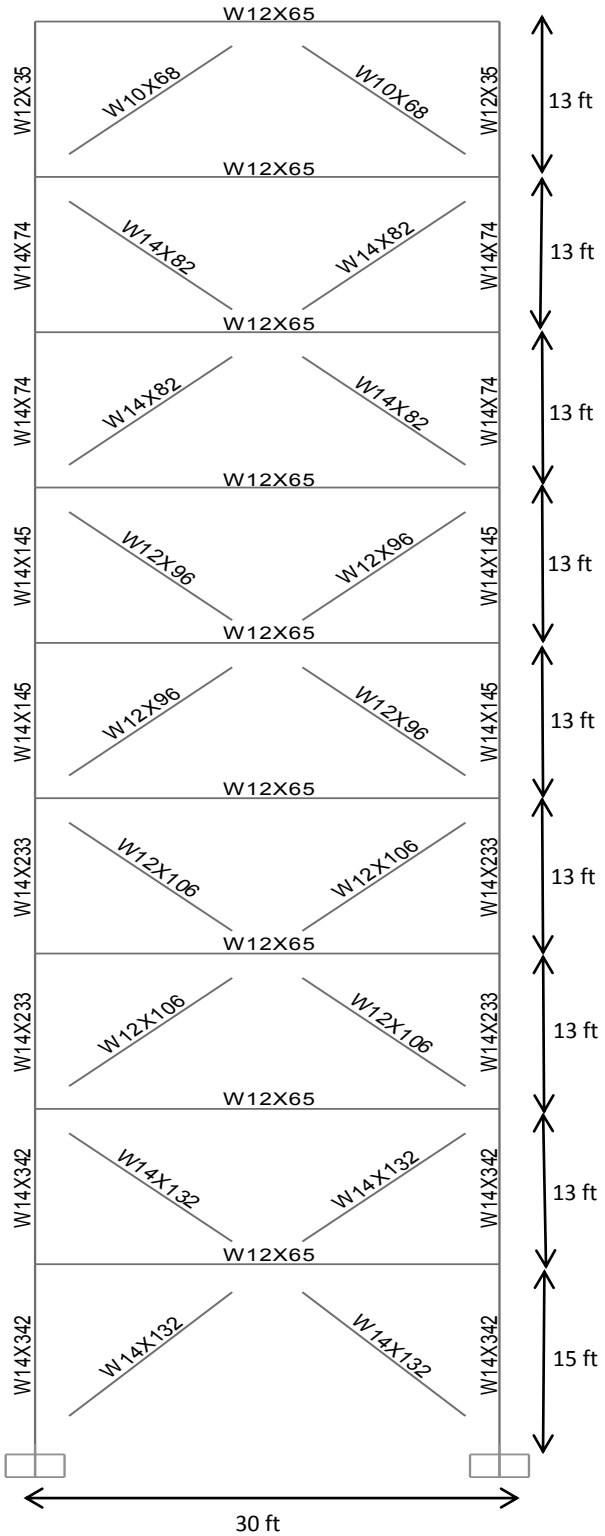

Figure 3.4 – 9SCBF with designed section sizes by ELF procedure

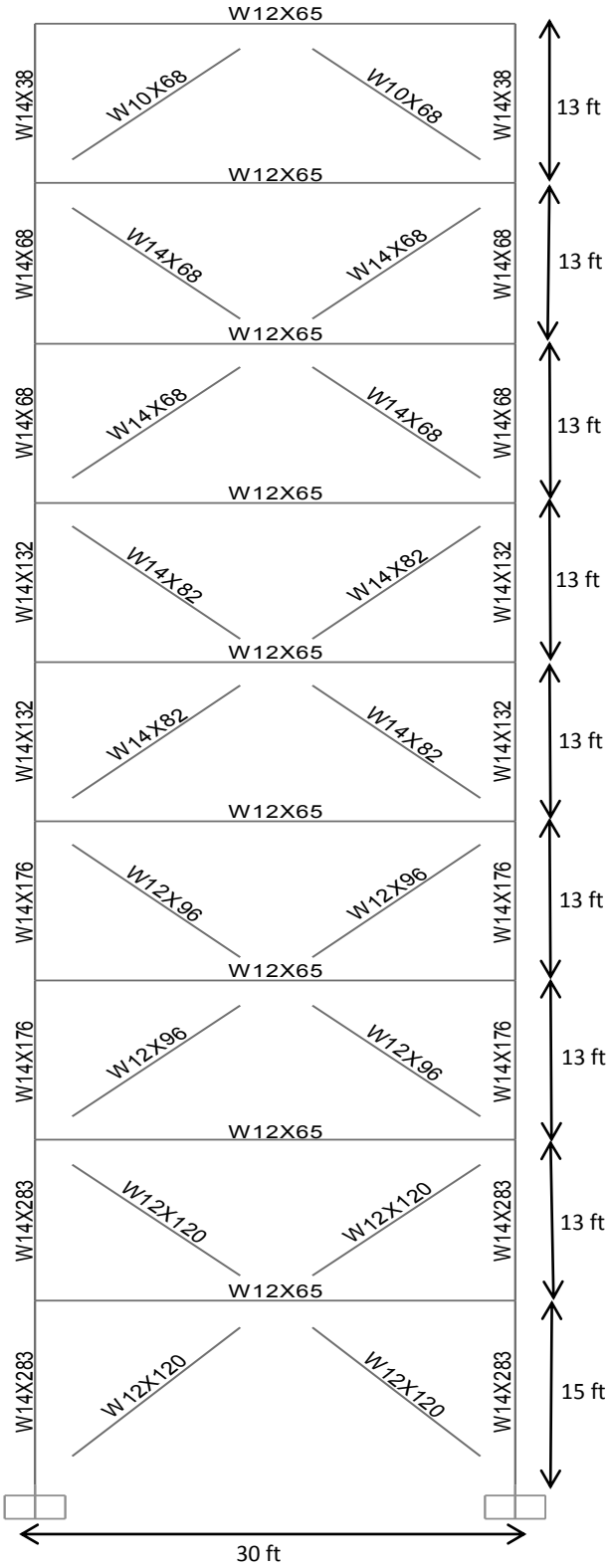

Figure 3.5 - 9SCBF with designed section sizes by RSA procedure

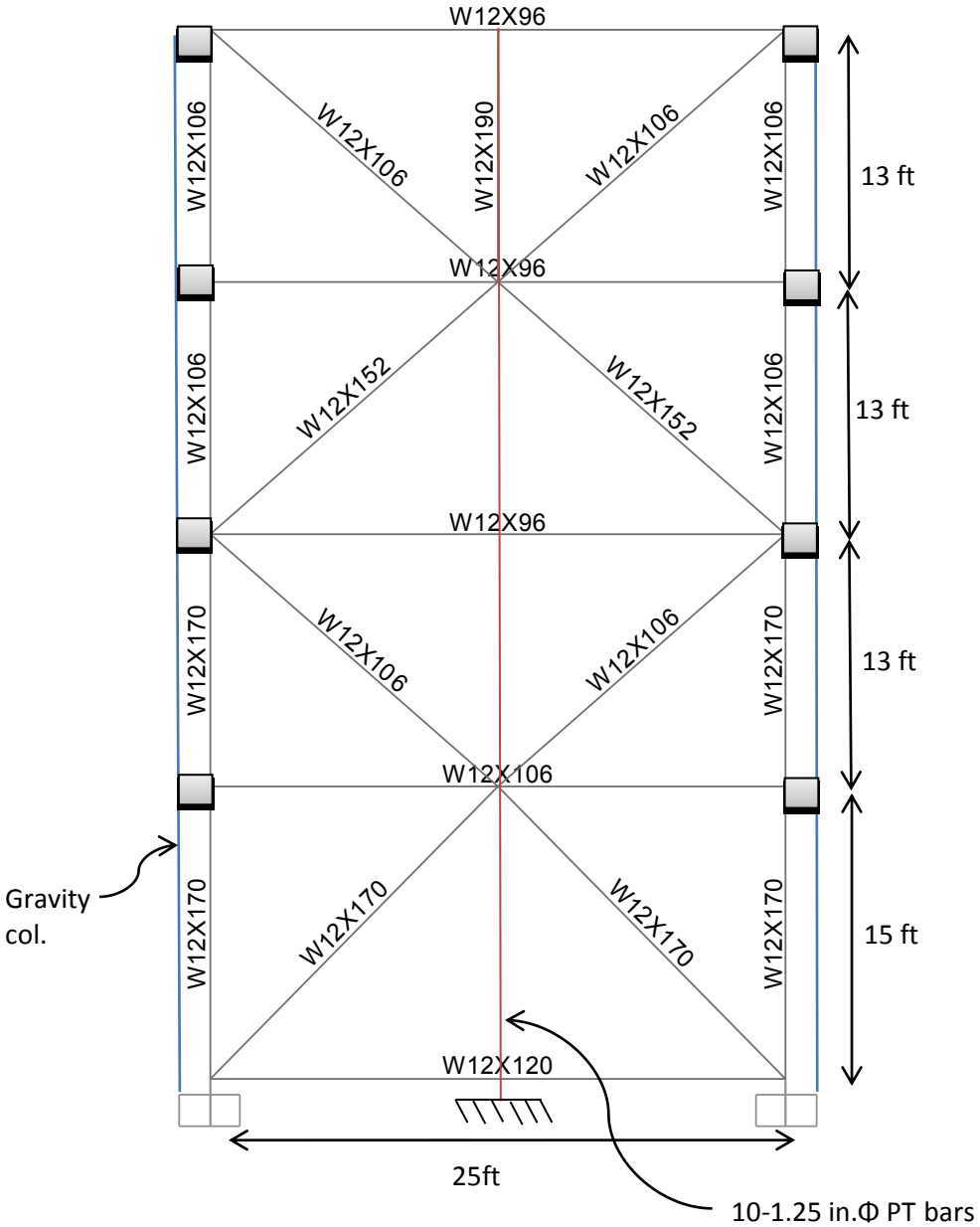

Figure 3.6 – Designed 4SC-CBF (Chancellor, 2013)

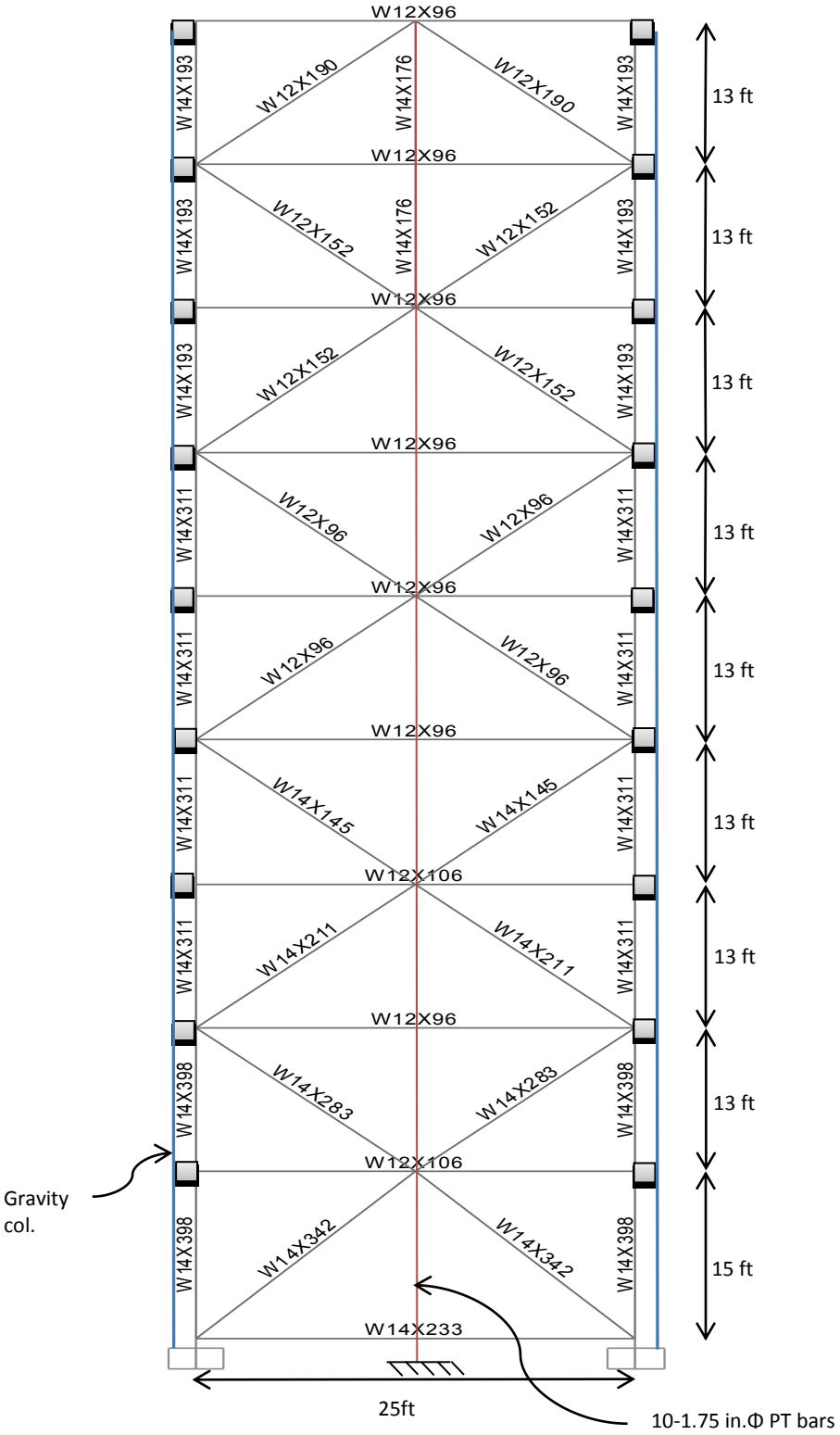

Figure 3.7 – Designed 9SC-CBF (Chancellor, 2013)

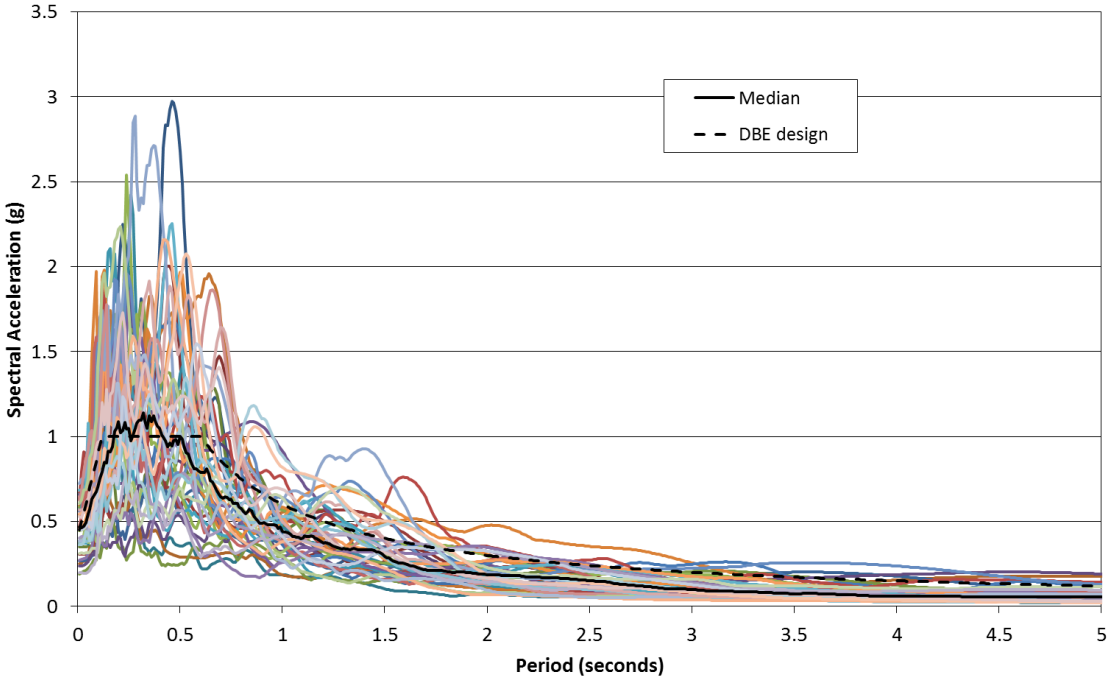

Figure 3.8 – Pseudo-acceleration response spectrum for ground motions in Far-Field record set scaled to DBE for 4-story buildings

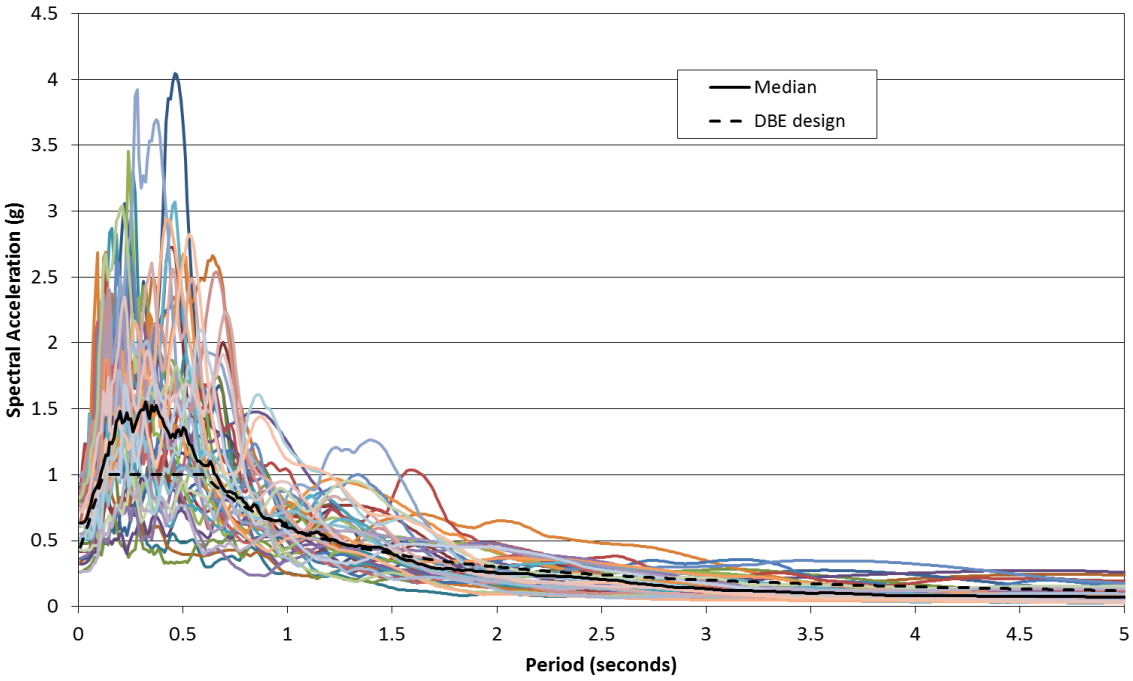

Figure 3.9 – Pseudo-acceleration response spectrum for ground motions in Far-Field record set scaled to DBE for 9-story buildings

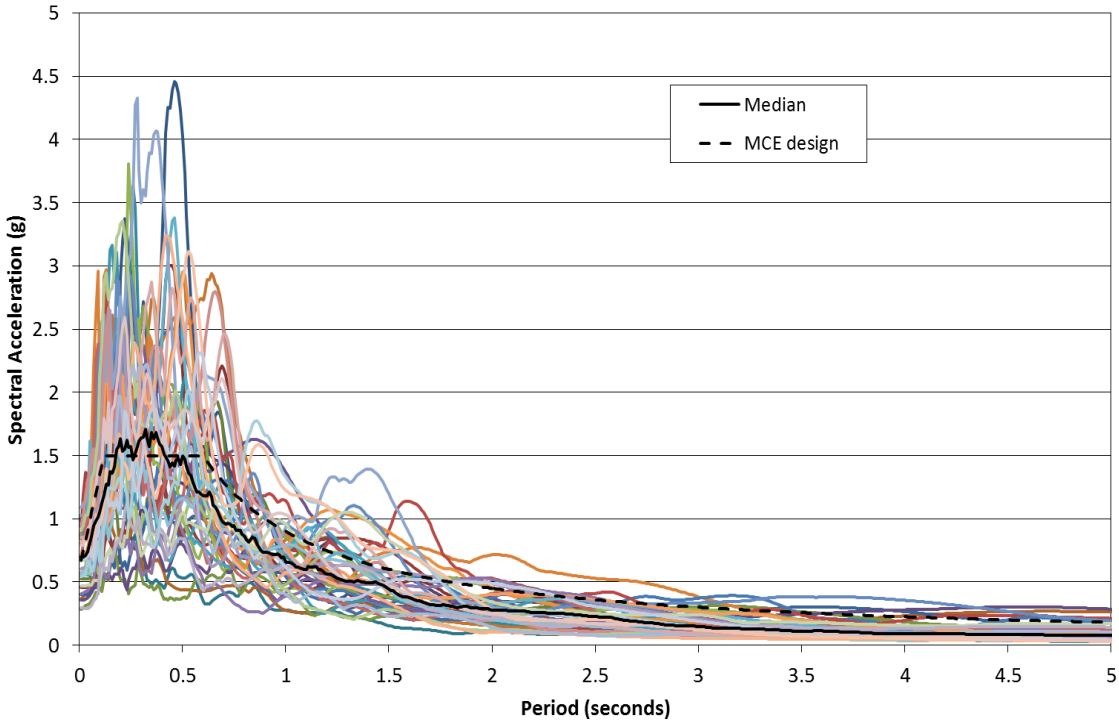

Figure 3.10 – Pseudo-acceleration response spectrum for ground motions in Far-Field record set scaled to MCE for 4-story buildings

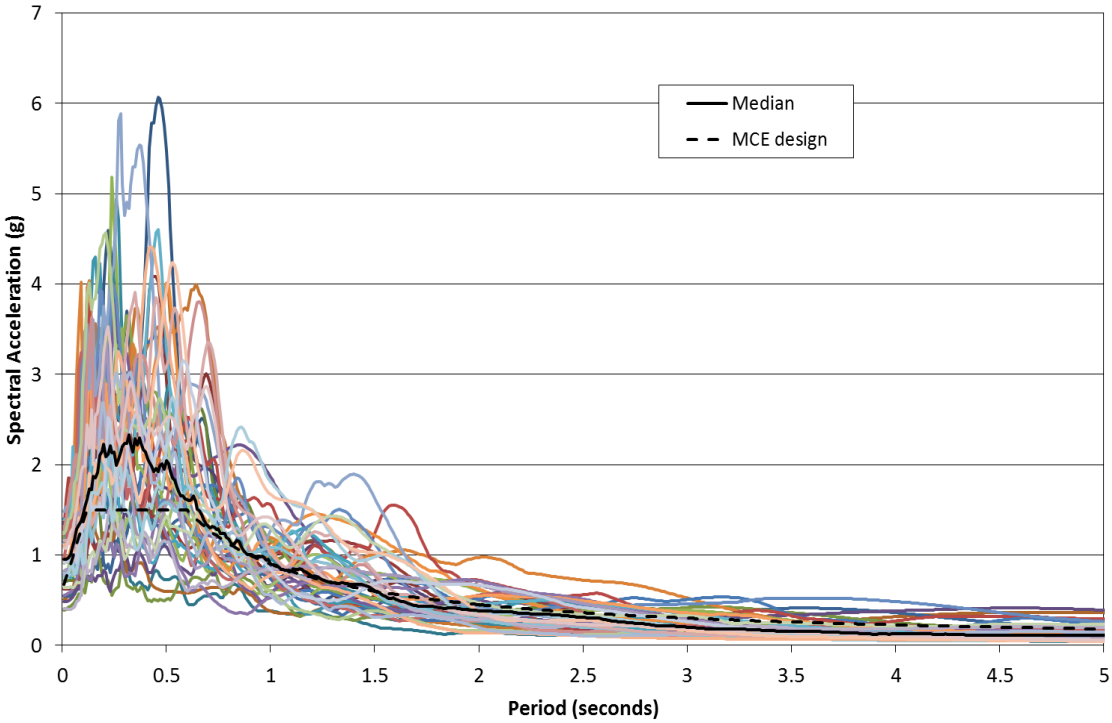

Figure 3.11 – Pseudo-acceleration response spectrum for ground motions in Far-Field record set scaled to MCE for 9-story buildings

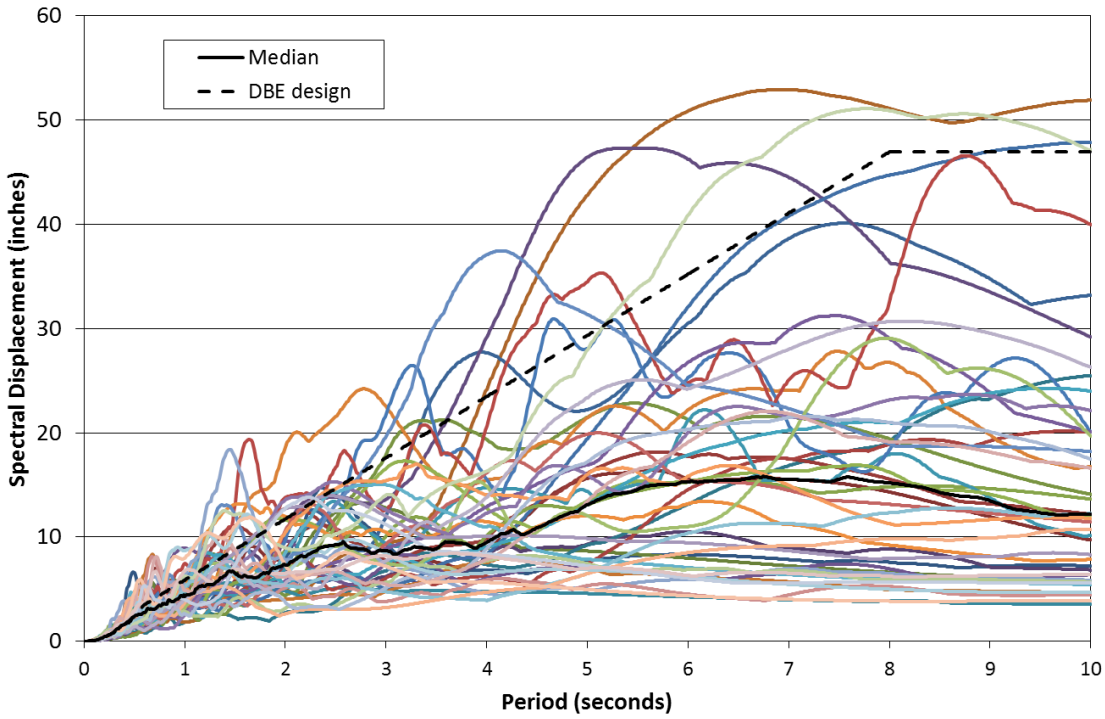

Figure 3.12 – Displacement response spectrum for ground motions in Far-Field record set scaled to DBE for 4-story buildings

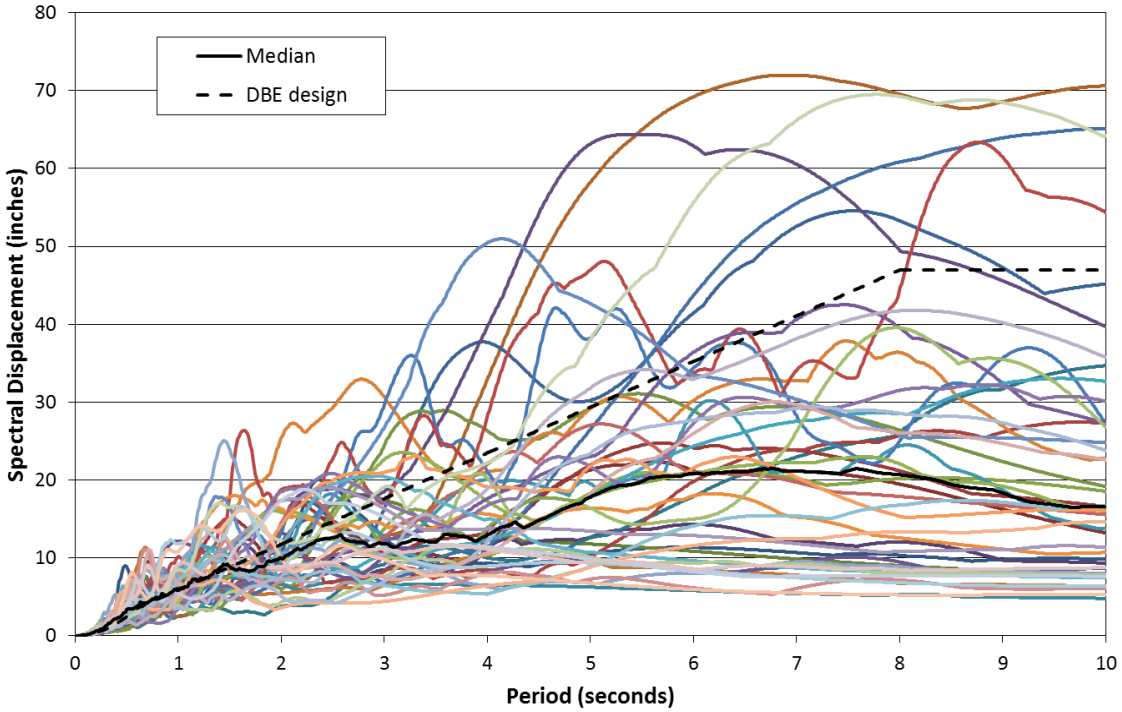

Figure 3.13 – Displacement response spectrum for ground motions in Far-Field record set scaled to DBE for 9-story buildings

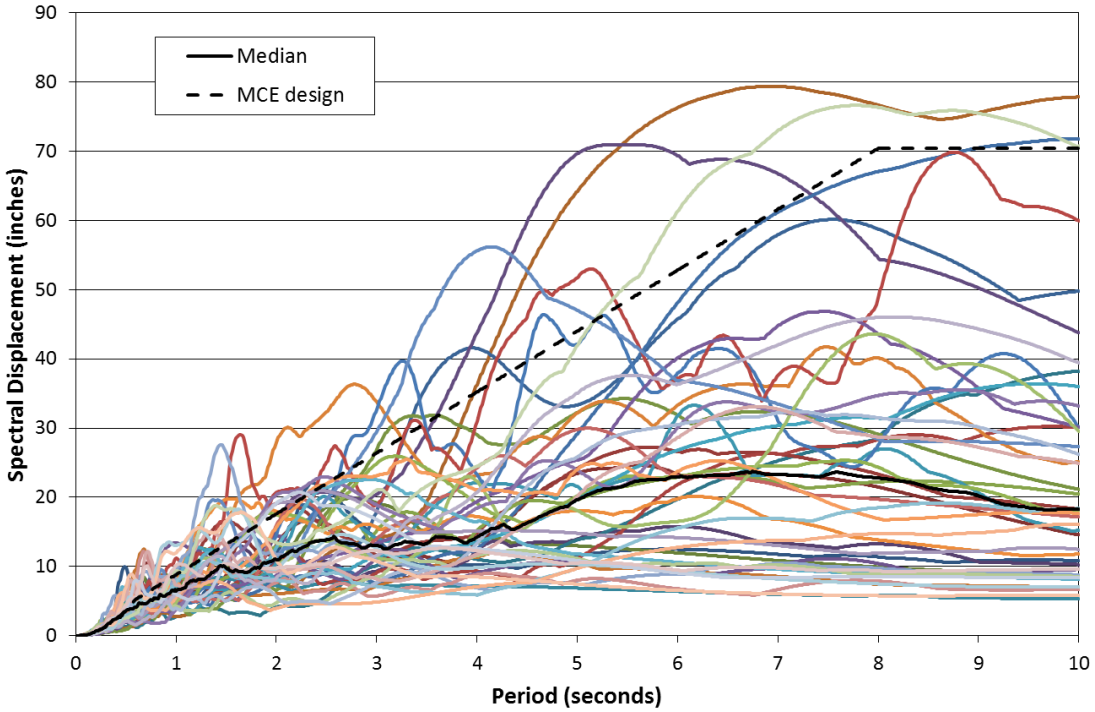

Figure 3.14 – Displacement response spectrum for ground motions in Far-Field record set scaled to MCE for 4-story buildings

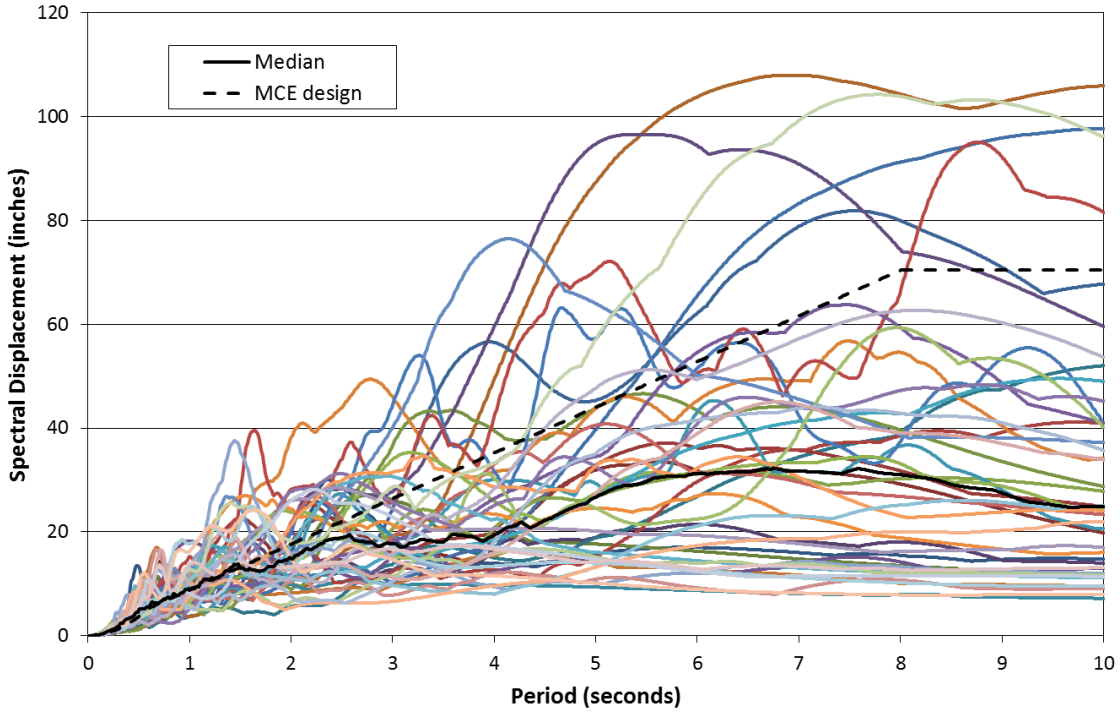

Figure 3.15 – Displacement response spectrum for ground motions in Far-Field record set scaled to MCE for 9-story buildings

CHAPTER 4

BUILDING DAMAGE ASSESSMENT

4.1 General

In performance based earthquake engineering (PBEE), "building losses" are estimated from a damage assessment. As mentioned in Chapter 2, Miranda (2010) stated that the total expected loss in a building is the summation of the losses associated with the building collapse case and the losses associated with the building non-collapse case. According to Miranda (2010), losses associated with the non-collapse case consist of the losses associated with the case when the damage is reparable, and the losses associated with the case when the damage is considered irreparable so that the building is demolished.

In this study, the damage assessment is similar in concept to that of Miranda (2010). Building damage is classified into two damage categories: damage corresponding to building collapse, i.e., a total building loss, and damage corresponding to building non-collapse. Damage associated with the non-collapse case are specified further and classified into two damage categories: reparable damage and irreparable damage. Irreparable damage corresponds to building demolition which leads to total building loss as in the collapse case.

The peak story drift (θ_m) is used as the structural engineering demand parameter (EDP) for the collapse assessment, and the peak residual story drift (θ_r) is used as the EDP for

the demolition assessment. Building damage is expressed in terms of probabilities, such as probability of collapse/non-collapse and probability of demolition/no demolition. In this chapter, the collapse/non-collapse and demolition/no demolition events are treated as independent events without any correlation. In Chapter 6, correlation between these events is considered.

The probabilities of collapse/non-collapse and demolition/no demolition described in Sections 4.2.2 and 4.3.2 are estimated using fragility functions. Development of the collapse/non-collapse and demolition/no demolition fragility functions is described in this chapter. A discussion of results is given for each damage case, illustrating the differences between the buildings used in this study. The buildings used in this study are the 4- and 9-story SCBF model buildings (referred to as 4SCBF and 9SCBF, respectively), and the 4- and 9-story SC-CBF model buildings (referred to as 4SC-CBF and 9SC-CBF, respectively) described in Chapter 3.

4.2 Building Collapse Assessment

A critical objective of the seismic design of buildings is protection against collapse. Local collapse or global collapse may occur as a result of earthquake loading. Local collapse, which is also known as vertical collapse, occurs when a vertical load carrying component fails, or when the shear transfer between horizontal and vertical components is lost. Global collapse occurs if most components in the system experience local collapse or if a single story displaces so extensively that P-delta effects overcome gravity load resistance

and dynamic instability occurs (Krawinkler et al., 2009). In this study, "collapse" refers to global collapse.

Collapse is triggered by large story drifts that result from P-delta effects and from deterioration in the strength and stiffness of the individual components. For this reason, the peak story drift (θ_m) is chosen as the EDP for building collapse.

To determine the values of the EDPs, nonlinear dynamic earthquake response analysis is needed. For this analysis, numerical models of the structures are created and subjected to selected earthquake ground motion records. The numerical models of the SCBFs and SC-CBFs used in this study are mentioned in Section 3.4.

Deterioration in the stiffness and strength of the components should be considered in a collapse assessment (Krawinkler et al., 2009). Therefore, the ability to represent stiffness and strength deterioration is an essential part of the model used in the nonlinear dynamic earthquake response analysis. In the numerical models used in this study, buckling of braces is modeled. The model accounts for deterioration of the braces in compression to some extent. Low-cycle fatigue and fracture of the braces is not considered in the models. This deterioration can be seen in results shown in Chapter 5. Beams and columns are modeled with fiber sections having a steel material model with the Bauschinger effect. No deterioration is included in the models for the beams and columns (Tahmasebi, 2014).

As mentioned in Chapter 3, the numerical models of the 4- and 9- story SCBFs and SC-CBFs are subjected to FEMA P695 Far-Field record set ground motions (FEMA, 2009) scaled to the DBE and MCE levels. According to FEMA P695, the Far-Field record set

can be used for the collapse evaluation of all Seismic Design Categories (FEMA, 2009). This record set includes ground motion records from large magnitude events. These large magnitude events are important for a building collapse assessment, because they dominate the collapse potential and have longer durations of shaking (FEMA, 2009). The ground motion records in the Far-Field record set are listed in Table 4.1 with the scale factors used for 4- and 9-story model buildings scaled to the DBE and MCE level intensities.

4.2.1 Development of Collapse – Non-Collapse Fragility Functions

There are two approaches to develop collapse fragility functions: One approach is the IM-based approach. In this approach, the collapse capacity of a structure subjected to a given ground motion is defined as the ground motion intensity, IM_c, at which the dynamic instability is observed. Incremental dynamic analysis (IDA) is performed to find IM_c. IM_c is often defined as the intensity at which a small increment of intensity causes a large increment in the lateral displacement (Krawinkler et al., 2009). IM_c values are obtained for a large number of ground motions and a statistical evaluation of IM_c is performed (Krawinkler et al., 2009). A probability distribution is fit to the IM_c values to develop the collapse fragility function.

The second approach is the EDP-based approach. In this approach, an EDP limit value, EDP_c, is used as the collapse indicator. EDP_c is defined to be the minimum value of the EDP corresponding to collapse. When the EDP value obtained from the dynamic analysis equals or exceeds EDP_c, the building is considered to be in the collapse condition (i.e.,

the collapse event has occurred). Both EDP and EDP_c are random variables. The probability of collapse when EDP equals a given value EDP_i is written as $P(C|EDP=EDP_i)$, where C represents the collapse event. This probability equals the probability that EDP_i equals or exceeds EDP_c, written as $P(EDP_i \geq EDP_c)$, which equals the probability that EDP_c is less than or equal to EDP_i, written as $P(EDP_c \leq EDP_i)$.

$P(EDP_c \leq EDP_i)$ is the cumulative probability distribution function for EDP_c, written as $CDF_{EDPc}(EDP_i)$. Therefore $P(C|EDP=EDP_i)=CDF_{EDPc}(EDP_i)$. In words, the probability of collapse when EDP has the given value EDP_i equals the CDF for EDP_c evaluated at EDP_i. More succinctly, $P(C|EDP) = CDF_{EDPc}(EDP)$, that is, the probability of collapse for a given value of EDP is estimated using the CDF for EDP_c, so the CDF for EDP_c is the collapse fragility function.

The peak story drift, θ_m, is selected as the EDP for collapse in this study. Figure 4.1(a), shows the CDF for the θ_m limit value, $\theta_{m,c}$. The CDF for $\theta_{m,c}$ in Figure 4.1(a) is assumed to follow a lognormal distribution and is defined by a median value, $\theta_{m,c,m}$, and the lognormal standard deviation, β_c. This CDF shown in Figure 4.1(a), has the following mathematical expression:

$$P(\theta_{m,c} \leq \theta_m) = \Phi\left(\frac{\ln(\theta_m) - \ln(\theta_{m,c,m})}{\beta_c}\right) \tag{4.1}$$

where,

$P(\theta_{m,c} \leq \theta_m)$ = the probability that $\theta_{m,c}$ is less than or equal to the given value of θ_m

$\theta_{m,c}$ = the θ_m limit value for collapse, which is the minimum value of θ_m corresponding to collapse

$\theta_{m,c,m}$ = the median value of $\theta_{m,c}$

β_c = the lognormal standard deviation of $\theta_{m,c}$

Φ = the standard normal cumulative distribution function

Figure 4.1(b) shows that the same function, the fragility function, expresses the probability of collapse for a given value of θ_m. The fragility function plotted in Figure 4.1(b) is given by the following mathematical expression:

$$P(C \mid \theta_m) = P(\theta_m \geq \theta_{m,c}) = \Phi\left(\frac{\ln(\theta_m) - \ln(\theta_{m,c,m})}{\beta_c}\right) \tag{4.2}$$

where,

$P(C| \theta_m)$ = the probability of collapse for a given θ_m

$P(\theta_m \geq \theta_{m,c})$ = the probability that θ_m exceeds $\theta_{m,c}$

θ_m = the peak story drift

$\theta_{m,c,m}$ = the median value of $\theta_{m,c}$

β_c = the lognormal standard deviation of $\theta_{m,c}$

Φ = the standard normal cumulative distribution function

In both Figures 4.1(a) and 4.1(b), $\theta_{m,c,m}$ is the median value of $\theta_{m,c}$. There is a 50% probability of collapse when θ_m is equal to $\theta_{m,c,m}$. As indicated in Figure 4.1(b), $P(C|\ \theta_m)$ increases with increasing θ_m and the complementary $P(NC|\ \theta_m)$ decreases with increasing θ_m, where NC represents the non-collapse event.

In this study, since the dynamic analyses are performed at only two ground motion intensity levels, namely the DBE and MCE, the collapse fragility curve is defined by using this EDP-based approach. Krawinkler et al. (2009) state that collapse is imminent at a story drift of less than 10%, even for frame structures having very ductile components. Therefore, $\theta_{m,c,m}$ is set equal to 0.10 or 10%. β_c is assumed to be 0.3 to account for the uncertainty in $\theta_{m,c}$.

Collapse and non-collapse are mutually exclusive events because the occurrence of collapse implies the non-occurrence of non-collapse. This relationship is illustrated in Figure 4.2 by a Venn diagram. The fragility function for the non-collapse case is obtained as follows:

$$P(NC \mid \theta_m) = 1 - P(C \mid \theta_m) \tag{4.3}$$

The collapse and non-collapse fragility functions used in this study are plotted in Figures 4.3 and 4.4.

4.2.2 Probability of Collapse and Probability of Non-Collapse

The collapse potential of a building is expressed as the probability of collapse. The probability of collapse for a given θ_m is found using Equation 4.2. The unconditional

probability of collapse for a given ground motion intensity level is estimated from the total probability theorem by convolving $P(C|\theta_m)$ with the probability density function for θ_m (for a given ground motion intensity level) as follows:

$$P(C) = \int_0^\infty P(C \mid \theta_m) \cdot f(\theta_m) \cdot d\theta_m \tag{4.4}$$

where,

P(C) = the probability of collapse

$P(C| \theta_m)$ = the probability of collapse for a given θ_m from the collapse fragility function (Equation 4.2)

$f(\theta_m)$ = the probability density function (PDF) for θ_m

The unconditional probability of non-collapse can be obtained in the same manner as follows:

$$P(NC) = 1 - P(C)$$
$$P(NC) = \int_0^\infty P(NC \mid \theta_m) \cdot f(\theta_m) \cdot d\theta_m = \int_0^\infty \left[1 - P(C \mid \theta_m)\right] \cdot f(\theta_m) \cdot d\theta_m \tag{4.5}$$

where,

P(NC) = the probability of non-collapse

$P(NC| \theta_m)$ = probability of non-collapse for a given θ_m from the non-collapse fragility function (Equation 4.3)

$f(\theta_m)$ = PDF for θ_m

The PDF for θ_m (for a given ground motion intensity level) in Equations 4.4 and 4.5 was obtained from dynamic analysis results for the model buildings. 44 different ground motion records were used in the dynamic analyses at each ground motion intensity level (i.e., at the DBE and MCE), so the PDF for θ_m (for a given ground motion intensity level) was estimated from 44 different θ_m values, one value of θ_m for each ground motion at the given intensity level. The lognormal PDF was used for θ_m since deformation-based EDPs such as θ_m have been shown to follow the lognormal distribution. The θ_m values for the 4- and 9-story model buildings under the DBE and MCE are given in Table 4.2 and Table 4.4; and the probability distribution parameters based on these θ_m data are given in Tables 4.3 and 4.5. Mean (μ), standard deviation (σ), lognormal mean (λ), and lognormal standard deviation (ζ) values of the θ_m data are given in these tables. The values given in these tables are rounded off to three significant decimal digits.

As it is seen from these tables, the mean peak story drifts of the 9-story model buildings are larger than the mean peak story drifts of the 4-story model buildings. Not much difference is observed in the mean peak story drifts between the SCBF and SC-CBF for both the 4- and 9-story model buildings. As expected, both systems have larger story drifts as the ground motion intensity level is increased from the DBE to MCE.

As shown in Table 4.4, the 9SC-CBF has a very large θ_m value (~80%) for ground motion-6 under the MCE. This is a very large value compared to the other 43 θ_m values and lies outside the overall pattern. For this reason, this θ_m value is treated as an outlier of

the θ_m data set for the 9-story SC-CBF under the MCE and is excluded from the probability distribution parameter (i.e., μ, σ, λ and λ) calculations.

Such a large peak story drift value is unexpected for an SC-CBF. The response of the 9SC-CBF under ground motion-6 scaled to the MCE was analyzed in detail to find the reason for this large θ_m value.

GM-6 is a ground motion from the Kocaeli, Turkey Earthquake in 1999 which had a magnitude of 7.5 (see Table 4.1). The pseudo-acceleration spectrum of GM-6 scaled to the MCE for the 9SC-CBF is plotted in Figure 4.5 together with the median spectrum for the ground motion set and the MCE design spectrum. The corresponding displacement spectra are plotted in Figure 4.6. From Figures 4.5 and 4.6, it is seen that after 3.5 seconds, both the spectral acceleration and spectral displacement of GM-6 increase rapidly with the period.

The initial fundamental period of the 9SC-CBF is around 1.3 seconds when both the columns are in contact with the foundation. During rocking, the effective period of the SC-CBF is lengthened with respect to the initial period (Roke et al., 2010). As a result of the period elongation, the acceleration demand is reduced (Seo, 2005), but larger non-linear displacements can be expected.

When GM-6 excites the rocking behavior of the 9SC-CBF, the system softens and the period elongates. In the long period region for GM-6, the spectral acceleration is increasing and the spectral displacement is increasing rapidly and this is the reason for the large peak story drifts. The rapid increase in the spectral displacement based on the

median and the design spectrum. For ground motions where the spectral acceleration decreases with increasing period, the period elongation can be beneficial in reducing the effect of the seismic excitation. However, as it is seen from Figure 4.5, the spectral acceleration of GM-6 increases with increasing period after a period of about 3.5 seconds.

P(C) and P(NC) values found using Equations 4.4 and 4.5 are given in Table 4.6 for the model buildings under the MCE and DBE. According to Table 4.6, the P(C) values are very small for all model buildings under both the DBE and MCE. Although the P(C) values are very small, there are some differences between the SCBF and SC-CBF model buildings, as well as between the 4-story and 9-story model buildings. As expected, the results in Table 4.6 show that P(C) increases with increasing ground motion intensity. The 9-story model buildings have a larger P(C) than the 4-story model buildings. Comparing the collapse performance of the SCBF and SC-CBF model buildings, it is seen that the 4SCBF has a larger P(C) than the 4SC-CBF under both the DBE and MCE. However, the 9SCBF has a lower P(C) than the 9SC-CBF both under the DBE and MCE.

When the statistical parameters of θ_m given in Tables 4.3 and 4.5 are compared for the model buildings, it is seen that μ and σ of θ_m are similar for the buildings with the same number of stories under both the DBE and MCE except one case. The one exception is between the 9SCBF and the 9SC-CBF under the MCE, where σ of θ_m for the 9SC-CBF is larger than σ of θ_m for the 9SCBF. The larger σ for the 9SC-CBF leads to the increased probability of collapse of the 9SC-CBF.

The values of the probabilities given in Table 4.6 are rounded off so that the sum of P(C) and P(NC) equals one, because the collapse and the non-collapse events are mutually exclusive.

4.3 Building Demolition Assessment

Post-earthquake inspections of buildings often observe significant residual drift. Past studies show that post-earthquake residual drift increases with increasing inelastic deformations during the earthquake (Ramirez and Miranda, 2009). Lateral force resisting systems designed to develop large inelastic deformations may have large residual deformations. These systems may perform well in terms of collapse prevention with a low P(C), but good earthquake performance may require more than collapse prevention. Buildings not collapsed by seismic excitations may have irreparable damage and large residual deformations. In such a situation, the most economical post-earthquake option may be to demolish the building. For this reason, residual deformations are considered to be important in determining the technical and economical reparability of building damage.

In this study, the peak residual story drift, θ_r, is used as the measure of the potential for post-earthquake building demolition.

4.3.1 Development of Demolition – No Demolition Fragility Functions

Demolition (D) and No Demolition (ND) fragility functions are developed using the EDP-based approach explained in Section 4.2.1.

The demolition fragility function is as follows:

$$P(D \mid \theta_r) = P(\theta_r \geq \theta_{r,d}) = \Phi\left(\frac{\ln(\theta_r) - \ln(\theta_{r,d,m})}{\beta_d}\right) \quad (4.6)$$

where,

$P(D| \theta_r)$ = the probability of demolition for a given θ_r

$P(\theta_r \geq \theta_{r,d})$ = the probability that θ_r exceeds $\theta_{r,d}$

θ_r = the peak residual story drift

$\theta_{r,d}$ = the θ_r limit value for demolition of the building, which is the minimum value of θ_r corresponding to demolition

$\theta_{r,d,m}$ = the median value of $\theta_{r,d}$

β_d = the lognormal standard deviation of $\theta_{r,d}$

Φ = the standard normal cumulative distribution function

Miranda (2010) states that residual drifts leading to demolition are in the range of 0.7 to 3%. Limited information is available for determining appropriate values for $\theta_{r,d}$. For this reason, the demolition fragility curve is adopted from the repair fragility given by ATC-58 (ATC, 2011) in this study. According to ATC-58 (ATC, 2011), the repair fragility function has a median $\theta_{r,d}$ value ($\theta_{r,d,m}$) of 1% and a dispersion (β_d) of 0.3. Furthermore, ATC-58 (ATC, 2011) uses a lognormal distribution for $\theta_{r,d}$, which is adopted for the present research.

D and ND are mutually exclusive events, since the building is either demolished or not. It can be said that demolition represents the irreparable damage case whereas no demolition represents the reparable damage case. This relationship is illustrated in Figure 4.7 using a Venn diagram. Considering this relationship between the D and ND events, the fragility curve for the no demolition case is as follows:

$$P(ND \mid \theta_r) = 1 - P(D \mid \theta_r) \tag{4.7}$$

The demolition and no demolition fragility functions used in the present study are plotted in Figures 4.8 and 4.9.

4.3.2 Probability of Demolition and Probability of No Demolition

The probability of demolition, P(D), and the probability of no demolition, P(ND), for a given θ_r are found using Equations 4.6 and 4.7. The unconditional probabilities of D and ND for a given ground motion intensity level are estimated as shown for P(C) and P(NC) in Section 4.2.2. P(D) and P(ND) are as follows, based on the total probability theorem:

$$P(D) = \int_0^\infty P(D \mid \theta_r) \cdot f(\theta_r) \cdot d\theta_r \tag{4.8}$$

$$\begin{aligned} P(ND) &= 1 - P(D) \\ P(ND) &= \int_0^\infty P(ND \mid \theta_r) \cdot f(\theta_r) \cdot d\theta_r = \int_0^\infty \left[1 - P(D \mid \theta_r)\right] \cdot f(\theta_r) \cdot d\theta_r \end{aligned} \tag{4.9}$$

where,

P(ND) = the probability of no demolition

$P(D)$ = the probability of demolition

$P(D|\theta_r)$ = the probability of demolition for a given θ_r (Equation 4.6)

$P(ND|\theta_r)$ = the probability of no demolition for a given θ_r (Equation 4.7)

$f(\theta_r)$ = the probability density function (PDF) for θ_r

The PDF for θ_r (for a given ground motion intensity level) in Equations 4.8 and 4.9 was obtained from dynamic analysis results for the model buildings. The PDF was estimated from 44 different θ_r values that were obtained for the 44 different ground motions at each ground motion intensity level. The lognormal PDF was used to represent this data. The peak residual story drifts for the 4- and 9-story model buildings under the DBE and MCE are given in Table 4.7 and Table 4.9; and the probability distribution parameters based on these θ_r data are listed in Tables 4.8 and 4.10. The values given in these tables are rounded off to three significant decimal digits.

Tables 4.7 and 4.9 show that both the 4- and 9-story SC-CBF model buildings have lower θ_r values than the SCBF model buildings. The 4SC-CBF has θ_r values very close to zero, with a mean in the range of 10^{-7}, so θ_r is treated as zero. This is an expected result, since the SC-CBF system with the controlled rocking action is able to concentrate structural damage into replaceable elements and eliminate residual drift (Roke et al., 2010).

Tables 4.7 and 4.9 show that the 9-story model buildings have larger θ_r than the 4-story model buildings for both systems. As expected, the buildings have larger θ_r under the MCE than the DBE.

Similar to θ_m, a very large θ_r value (~80%) is obtained for the 9SC-CBF under ground motion-6 at the MCE level. This value is treated as an outlier of the θ_r data set for the 9SC-CBF under MCE since it is much larger than the rest of the data. This value is excluded from the probability distribution parameter (i.e., μ, σ, λ and λ) calculations. The reasons for this unexpected θ_r under GM-6 are discussed in Section 4.2.2.

P(D) and P(ND) values are calculated using Equations 4.8 and 4.9. The results are given in Table 4.11 for all model buildings under the MCE and DBE. The values of probabilities given in Table 4.11 are rounded off so that the sum of P(D) and P(ND) equals one, because they are mutually exclusive. The results in Table 4.11 show that P(ND) is greater than P(D) for all model buildings. Both the 4- and 9-story SC-CBF model buildings have much lower P(D) than the 4- and 9-story SCBF model buildings, because the self-centering design greatly reduces the residual drift. For example, the 9SCBF model building has a 26% probability of demolition after the MCE, while the 9SC-CBF has a 8% probability of demolition after the MCE.

Table 4.1 – Far-Field ground motion record set scale factors (S.F.) for DBE and MCE

ID No.	Earthquake		DBE S.F.		MCE S.F.	
	M	Name	4-story	9-story	4-story	9-story
1-2	6.9	Kobe, Japan	1.319	1.795	1.978	2.692
3-4	6.9	Kobe, Japan	1.436	1.954	2.153	2.930
5-6	7.5	Kocaeli, Turkey	1.656	2.254	2.484	3.381
7-8	7.5	Kocaeli, Turkey	0.852	1.159	1.278	1.739
9-10	7.6	Chi-Chi, Taiwan	0.539	0.733	0.808	1.100
11-12	6.5	Friuli, Italy	1.880	2.559	2.820	3.838
13-14	7.6	Chi-Chi, Taiwan	1.212	1.649	1.817	2.473
15-16	7.1	Duzce, Turkey	0.790	1.074	1.184	1.612
17-18	7.4	Manji, Iran	1.076	1.465	1.614	2.197
19-20	6.5	Imperial Valley	1.584	2.155	2.376	3.233
21-22	6.5	Imperial Valley	1.227	1.669	1.840	2.504
23-24	7.1	Hector Mine	1.377	1.874	2.066	2.811
25-26	6.6	San Fernando	2.596	3.533	3.894	5.299
27-28	6.5	Superstition Hills	1.043	1.420	1.565	2.130
29-30	6.5	Superstition Hills	1.526	2.076	2.289	3.115
31-32	6.9	Loma Prieta	1.365	1.858	2.048	2.787
33-34	6.9	Loma Prieta	1.093	1.487	1.639	2.231
35-36	7.0	Cape Mendocino	0.983	1.337	1.474	2.006
37-38	7.3	Landers	1.360	1.851	2.040	2.776
39-40	7.3	Landers	1.277	1.738	1.916	2.607
41-42	6.7	Northridge	0.869	1.183	1.304	1.774
43-44	6.7	Northridge	1.087	1.480	1.631	2.220

Table 4.2 – Peak story drift (θ_m) of 4-story model buildings from dynamic analysis

	4SCBF		4SC-CBF	
GM	DBE	MCE	DBE	MCE
1	0.014	0.023	0.009	0.014
2	0.014	0.022	0.009	0.013
3	0.018	0.027	0.014	0.018
4	0.014	0.019	0.010	0.016
5	0.005	0.008	0.003	0.005
6	0.003	0.004	0.004	0.007
7	0.007	0.010	0.005	0.009
8	0.006	0.009	0.012	0.024
9	0.004	0.005	0.006	0.008
10	0.004	0.006	0.009	0.015
11	0.010	0.014	0.009	0.015
12	0.017	0.029	0.011	0.014
13	0.014	0.015	0.007	0.010
14	0.015	0.027	0.011	0.017
15	0.008	0.015	0.008	0.016
16	0.015	0.026	0.019	0.026
17	0.010	0.019	0.008	0.011
18	0.009	0.019	0.010	0.022
19	0.006	0.017	0.009	0.011
20	0.014	0.041	0.013	0.034
21	0.010	0.011	0.007	0.012
22	0.007	0.014	0.007	0.009
23	0.006	0.010	0.009	0.018
24	0.012	0.022	0.017	0.038
25	0.008	0.024	0.015	0.027
26	0.009	0.008	0.007	0.010
27	0.009	0.016	0.010	0.018
28	0.005	0.009	0.005	0.006
29	0.008	0.021	0.011	0.015
30	0.009	0.018	0.010	0.012
31	0.017	0.034	0.021	0.031
32	0.018	0.017	0.010	0.016
33	0.009	0.014	0.006	0.009
34	0.007	0.010	0.008	0.019
35	0.011	0.024	0.012	0.019

Table 4.2 – Peak story drift (θ_m) of 4-story model buildings from dynamic analysis (cont'd)

	4SCBF		4SC-CBF	
GM	DBE	MCE	DBE	MCE
36	0.017	0.013	0.007	0.012
37	0.009	0.014	0.007	0.009
38	0.021	0.027	0.014	0.024
39	0.007	0.028	0.014	0.023
40	0.005	0.006	0.006	0.016
41	0.012	0.036	0.020	0.023
42	0.016	0.035	0.020	0.028
43	0.011	0.022	0.010	0.019
44	0.018	0.026	0.011	0.014

Table 4.3 – Statistics for peak story drift (θ_m) of 4-story model buildings from dynamic analysis

	4SCBF		4SC-CBF	
	DBE	MCE	DBE	MCE
$\boldsymbol{\mu}$	0.011	0.019	0.010	0.017
$\boldsymbol{\sigma}$	0.005	0.009	0.004	0.008
$\boldsymbol{\lambda}$	-4.622	-4.091	-4.672	-4.191
$\boldsymbol{\zeta}$	0.412	0.459	0.408	0.433

Table 4.4 – Peak story drift (θ_m) of 9-story model buildings from dynamic analysis

	9SCBF		9SC-CBF	
GM	DBE	MCE	DBE	MCE
1	0.016	0.032	0.023	0.035
2	0.022	0.031	0.019	0.031
3	0.018	0.024	0.018	0.026
4	0.018	0.025	0.012	0.019
5	0.007	0.008	0.005	0.014
6	0.010	0.021	0.018	0.804*
7	0.012	0.033	0.027	0.059
8	0.032	0.022	0.013	0.021
9	0.008	0.014	0.019	0.037
10	0.012	0.023	0.043	0.076
11	0.014	0.017	0.010	0.018
12	0.023	0.025	0.010	0.020
13	0.018	0.023	0.009	0.020
14	0.022	0.028	0.015	0.023
15	0.015	0.015	0.015	0.022
16	0.020	0.029	0.009	0.015
17	0.012	0.016	0.017	0.023
18	0.021	0.019	0.017	0.028
19	0.022	0.034	0.026	0.028
20	0.034	0.044	0.026	0.042
21	0.020	0.034	0.019	0.026
22	0.017	0.021	0.011	0.021
23	0.018	0.020	0.010	0.011
24	0.018	0.025	0.014	0.020
25	0.028	0.049	0.037	0.052
26	0.015	0.023	0.011	0.022
27	0.022	0.025	0.012	0.016
28	0.028	0.030	0.018	0.024
29	0.017	0.023	0.021	0.036
30	0.016	0.025	0.019	0.038
31	0.019	0.017	0.019	0.021
32	0.019	0.020	0.010	0.019
33	0.019	0.021	0.006	0.011
34	0.021	0.035	0.019	0.025
35	0.019	0.023	0.009	0.013

* data considered to be outlier

Table 4.4– Peak story drift (θ_m) of 9-story model buildings from dynamic analysis (cont'd)

	9SCBF		9SC-CBF	
GM	DBE	MCE	DBE	MCE
36	0.017	0.023	0.015	0.026
37	0.014	0.021	0.007	0.011
38	0.030	0.023	0.013	0.028
39	0.034	0.051	0.024	0.054
40	0.017	0.016	0.007	0.028
41	0.024	0.028	0.012	0.023
42	0.022	0.031	0.013	0.021
43	0.019	0.031	0.014	0.025
44	0.022	0.028	0.010	0.023

Table 4.5 – Statistics for peak story drift (θ_m) of 9-story model buildings from dynamic analysis

	9SCBF		9SC-CBF	
	DBE	MCE	DBE	MCE
μ	0.019	0.026	0.016	0.026
σ	0.006	0.008	0.008	0.014
λ	-3.987	-3.714	-4.242	-3.766
ζ	0.308	0.322	0.458	0.493

Table 4.6 – Collapse and Non-Collapse Probabilities of model buildings

Frame	Hazard	P(C)	P(NC)
4SCBF	DBE	3.00E-06	9.99997E-01
	MCE	5.60E-04	9.9944E-01
4SC-CBF	DBE	1.50E-06	9.999985E-01
	MCE	1.70E-04	9.9983E-01
9SCBF	DBE	4.50E-05	9.99955E-01
	MCE	6.70E-04	9.9933E-01
9SC-CBF	DBE	2.00E-04	9.998E-01
	MCE	5.60E-03	9.944E-01

Table 4.7 – Peak residual story drift (θ_r) of 4-story model buildings from dynamic analysis

GM	4SCBF		4SC-CBF	
	DBE	MCE	DBE	MCE
1	6.972E-04	5.559E-03	8.734E-09	7.292E-06
2	1.060E-03	3.095E-03	4.485E-07	1.683E-06
3	2.887E-03	7.350E-03	4.851E-12	5.942E-11
4	1.223E-03	2.393E-03	6.356E-12	1.502E-11
5	1.965E-07	5.859E-04	1.328E-13	1.733E-13
6	1.371E-09	1.771E-06	6.646E-14	5.754E-13
7	2.633E-04	5.246E-04	1.877E-12	4.434E-07
8	1.523E-05	5.028E-04	1.932E-12	2.812E-08
9	1.703E-07	4.535E-04	2.949E-14	4.434E-07
10	6.954E-06	8.072E-04	2.935E-13	4.462E-07
11	2.890E-04	8.966E-04	9.204E-10	1.802E-06
12	1.422E-03	7.099E-03	3.269E-07	4.631E-06
13	1.475E-03	1.581E-03	7.757E-10	3.675E-08
14	2.504E-03	8.384E-03	3.294E-07	2.962E-10
15	3.416E-04	3.067E-03	1.851E-09	4.900E-10
16	2.133E-03	7.377E-03	1.957E-11	2.279E-06
17	9.101E-04	2.797E-03	5.791E-10	3.269E-08
18	2.235E-04	2.634E-03	4.432E-07	3.719E-07
19	2.040E-04	7.078E-04	6.735E-11	4.089E-10
20	6.639E-04	1.825E-03	6.135E-11	5.180E-03
21	2.956E-04	5.503E-04	3.813E-07	3.717E-06
22	7.824E-04	1.400E-03	2.093E-10	3.761E-07
23	5.389E-04	5.725E-04	1.538E-11	7.989E-10
24	1.019E-03	5.405E-03	3.308E-12	4.513E-11
25	6.653E-04	2.977E-03	1.072E-07	5.894E-06
26	4.501E-04	1.398E-03	6.425E-11	3.381E-09
27	6.872E-04	2.880E-03	3.066E-11	1.628E-10
28	3.752E-06	6.875E-04	1.928E-12	3.294E-07
29	2.736E-04	2.493E-03	4.730E-07	2.670E-07
30	4.386E-04	3.063E-03	4.394E-07	4.432E-07
31	1.468E-03	5.050E-03	3.232E-07	8.301E-06
32	1.066E-03	8.861E-04	6.963E-12	5.711E-07
33	2.931E-04	4.933E-04	4.484E-07	6.605E-07
34	4.390E-04	2.071E-04	3.322E-11	4.561E-07
35	1.350E-03	6.265E-03	5.184E-10	3.245E-07

Table 4.7 – Peak residual story drift (θ_r) of 4-story model buildings from dynamic analysis (cont'd)

	4SCBF		4SC-CBF	
GM	DBE	MCE	DBE	MCE
36	1.129E-03	2.311E-03	9.911E-09	6.070E-07
37	4.447E-04	2.053E-03	4.428E-07	4.598E-07
38	3.478E-03	3.668E-03	3.943E-07	2.523E-05
39	8.926E-04	9.997E-03	4.343E-13	3.416E-10
40	2.615E-06	4.536E-04	5.816E-13	6.214E-10
41	5.002E-04	3.704E-03	2.347E-12	1.052E-08
42	1.693E-03	6.949E-03	7.721E-11	1.806E-09
43	9.374E-04	6.025E-03	4.434E-07	5.209E-07
44	1.545E-03	3.108E-03	4.360E-07	4.179E-06

Table 4.8 – Statistics for residual peak story drift (θ_r) of 4-story model buildings from dynamic analysis

	4SCBF		4SC-CBF	
	DBE	MCE	DBE	MCE
$\boldsymbol{\mu}$	8.344E-04	2.960E-03	1.241E-07	1.194E-04
$\boldsymbol{\sigma}$	7.925E-04	2.583E-03	1.900E-07	7.806E-04
$\boldsymbol{\lambda}$	-7.410	-6.106	-16.506	-10.923
$\boldsymbol{\zeta}$	0.802	0.752	1.099	1.944

Table 4.9 – Peak residual story drift (θ_r) of 9-story model buildings from dynamic analysis

GM	9SCBF		9SC-CBF	
	DBE	MCE	DBE	MCE
1	2.908E-03	2.433E-02	1.361E-03	2.743E-03
2	2.251E-03	8.991E-03	1.495E-03	3.369E-03
3	2.078E-03	1.796E-03	8.360E-07	1.988E-03
4	1.052E-03	3.412E-03	1.805E-05	8.943E-04
5	1.836E-06	4.034E-04	4.857E-07	6.284E-10
6	6.559E-04	2.674E-03	4.857E-07	8.036E-01*
7	8.210E-04	1.407E-02	4.758E-04	1.132E-02
8	9.247E-03	9.547E-03	5.405E-04	4.793E-04
9	4.119E-04	1.276E-03	4.857E-07	3.894E-07
10	9.523E-04	3.158E-03	4.321E-07	5.916E-02
11	1.875E-03	3.597E-03	1.495E-03	4.536E-03
12	2.866E-03	5.096E-03	1.742E-03	8.452E-04
13	1.183E-03	3.215E-03	3.897E-04	3.886E-03
14	1.755E-03	4.800E-03	1.158E-03	5.001E-03
15	3.209E-03	1.445E-02	1.189E-03	5.551E-03
16	1.001E-03	1.797E-03	4.796E-04	1.402E-03
17	8.692E-04	1.707E-03	9.342E-04	1.621E-03
18	6.936E-03	1.876E-02	1.104E-03	1.234E-03
19	4.942E-03	1.723E-02	3.082E-04	5.940E-04
20	1.261E-03	2.985E-02	7.405E-04	7.795E-04
21	1.125E-02	2.078E-02	5.375E-06	9.305E-04
22	1.240E-03	6.589E-03	6.599E-04	1.377E-03
23	8.977E-04	2.869E-03	3.029E-05	4.928E-07
24	5.200E-03	2.111E-03	6.947E-04	1.593E-03
25	5.765E-03	1.521E-02	1.450E-03	1.793E-03
26	1.218E-03	6.970E-03	4.501E-04	4.065E-04
27	5.970E-03	5.691E-03	1.512E-07	1.799E-03
28	2.634E-03	8.439E-03	5.929E-04	5.050E-04
29	1.514E-03	1.152E-02	6.482E-04	1.019E-02
30	1.657E-03	9.900E-03	5.960E-04	4.181E-03
31	2.742E-03	1.291E-02	5.164E-04	1.943E-03
32	1.361E-03	7.383E-03	9.028E-04	1.619E-03
33	1.485E-03	1.836E-03	6.413E-04	9.966E-04
34	4.215E-03	8.892E-03	1.789E-09	1.198E-03
35	2.006E-03	4.849E-03	4.735E-07	1.835E-05

* data considered to be outlier

Table 4.9 – Peak residual story drift (θ_r) of 9-story model buildings from dynamic analysis (cont'd)

GM	9SCBF		9SC-CBF	
	DBE	MCE	DBE	MCE
36	4.534E-03	8.699E-03	1.811E-03	4.794E-03
37	9.292E-04	2.318E-03	2.828E-05	6.367E-04
38	3.949E-03	6.002E-03	6.771E-04	4.460E-03
39	1.010E-02	6.874E-03	6.328E-04	6.671E-05
40	1.195E-03	1.005E-03	6.723E-09	3.572E-05
41	2.454E-03	1.385E-03	4.468E-07	1.098E-03
42	1.948E-03	3.011E-03	1.684E-04	9.849E-04
43	4.315E-03	1.106E-02	5.113E-04	3.571E-04
44	2.182E-03	5.971E-03	9.688E-04	2.946E-03

Table 4.10 – Statistics for residual peak story drift (θ_r) of 9-story model buildings from dynamic analysis

	9SCBF		9SC-CBF	
	DBE	MCE	DBE	MCE
$\boldsymbol{\mu}$	0.003	0.008	0.001	0.003
$\boldsymbol{\sigma}$	0.003	0.007	0.001	0.009
$\boldsymbol{\lambda}$	-6.142	-5.132	-7.765	-6.688
$\boldsymbol{\zeta}$	0.767	0.743	0.786	1.432

Table 4.11 – Demolition and No Demolition Probabilities of model buildings

Frame	Hazard	P(D)	P(ND)
4SCBF	DBE	5.38E-04	9.99462E-01
	MCE	3.23E-02	9.677E-01
4SC-CBF	DBE	0.000	1.000
	MCE	6.65E-04	9.9934E-01
9SCBF	DBE	3.14E-02	9.686E-01
	MCE	2.57E-01	7.43E-01
9SC-CBF	DBE	8.84E-05	9.99E-01
	MCE	7.78E-02	9.22E-01

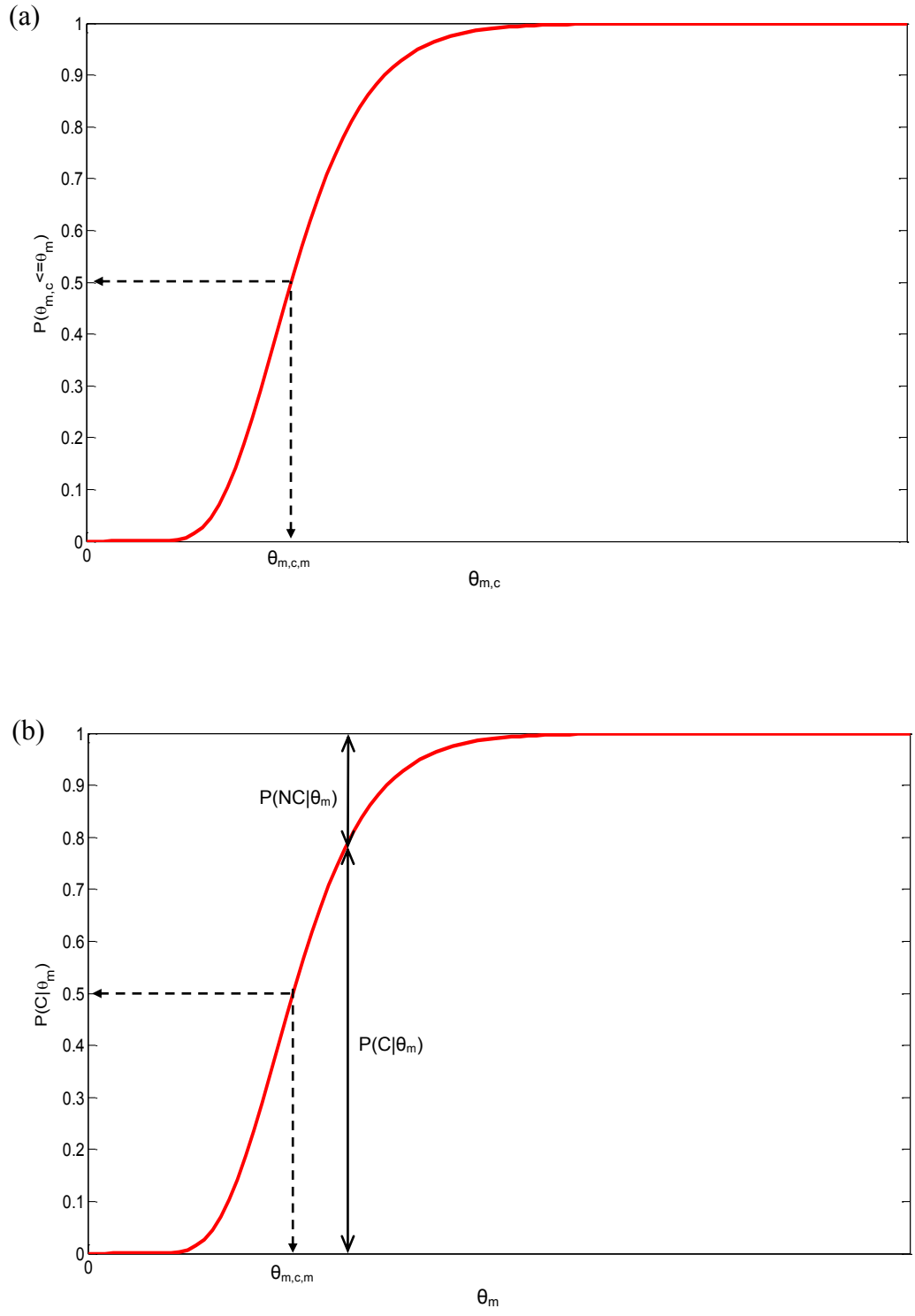

Figure 4.1 – (a) CDF for $\theta_{m,c}$, (b) collapse fragility function $P(C|\theta_m)$

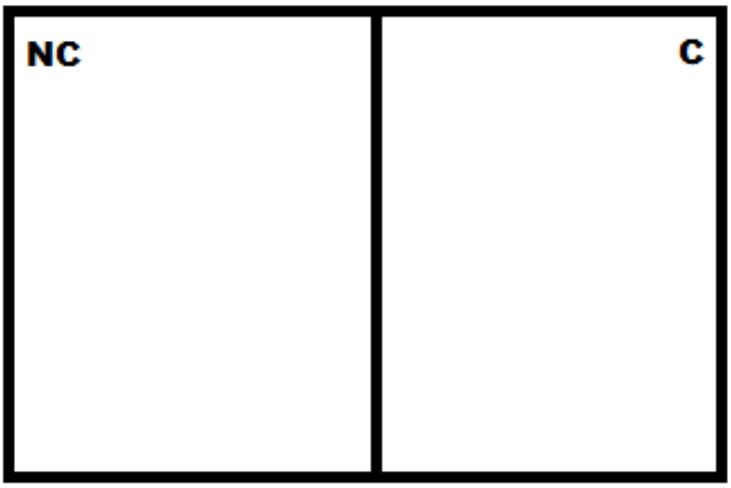

Figure 4.2 – Venn diagram illustration of C and NC events

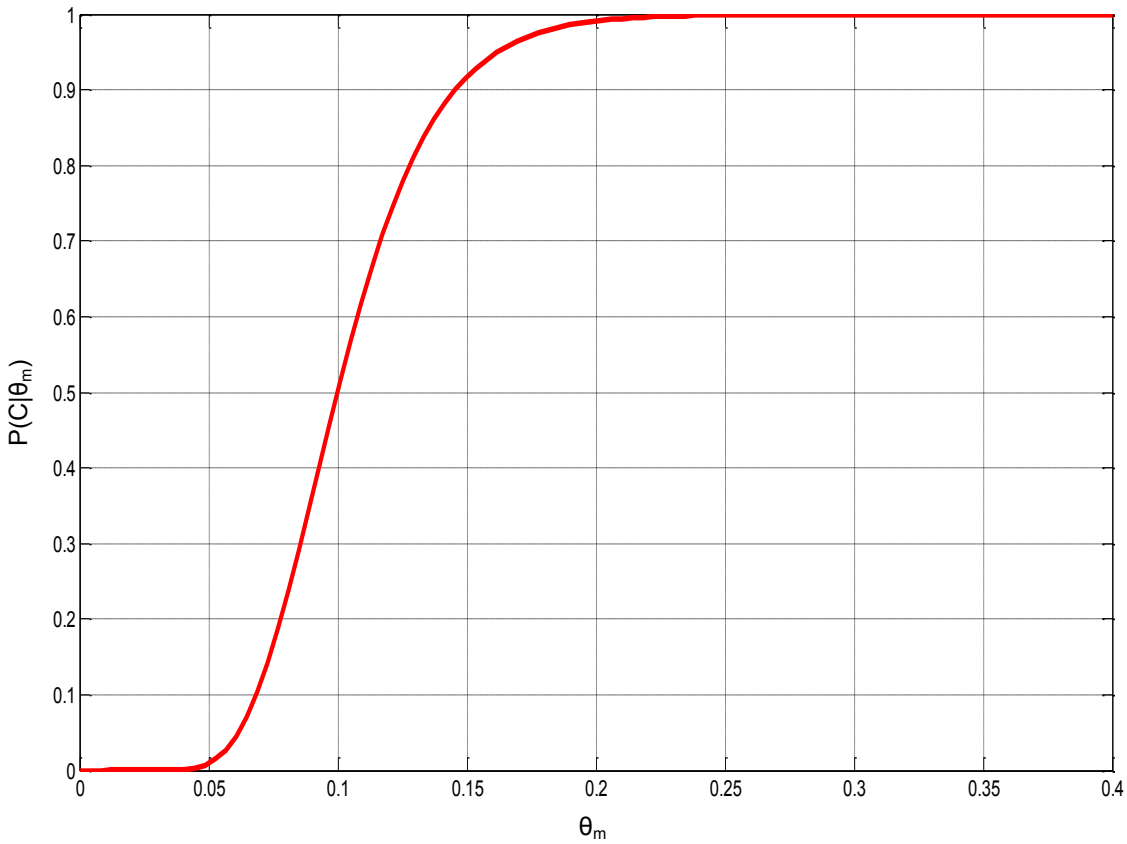

Figure 4.3 – Collapse fragility function

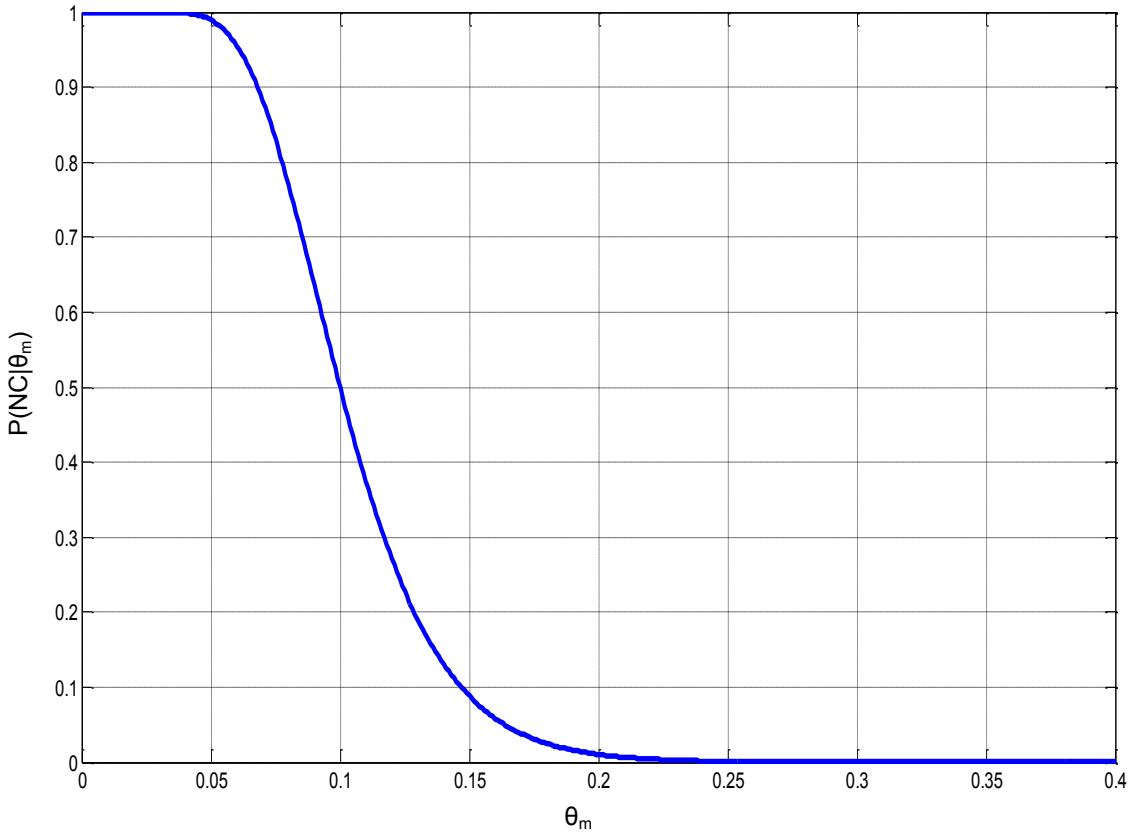

Figure 4.4 – Non-Collapse fragility function

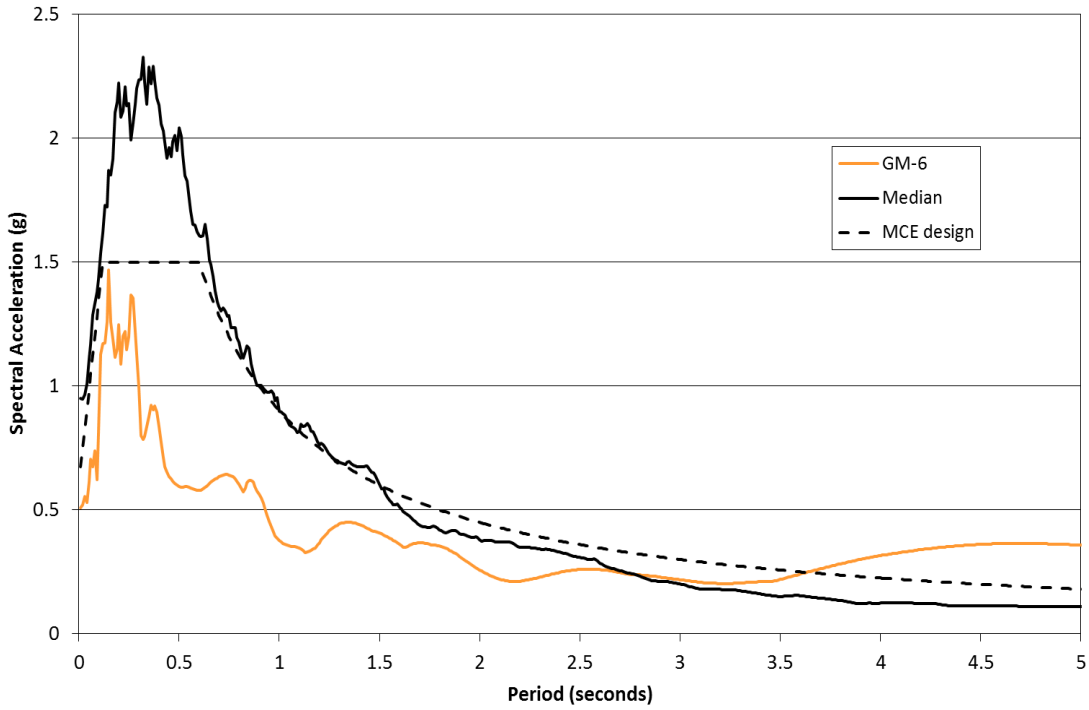

Figure 4.5 – Pseudo-acceleration response spectrum for ground motion-6 in Far-Field record set scaled to MCE for 9-story SC-CBF

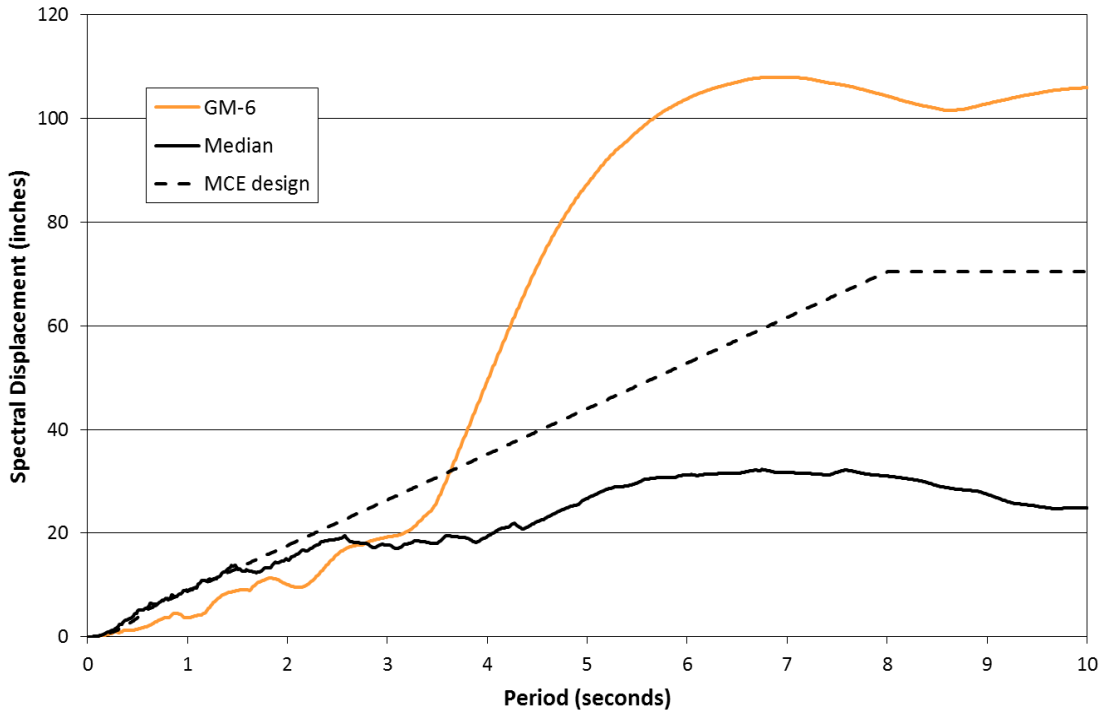

Figure 4.6 – Displacement response spectrum for ground motion-6 in Far-Field record set scaled to MCE for 9-story SC-CBF

Figure 4.7 – Venn diagram illustration of D and ND events

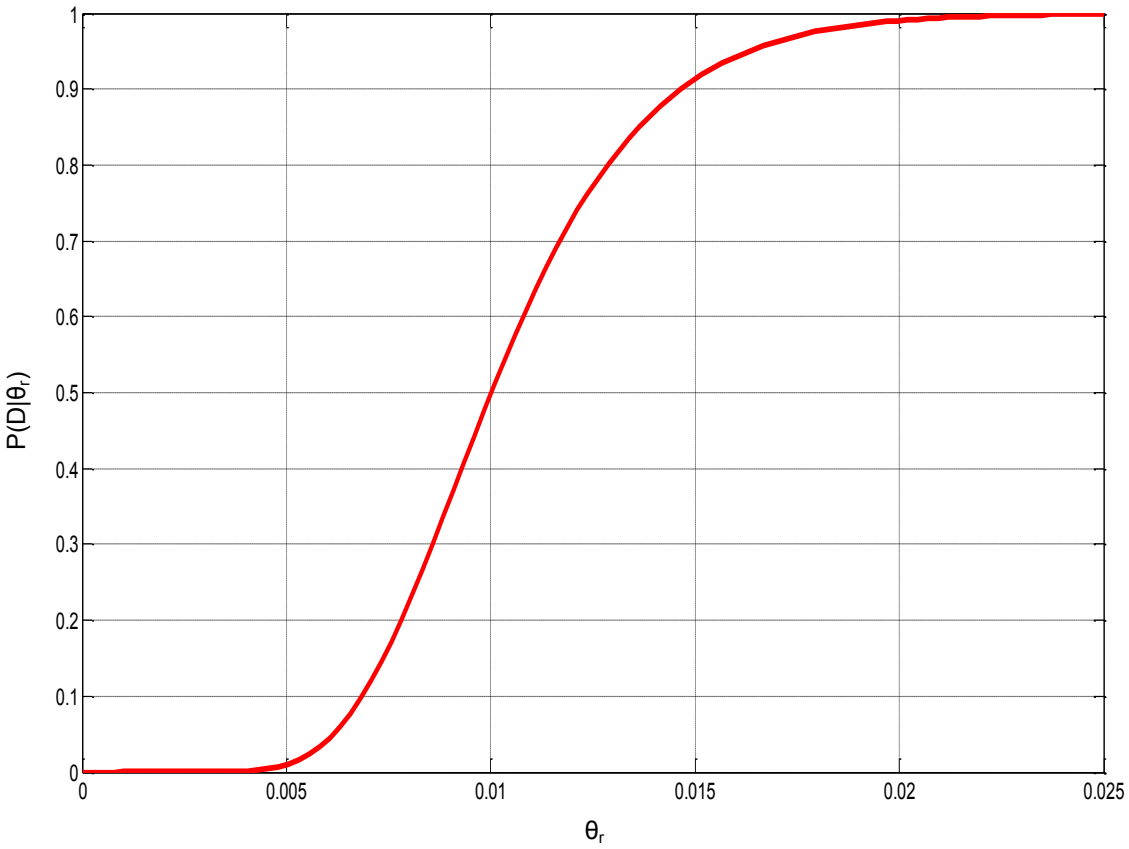

Figure 4.8 –Demolition fragility function

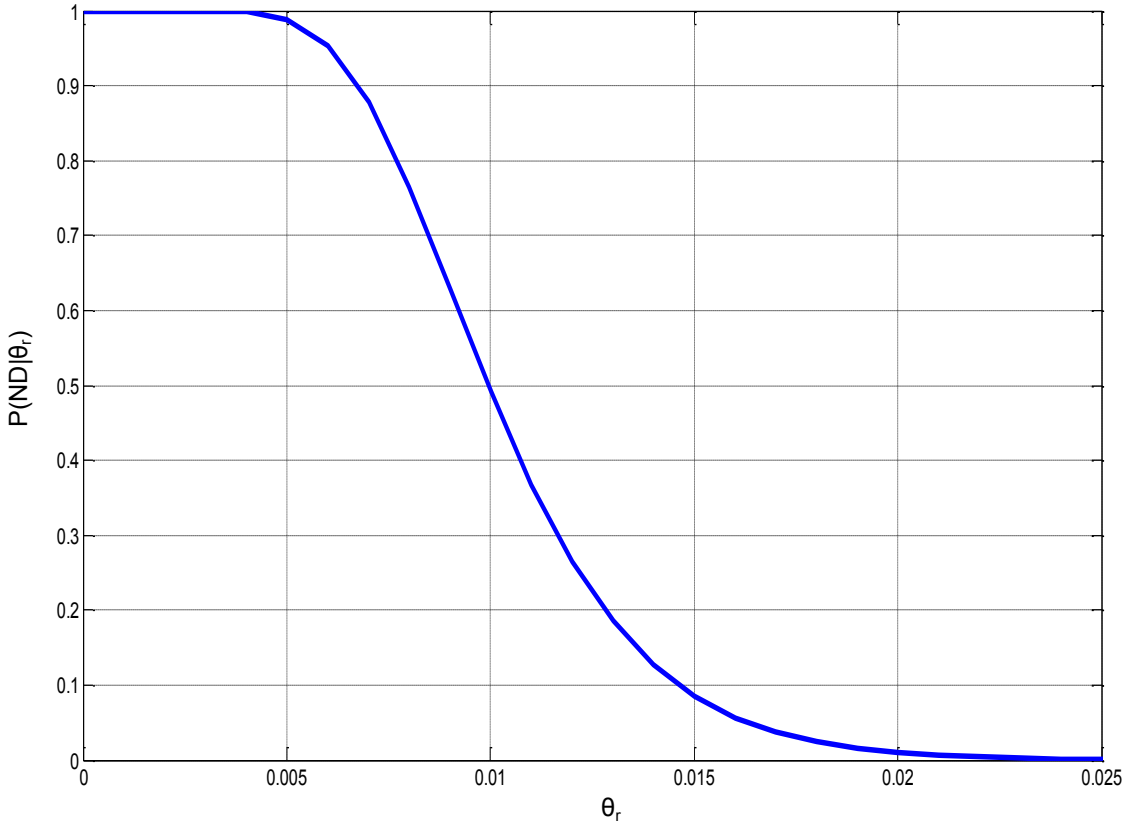

Figure 4.9 – No Demolition fragility function

CHAPTER 5

DAMAGE ASSESSMENT OF DIAGONAL BRACES

5.1 General

SCBFs act as vertical trusses, transferring the lateral forces through the diagonal braces, beams, and columns. The braces are the main components in SCBFs that resist story shear due to lateral forces. The resistance of SCBFs to seismic loading is based on the capacity of braces to resist the story shear and to undergo inelastic deformations in compression and in tension. Buckling of the braces in compression and yielding of the braces in tension leads to residual lateral drift after an earthquake. For this reason, the damage of the braces is a significant aspect of the performance of an SCBF.

In the elastic range, SC-CBFs deform similarly to SCBFs. However, the rocking action of the SC-CBF and yielding of the PT bars limit the internal forces that can develop in the members of an SC-CBF (Chancellor et al., 2012). The seismic performance of an SC-CBF depends mainly on the rocking behavior and the PT bars. When lateral forces acting on an SC-CBF are large enough to decompress one column, the column base lifts up from the foundation. At this point, the lateral stiffness of the system is reduced and the lateral stiffness is mainly controlled by the properties of the PT bars. As the lateral drift continues to increase, the lateral stiffness reduces further as a result of PT bar yielding. Yielding of the PT bars is the first indication of plastic system behavior. With increasing lateral drift, the frame members may begin to yield as well. Eventually, the frame

members may fail (Chancellor, 2013). According to the performance-based seismic design procedure for SC-CBFs, yielding of the PT bars is limited under the DBE but is permitted under the MCE (Roke et al., 2010). Frame members are designed using capacity design principles to remain essentially elastic under the DBE. Some member yielding is permitted under the MCE. Braces in SC-CBFs are not expected to undergo large inelastic deformations.

In this study, damage to brace members is estimated as a function of an EDP using fragility functions; the probability of being in or beyond a given damage state is captured by a fragility function. Residual out-of-plane (OOP) displacement at the location of the mid-length of the brace, normalized by the brace length, Δ_{or}, is the EDP selected for estimating the brace damage. This EDP is used because it can be easily observed and measured in a post-earthquake inspection.

This chapter summarizes the development of the fragility functions that permit damage in the braces to be estimated. Estimates of damage to braces in the model buildings under the DBE and MCE are made.

5.2 Inelastic Seismic Behavior of Braces

Elastic design of SCBFs is uneconomical and SCBFs are designed to sustain inelastic deformations (Lumpkin, 2009). The design of an SCBF requires that beams and columns in the system should remain undamaged under the DBE to protect the gravity load carrying capability of the SCBF system while the braces yield in tension and buckle in compression. For this reason, the beams and columns in an SCBF are designed to resist

gravity loads together with the maximum anticipated brace forces. The braces are designed to meet the compressive strength requirements as well as code specified slenderness and width-to-thickness ratio limits. It should be noted that the tensile capacity of a brace is typically greater than its compressive capacity, which is controlled by buckling.

A typical brace response under cyclic loading is shown in Figure 5.1. Tremblay (2002) describes the hysteretic behavior of this brace under quasi-static loading. A summary of this description is as follows: The brace was first loaded in tension, when the load was reversed it buckled in compression in the first cycle. After buckling occurred, the compressive strength started to decrease and a plastic hinge formed near the brace mid-length. With load reversal, the brace straightened through inelastic rotation in the plastic hinge. During the following cycles, the compressive resistance decreased due to the Baushinger effect and the residual out-of-plane displacements from previous cycles. In tension, the brace reached the yield capacity and exhibited some strain hardening. With every load cycle, the permanent axial elongation increased. As the axial elongation increased, the inelastic rotation of the mid-length plastic hinge increased. Then, local buckling at the hinge location caused a further reduction in the brace compressive resistance. Finally, after local buckling, the brace fractured at the plastic hinge when it was loaded in tension.

In an SCBF with a tension-compression X-bracing configuration, when the tension brace in the given story is at its yield capacity, the story shear reaches a maximum value. As the compression brace strength degrades due to buckling, the force in the tension brace

remains constant or increases slightly due to strain hardening. As a result of this action, the story shear capacity decreases although there is some strain hardening in the tension brace. After the strength loss in the compression brace, the interior columns must carry the difference between the vertical components of the compression and tension brace forces together with the gravity loads.

A common configuration of braces in practice is an arrangement that provides two braces in each story, one in tension and one in compression. The braced frames used in the model buildings of this study (see Chapter 3) have a multi-story X-bracing configuration.

5.3 Development of Fragility Curves for Brace Damage

5.3.1Formulation of Brace Damage Fragility Functions

As explained in Section 4.2.1, fragility functions provide the probability that a building reaches or exceeds a level of damage (i.e., a damage state or damage condition), as a function of (or conditioned on) a structural demand parameter (EDP) (Baker, 2008). One such fragility function is required for each component and each damage state. As explained in Section 4.2.1, the fragility function which represents the conditional probability of a component being in a damage state (conditioned on an EDP) is equivalent to the CDF for the limit value of the EDP (the minimum value of the EDP corresponding to the damage state). A lognormal distribution is often used for fragility functions because it often fits structural damage data well, and because the lognormal distribution has zero probability density when the EDP value is less than or equal to zero (Porter et al., 2007).

In this study, the brace damage fragility functions use the residual out-of-plane (OOP) displacement of brace mid-length normalized by the brace length, Δ_{or}, as the EDP. Three damage states are considered, as discussed later.

The fragility functions can be written as follows:

$$P(DS \geq DS_i \mid \Delta_{or}) = P(\Delta_{or} \geq \Delta_{or,i}) = \Phi\left(\frac{\ln(\Delta_{or}) - \ln(\Delta_{or,i,m})}{\beta_i}\right) \quad (5.1)$$

where,

DS = the damage state

DS_i = damage state i

$\Delta_{or,i}$ = the Δ_{or} limit value for damage state i, which is the minimum value of Δ_{or} corresponding to damage state DS_i or worse

$\Delta_{or,i,m}$ = the median value of $\Delta_{or,i}$

β_i = the lognormal standard deviation of $\Delta_{or,i}$

Φ = the standard normal cumulative distribution function

$\Delta_{or,i,m}$ and β_i must be established for each DS_i.

$\Delta_{or,i,m}$ in Equation 5.1 is the limit value for Δ_{or} for which the probability of being in damage state DS_i (or worse) is 50%. When Δ_{or} obtained from dynamic analysis (or observed after a test or after an earthquake) exceeds $\Delta_{or,i}$, the braces are considered to be in damage state DS_i (or worse).

Note that $\Delta_{or,i,}$ is not deterministic, but is a random variable. The lognormal standard deviation β_i is used as the measure of dispersion of $\Delta_{or,i}$. It considers the uncertainty in the limit value for Δ_{or} corresponding to damage state DS_i. Without any dispersion (i.e., when β_i=0), the fragility functions would plot as straight vertical lines and the damage states are separated from each other with these lines. Brace fragility functions with β_i=0 are shown in Figure 5.2(a). As seen in this figure, damage states are separated by vertical lines at deterministic limit values. Damage states are represented as the range between the deterministic limit values in Figure 5.2(a). Figure 5.2(b) shows fragility functions for brace damage plotted with β_i not equal to zero. The definition of $\Delta_{or,i,m}$ is seen in Figure 5.2(b). Damage states are represented as the range between the uncertain limit values in Figure 5.2(b). When Δ_{or} obtained from dynamic analysis exceeds the limit value of a damage state (either $\Delta_{or,1}$ or $\Delta_{or,2}$), the braces are considered to be in that damage state or worse.

5.3.2 Definition of Damage States

In this study, three discrete damage states are used to quantify the damage of the braces. These damage states are defined according to the repair actions that would be taken as a result of observed damage. The damage states are as follows:

DS_0: There is no damage in this damage state. The braces retain all of their pre-earthquake strength and stiffness. No repairs are needed. This damage state is represented by either DS_0 or NR (no repair).

DS_1: The damage of the braces is slight. The expected strength loss at this level of damage is recoverable with a repair action consisting of brace straightening (BS) by heat straightening. In the heat straightening process, a limited amount of heat is applied to the plastically deformed regions in a specific pattern with repetitive heating and cooling cycles (Kowalkowski and Varma, 2007). This damage state is represented by either DS_1 or BS (brace straightening).

DS_2: At this level of damage, the brace member is damaged significantly. High residual deformations are observed in the brace. A large strength loss is expected; therefore the brace needs to be replaced (BR). This damage state is represented by either DS_2 or BR (brace replacement).

5.3.3 Definition of Damage State Limits

To define the damage fragility functions, limit values for each damage state are needed. These damage state limits correspond to the minimum value of the EDP (i.e., Δ_{or}) corresponding to the damage state. Two damage state limits are used in this study:

$\Delta_{or,1}$: This damage state limit is the minimum value of Δ_{or} corresponding to damage state DS_1 and separates DS_0 and DS_1. As illustrated in Figure 5.2, Δ_{or} values smaller than $\Delta_{or,1}$ correspond to DS_0 and Δ_{or} values greater than $\Delta_{or,1}$ correspond to DS_1 (or DS_2). The median value of $\Delta_{or,1}$, defined as $\Delta_{or,1,m}$, corresponds to 50% probability of being in damage state DS_1 (or worse, i.e., DS_2).

Δ_{or_2}: This damage state limit is the minimum value of Δ_{or} corresponding to damage state DS_2 and separates DS_1 and DS_2. As illustrated in Figure 5.2, Δ_{or} values smaller than $\Delta_{or,2}$

correspond to DS_1 (or DS_0) and Δ_{or} values greater than $\Delta_{or,2}$ correspond to DS_2. The median value of $\Delta_{or,2}$, defined as $\Delta_{or,2,m}$, corresponds to 50% probability of being in DS_2.

5.3.3.1 Experimental Results Used to Define Median Damage State Limits

The level of residual OOP displacement corresponding to the damage states and the associated repair actions from actual buildings after earthquakes would be useful for the present study. However, information of this type is not available in the literature. Therefore, the results of a previous experimental study are used to establish the limit values for Δ_{or} associated with the defined damage states.

The results of brace tests, which are a part of the National Science Foundation program CMS-0619161 "International Hybrid Simulation of Tomorrow's Braced Frame Systems", are used (Powell, 2009). The test data is found at the NEES Project Warehouse website (NEEShub). The main goal of this project was to understand the nonlinear behavior of SCBFs under severe seismic loading.

The tests were performed at the University of Washington Structures Laboratory. The test setup consists of a single bay, single story frame system with a diagonal brace. The same test setup was used for various brace sections. Since all the brace sections studied in the present research are wide flange brace sections, the results from one test with a wide flange brace (WF-23) are used. The test setup drawing for specimen WF-23 is shown in Figure 5.3. The out-of-plane movement of the beams and columns was restricted in the test setup; the beams and columns displace in-plane. The braces and gusset plates are not restrained and free to displace out-of-plane when the braces buckle under compression.

The system was subjected to pseudo-static loading with a focus on the diagonal brace and gusset plate connections (Powell, 2009).

Potential yield mechanisms and failure modes in this test are described by Powell (2009). Potential yield mechanisms are associated with inelastic behavior that does not cause a rapid reduction in the system strength. On the other hand, failure modes are associated with inelastic behavior and brittle failure which result in a significant loss of system strength. Figure 5.4 shows the typical yield and failure mechanisms of SCBFs.

Damage levels described by Powell (2009) are given in Table 5.1. The descriptions of these damage levels are based on component-based observations and do not necessarily coincide with the damage states of a complete SCBF system. Table 5.2 relates each damage state to performance levels that are explained in Chapter 2 (Powell, 2009).

Specimen WF-23 was subjected to 41 loading cycles before failure. The frame displacements during the loading cycles are shown in Figure 5.5. The results of the test are given in Table 5.3, including maximum (max) and minimum (min) drift ratios, max and min lateral loads resisted by the frame, and the progression of damage to the braces (Powell, 2009). Table 5.3 also indicates the test cycles at which damage was first observed.

Damage of braces in compression is important for specifying the damage state limits for the present study. As seen in Table 5.3, the brace experienced Y1, B1, Y3, B2, and Y5 type damage under compression in the WF-23 test according to Powell (2009). Initial yielding (Y1) in compression was first observed in the flanges of the brace at -0.18%

drift. At -0.38% drift, the OOP displacement of brace mid-length was measured as 4 in. This level of OOP displacement exceeds 2% of the brace length, which is considered by Powell (2009) to be initial buckling (B1), as shown in Table 5.1. At -0.38% drift, moderate yielding (Y3) was observed at the brace mid-length. The OOP displacement at the brace mid-length was 5.14 in., identified as moderate buckling (B2), at -0.49% drift. Beyond this drift level, yielding at the mid-length of the brace continued to increase and a hinge formed. At -0.83% drift, severe yielding (Y5) was observed at the brace mid-length. The specimen failed at 2.32% drift because of a weld fracture, not because of brace fracture.

The WF-23 test results are plotted in Figures 5.6, 5.7 and 5.8. These figures were plotted using the data obtained from the NEES Project Warehouse database (NEEShub). The brace axial force is plotted against drift in Figure 5.6 to obtain the brace hysteresis curve. Figure 5.6 shows that the axial force increases with increasing positive drift when the brace is in tension. In compression, the largest brace axial force was recorded just before buckling. After buckling, the compressive strength decreases with increasing negative drift. The OOP displacement is plotted against drift in Figure 5.7 and the brace axial force is plotted against OOP displacement in Figure 5.8. These figures show that the OOP displacement of the brace increases with the decreasing compressive force (especially after buckling) and decreases with the increasing tensile force, as expected.

It should be kept in mind that in this test, a single diagonal brace was used. This configuration exhibits an unsymmetric response, with different resistance from the brace

in tension or in compression. In actual SCBF systems, a pair of braces, one in tension and one in compression is often used, resulting in nearly equal resistance in each direction.

5.3.3.2 Definition of Damage State Limits from Experimental Results

According to the experimental results described in Section 5.3.3.1, damage state B1 was initially selected as the lower limit of DS_1 and damage state Y5 was initially selected as the lower limit of DS_2. Based on the information in Tables 5.1 and 5.2, B1 and Y5 are defined as follows:

- B1: Initial buckling of the brace which does not affect the strength of the system. Repairs are not required for IO.
- Y5: Severe yielding of the brace section with residual deformation. There is some loss of strength but not enough to cause collapse. The brace needs to be replaced.

The definitions of B1 and Y5 appear to have some similarities with the definitions of DS_1 and DS_2, respectively. Therefore, the test data associated with damage state B1 was initially used to determine $\Delta_{or,1,m}$ and the test data associated with damage state Y5 was initially used to determine $\Delta_{or,2,m}$. Note that, the OOP displacement values given in the test results (Powell, 2009) are not the residual displacements. The residual OOP displacements were determined from the test data.

By using brace hysteresis curves for specimen WF-23 obtained from the data available on the NEES Project Warehouse website (NEEShub), the residual OOP displacements of brace mid-length were determined. The residual OOP displacement is assumed to be the

OOP displacement that the brace has at its mid-length when the axial force is zero during the cyclic loading.

The compression force capacity at first buckling of WF-23 was found as 167 kips from brace hysteresis curve given in Figure 5.6. After first buckling, the compressive strength of the brace starts to decrease. 167 kips is used as the reference capacity for estimating the loss in compressive force capacity of the brace.

In Table 5.3, the loading cycle numbers at which the corresponding damage state is first observed are given. These cycles are used to identify damage state limits for B1 and Y5, defined as $\Delta_{or,B1}$ and $\Delta_{or,Y5}$, respectively. $\Delta_{or,B1}$ and $\Delta_{or,Y5}$ are deterministic values established from the WF-23 test data. It was mentioned earlier that the test had 41 load cycles as shown in Figure 5.5. According to Table 5.3, damage state B1 was first observed from cycle 19 to 20, and damage state Y5 was first observed from cycle 25 to 26 (Powell, 2009). Therefore, cycle 19 to 20 was defined as cycle B1 and cycle 25 to 26 was defined as cycle Y5. These cycles are shown on the brace hysteresis curve in Figure 5.9. Similarly, the data from Figures 5.7 and 5.8 are plotted again with cycle B1 and cycle Y5 marked on them in Figures 5.10 and 5.11, respectively. Cycle B1 and cycle Y5 were considered initially as the cycles defining the damage state limit values $\Delta_{or,1,m}$ and $\Delta_{or,2,m}$.

Determination of $\Delta_{or,1,m}$

In cycle B1 (cycle 19 to 20), the peak compression force at buckling was 111.1 kips which is 33% less than the compression force capacity of the brace. A 33% capacity loss

is thought to be too large to correspond to $\Delta_{or,1,m}$. As mentioned earlier, $\Delta_{or,1,m}$ is the median of $\Delta_{or,1}$ which is the limit value for damage state DS_1. DS_1 represents a damage state without considerable strength loss so that damage can be repaired by minor repair actions such as brace straightening. More importantly, $\Delta_{or} \leq \Delta_{or,1}$ corresponds to damage state DS_0, for which the brace retains all of its pre-earthquake strength and stiffness. For this reason, the test data used to define $\Delta_{or,1,m}$ was reconsidered. Alternative load cycles are selected from the brace hysteresis curve to define $\Delta_{or,1,m}$, and the results are compared with $\Delta_{or,B1}$ in Table 5.4.

Cycle 15 to 16, defined as cycle 1-alt-1, was considered for determining $\Delta_{or,1,m}$. Cycle 17 to 18, defined as cycle 1-alt-2, was also considered. These alternative cycles are shown on the brace hysteresis curve together with cycle B1 in Figure 5.12. Each cycle is plotted individually in Figures 5.13 through 5.18. The points of residual OOP displacements and the peak compression forces are marked on these figures. The results from each cycle are tabulated in Table 5.4 for comparison.

According to the data given in Table 5.4, cycle 1-alt-1 has the lowest values among the three cycles. The compression force capacity loss is about 5%, and Δ_{or} is about 0.3% (i.e., L/333) at the end of cycle 1-alt-1. As indicators of the limit between DS_0 and DS_1, these values are conservative. For the cycle 1-alt-2, the compression force capacity loss is about 20%, and Δ_{or} is about 1% (i.e., L/100) at the end. Since the brace damage state is assumed to be determined in a post-earthquake inspection, the potential for observing the limit value of Δ_{or} is important. When the potential for observing Δ_{or} in an inspection is considered, the value 0.3% from cycle 1-alt-1 is considered to be too small to observe.

However, Δ_{or}=1% from cycle 1-alt-2 would be easier observed. For this reason, cycle 1-alt-2 was selected to determine $\Delta_{or,1,m}$, and $\Delta_{or,1,m}$ is set to 1%. $\Delta_{or,1,m}$ represents the median of the $\Delta_{or,1}$ data and the uncertainty in $\Delta_{or,1}$ is considered by a specified dispersion value, as discussed later.

Determination of $\Delta_{or,2,m}$

In cycle Y5 (cycle 25 to 26), the peak compression force at buckling was 69.96 kips which is 60% less than the compression force capacity of the brace. A 60% capacity loss is considered to be too large for the limit between DS_1 and DS_2. As mentioned earlier, $\Delta_{or,2,m}$ is the median of $\Delta_{or,2}$ which is the limit value for damage state DS_2. DS_2 represents major brace damage with significant strength loss so that the brace needs to be replaced. $\Delta_{or,1,m} \leq \Delta_{or} \leq \Delta_{or,2,m}$ corresponds to damage state DS_1 and $\Delta_{or} \geq \Delta_{or,2,m}$ corresponds to damage state DS_2. For this reason, the test data used to define $\Delta_{or,2,m}$ was reconsidered. Alternative load cycles were selected from the brace hysteresis curve to define $\Delta_{or,2,m}$, and the results are compared with $\Delta_{or,Y5}$ in Table 5.5.

Cycle 22 to 23, defined as cycle 2-alt-1, was considered for determining $\Delta_{or,2,m}$. Cycle 24 to 25, defined as cycle 2-alt-2, was also considered. These alternative cycles are shown on the brace hysteresis curve together with the cycle Y5 in Figure 5.19. Each cycle is plotted individually in Figures 5.20 through 5.25. The points of residual OOP displacements and the peak compression forces are marked on these figures. The results obtained from each cycle are tabulated in Table 5.5 for comparison.

According to the data given in Table 5.5, cycle 2-alt-1 has the lowest values among the three cycles. The compression force capacity loss is about 45%, and Δ_{or} is about 2.5% (i.e., L/40) at the end of cycle 2-alt-1. For the cycle 2-alt-2, the compression force capacity loss is about 53%, and Δ_{or} is about 3.5% (i.e., L/29) at the end. Either cycle could be used to define $\Delta_{or,2,m}$; however cycle 2-alt-1 was selected to determine $\Delta_{or,2,m}$ and $\Delta_{or,2,m}$ is set to 2.5%.

5.3.4 Brace Fragility Functions

After determining $\Delta_{or,1,m}$ and $\Delta_{or,2,m}$, brace damage fragility functions for DS_1 and DS_2 are obtained and plotted in Figure 5.26. Fragility curves for B1 (or worse) and Y5 (or worse) as identified by Powell (2009) are also plotted in Figure 5.26. To the represent the dispersion in the damage state limit values, β_1 and β_{B1} are taken as 0.2; and β_2 and β_{Y5} are taken as 0.3. Figure 5.26 shows that damage state DS_1 is reached at a smaller Δ_{or} than B1 and damage state DS_2 is reached at a smaller Δ_{or} than Y5.

5.4 Brace Damage State Probabilities

Fragility functions developed for the braces were used to estimate the probability that the braces would be in a specific damage state (or worse) as a function of Δ_{or} when the model buildings are subjected to earthquake loading at a given ground motion input level. The conditional probability that a brace will be damaged to damage state DS_i or a more severe damage state (i.e., DS_i or worse) is found by using the fragility function given in Equation 5.1. The conditional probability that the brace will be damaged to damage state DS_i is obtained as follows (Aslani and Miranda, 2005):

$$P(DS = DS_i \mid \Delta_{or}) = \begin{cases} 1 - P(DS \geq DS_{i+1} \mid \Delta_{or}) & i = 0 \\ P(DS \geq DS_i \mid \Delta_{or}) - P(DS \geq DS_{i+1} \mid \Delta_{or}) & 1 \leq i < m \\ P(DS \geq DS_i \mid \Delta_{or}) & i = m \end{cases} \quad (5.2)$$

where,

DS_0 (i=0) corresponds to no damage (i.e., no repair)

$P(DS=DS_i|\Delta_{or})$ = probability that the brace is in the damage state DS_i

$P(DS\geq DS_i|\Delta_{or})$ = the brace damage fragility function for DS_i (i^{th} damage state) from Equation 5.1

m = number of damage states defined for the component (where m=2 for this study)

The generalized form of Equation 5.2 is written for this study as follows:

$$P(DS = DS_0 \mid \Delta_{or}) = P(NR \mid \Delta_{or}) = 1 - P(DS \geq DS_1 \mid \Delta_{or}) \quad (5.3)$$

$$P(DS = DS_1 \mid \Delta_{or}) = P(BS \mid \Delta_{or}) = P(DS \geq DS_1 \mid \Delta_{or}) - P(DS \geq DS_2 \mid \Delta_{or}) \quad (5.4)$$

$$P(DS = DS_2 \mid \Delta_{or}) = P(BR \mid \Delta_{or}) = P(DS \geq DS_2 \mid \Delta_{or}) \quad (5.5)$$

The conditional probabilities for each damage state from Equations 5.3, 5.4 and 5.5 are shown schematically in Figure 5.27. As seen in Figure 5.27, the individual brace damage state probabilities add up to 1. The conditional probabilities obtained from Equations 5.3, 5.4 and 5.5 are used in the damage assessment presented in Chapter 6.

Repair actions corresponding to each damage state are illustrated using the Venn diagram in Figure 5.28. According to Figure 5.28, the no repair or worse condition (NR') fills the sample space and its probability is equal to 100%. This means, in every case, the probability that the brace remains undamaged or worse (DS_1 or DS_2) is 100%. The brace straightening or worse condition (BS') is a subset of the NR' condition and has a smaller probability than NR'. Likewise, the brace replacement (BR) condition is a subset of the BS' condition and has the least probability.

The probability of the BS' condition (P(BS')) is the probability that the brace is in damage state DS_1 or DS_2 so that BS (brace straightening) or BR (brace replacement) may be needed. In Figure 5.28, the light grey area plus the dark grey area of the Venn diagram is associated with P(BS'). In Figure 5.27, P(BS') is shown as $P(DS \geq DS_1 | \Delta_{or})$. Likewise, the probability of BR condition (P(BR)) is the probability that the brace is in damage state DS_2 so that BR (brace replacement) is needed. In Figure 5.28, the dark grey area of the Venn diagram represents P(BR). In Figure 5.27, P(BR) is shown as $P(DS \geq DS_2 | \Delta_{or})$.

The light grey area of the Venn diagram shown in Figure 5.28 represents the probability that the brace is in damage state DS_1 only, P(BS). In other words, it represents the probability that Δ_{or} is between $\Delta_{or,1}$ and $\Delta_{or,2}$. Similarly, the white area of the Venn diagram shown in Figure 5.28 represents the probability that the brace is undamaged, P(NR), and it represents the probability that Δ_{or} is less than $\Delta_{or,1}$.

Equations 5.1 and 5.2 give the brace damage state probabilities conditioned on Δ_{or}. The unconditional probabilities are obtained as follows from total probability theory by convolving the fragility functions with the PDF for Δ_{or}:

$$P(DS \geq DS_0) = P(NR') = 1 \tag{5.6}$$

$$P(DS \geq DS_1) = P(BS') = \int_0^\infty P(DS \geq DS_1 \mid \Delta_{or}) \cdot f(\Delta_{or}) \cdot d\Delta_{or} \tag{5.7}$$

$$P(DS \geq DS_2) = P(BR) = \int_0^\infty P(DS \geq DS_2 \mid \Delta_{or}) \cdot f(\Delta_{or}) \cdot d\Delta_{or} \tag{5.8}$$

where,

$P(DS \geq DS_i)$ = the probability that the brace will be in damage state DS_i (or worse)

$P(DS \geq DS_i|\Delta_{or})$ = the brace damage fragility function from Equation 5.1

$f(\Delta_{or})$ = the probability density function (PDF) for Δ_{or}

The PDF for Δ_{or} in Equations 5.7 and 5.8 is specific for each brace in the model buildings and is obtained from the dynamic earthquake response analysis results. In Chapter 3, the dynamic earthquake response analysis of the 4- and 9-story SCBF and SC-CBF model buildings was described. The FEMA P695 Far-Field ground motion set which includes 44 different ground motion records was used in these analyses. From the 44 ground motions, 44 different residual OOP displacements were obtained for each brace, and were normalized by the brace length to obtain 44 values of Δ_{or}. The mean and standard deviation of these 44 values were obtained, and the PDF of Δ_{or} for each brace was

obtained. The lognormal distribution was chosen for the Δ_{or} PDF. The process was repeated for each model building and for both the DBE and MCE intensity levels. The probability distribution parameters for Δ_{or} for each brace of each model building are given in Tables 5.6 through Table 5.9. The values listed in these tables are rounded off to 3 significant decimal digits. Values around 10^{-6} to 10^{-7} or less are rounded to zero.

The damage state probabilities for each brace in the model buildings are found from Equations 5.7 and 5.8. The results for the 4-story model buildings are given in Table 5.10, and the results for the 9-story model buildings are given in Table 5.11 for both the DBE and MCE intensity levels. In Tables 5.10 and 5.11, P(B1 or worse) and P(Y5 or worse) are given in addition to $P(DS \geq DS_1)$ and $P(DS \geq DS_2)$ to see the difference between them. The values listed in these tables are rounded off to 3 significant decimal digits. Values around 10^{-6} to 10^{-7} or less are rounded to zero.

According to the results in Tables 5.10 and 5.11, it is seen that $P(DS \geq DS_1)$ values are greater than the P(B1 or worse) values. Similarly, $P(DS \geq DS_2)$ values are greater than the P(Y5 or worse) values. This shows that changing $\Delta_{or,B1}$ and $\Delta_{or,Y5}$ to $\Delta_{or,1,m}$ and $\Delta_{or,2,m}$ respectively, increases the brace damage probabilities. The expected need for repair actions is strongly influenced by the definition of the damage state limits from experimental data and observations.

According to the brace damage probabilities for the 4-story model buildings given in Table 5.10, the brace damage probabilities for the 4SC-CBF are almost zero. For this reason the braces of this building are considered to be damage free under the DBE and MCE level earthquakes. On the other hand, damage is expected in the braces of the

4SCBF. Results from Table 5.10 show that brace damage for the 4SCBF is concentrated in the 1st story braces, with the highest brace damage probabilities. Some damage is also expected in the 2nd and 4th story braces.

According to the brace damage probabilities for the 9-story model buildings given in Table 5.11, the brace damage is concentrated in the 5th, 6th and 7th story braces of the 9SC-CBF, where the brace damage probabilities are higher. The damage probabilities for the lower story braces are very small (almost zero) for this frame, so that they are considered to be undamaged. This result is expected for SC-CBFs, because in the design of SC-CBFs, higher mode forces affect upper stories, as mentioned in Section 3.3.2. On the other hand, results from Table 5.11 show that the brace damage is more uniformly distributed over the stories in the 9SCBF.

When the brace damage probabilities are compared on the basis of the number of stories, it is seen that the 9-story model buildings have more brace damage and require more expensive repair actions than the 4-story model buildings.

As expected, more brace damage is observed in both 4- and 9-story model buildings under the MCE level than the DBE level. In other words, more repair actions are needed after an MCE level event, as expected.

When considering which repair action to apply to a damaged brace, the damage probabilities are not the only decision parameters. There are some limitations for the use of heat straightening that should be kept in mind. Heat straightening increases the yield and ultimate stresses, and decreases the ductility of the repaired steel. For this reason, it is

recommended that heat straightening should not be applied more than twice to the same region if it is re-damaged (Avent and Mukai, 2001). If a repaired section may be damaged again, the changes in mechanical properties and the possibility of cracking should be considered when heat straightening is considered as the repair action.

Table 5.1 – Brace Damage Levels (Powell, 2009)

Symbol	Description	Detailed Description
Y1	Initial/Mild Yielding	Yield lines cover half the component width/depth
Y3	Moderate Yielding	Yield lines cover most of the component width/depth
Y5	Severe Yielding	Nearly all of the component is yielded with wide stretching yield lines
B1	Initial Buckling/Local Deformation	OOP of brace reaches 2% of brace length; when initial OOP buckling or deformation of component becomes visible
B2	Moderate Buckling/Local Deformation	OOP displacement of brace is greater than member depth; when buckling or deformation is greater than member depth
B3	Severe Buckling/Local Deformation	OOP displacement of brace exceeds twice the member depth, local pinching and severe deformation of component
BC	Brace Compressive Failure	Large local deformations (cupping and bulging) at plastic hinge location of brace in compression
BF	Brace Fracture	Brace begins to tear or it is completely fractured

Table 5.2 – Damage States for Performance Based Design (Powell, 2009)

SCBF Damage States for Performance Based Design		
	Brace	Performance Based Description
Minor	Y1; B1	Superficial damage not affecting strength of system. Repairs not required for IO.
Moderate	Y3; B2	Some obvious yielding or residual deformation. Minimal loss of strength. Repairs possibly required for IO perception.
Severe	Y5; BC	Severe visual yielding and residual deformations. Some loss of strength but okay for LS and CP. Component would have to be replaced.
Failure	BF	Fracture of component. Major loss of strength and potential for system failure or collapse. Beyond LS and possibly CP.

Table 5.3 – Peak Results of WF-23 Test (Powell, 2009)

Cycle		Drift Ratio			Load (kips)		Brace Damage	
From	To	Min	Max	Range	Min	Max	Comp	Tens
1	6	-0.06	0.07	0.12	-69.5	78.8		
7	8	-0.09	0.10	0.18	-99.4	112.1		Y1
9	10	-0.12	0.13	0.25	-120.8	141.0		
11	16	-0.18	0.16	0.35	-128.5	173.6	Y1	
17	18	-0.27	0.20	0.48	-121.0	193.9		
19	20	-0.38	0.24	0.62	-107.0	215.4	B1; Y3	
21	22	-0.49	0.29	0.78	-100.0	232.2	B2	
23	24	-0.67	0.40	1.07	-103.7	255.5		Y3
25	26	-0.83	0.53	1.36	-109.1	264.9	Y5	
27	28	-1.16	0.74	1.90	-121.8	291.7		
29	30	-1.48	0.98	2.47	-135.5	305.4		
31	32	-1.80	1.23	3.02	-141.5	316.5		
33	34	-2.15	1.48	3.63	-145.6	324.9		
35	36	-2.49	1.77	4.26	-148.4	330.8		
37	38	-2.86	2.05	4.91	-149.5	336.3		
39	40	-3.21	2.35	5.56	-137.3	338.2		
41	41	-	2.32	-	-	243.5		

Table 5.4 – Comparison of Δ_{or} values from several load cycles for determining Δ_{or_1}

	Cycle		Compression Capacity (kips)	Compression Capacity Loss (%)	Residual OOP Displ. (in.)	Δ_{or} (%)
	From	To				
B1	19	20	111.1	~33	2.6	~1.5
1-alt-1	15	16	157.6	~5	0.45	~0.3
1-alt-2	17	18	136.5	~20	1.55	~1

Table 5.5 – Comparison of Δ_{or} values from several load cycles for determining Δ_{or_2}

	Cycle		Compression Capacity (kips)	Compression Capacity Loss (%)	Residual OOP Displ. (in.)	Δ_{or} (%)
	From	To				
Y5	25	26	69.96	~60	6.5	~4
2-alt-1	22	23	90.3	~45	3.9	~2.5
2-alt-2	24	25	78.2	~53	5.5	~3.5

Table 5.6 – Probability Distribution Parameters for 4-story SCBF Braces

Brace	4 story SCBF							
	DBE				MCE			
	Normal mean (μ)	Normal std. dev. (σ)	Lognormal mean (λ)	Lognormal std. dev. (ζ)	Normal mean (μ)	Normal std. dev. (σ)	Lognormal mean (λ)	Lognormal std. dev. (ζ)
1LB	0.022	0.014	-3.991	0.584	0.038	0.022	-3.400	0.525
2LB	0.001	0.002	-8.130	1.435	0.005	0.013	-6.334	1.424
3LB	0.001	0.004	-8.577	1.752	0.001	0.007	-8.630	1.929
4LB	0.008	0.008	-5.143	0.811	0.010	0.010	-4.945	0.810
1RB	0.021	0.014	-4.032	0.611	0.037	0.020	-3.423	0.506
2RB	0.000	0.001	-8.587	1.293	0.004	0.012	-6.649	1.500
3RB	0.001	0.004	-8.637	1.750	0.002	0.008	-7.552	1.652
4RB	0.006	0.008	-5.592	1.003	0.012	0.010	-4.757	0.772

Table 5.7 – Probability Distribution Parameters for 4-story SC-CBF Braces

Brace	4 story SC-CBF							
	DBE				MCE			
	Normal mean (μ)	Normal std. dev. (σ)	Lognormal mean (λ)	Lognormal std. dev. (ζ)	Normal mean (μ)	Normal std. dev. (σ)	Lognormal mean (λ)	Lognormal std. dev. (ζ)
1LB	0.000	0.000	-11.838	0.134	0.000	0.000	-12.073	0.400
2LB	0.000	0.000	-10.571	0.155	0.000	0.000	-10.956	0.478
3LB	0.000	0.000	-8.672	0.162	0.000	0.000	-9.053	0.485
4LB	0.000	0.000	-8.854	0.145	0.000	0.000	-9.238	0.477
1RB	0.000	0.000	-11.838	0.134	0.000	0.000	-12.132	0.404
2RB	0.000	0.000	-10.571	0.155	0.000	0.000	-10.957	0.479
3RB	0.000	0.000	-8.672	0.162	0.000	0.000	-9.041	0.489
4RB	0.000	0.000	-8.854	0.145	0.000	0.000	-9.234	0.473

0.000 means value less than $1x10^{-6}$

Table 5.8 – Probability Distribution Parameters for 9-story SCBF Braces

Brace	9 story SCBF							
	DBE				MCE			
	Normal mean (μ)	Normal std. dev. (σ)	Lognormal mean (λ)	Lognormal std. dev. (ζ)	Normal mean (μ)	Normal std. dev. (σ)	Lognormal mean (λ)	Lognormal std. dev. (ζ)
1LB	0.022	0.016	-4.054	0.660	0.044	0.023	-3.243	0.495
2LB	0.001	0.003	-8.537	1.636	0.009	0.022	-5.583	1.357
3LB	0.017	0.017	-4.462	0.853	0.035	0.027	-3.591	0.689
4LB	0.002	0.008	-7.544	1.658	0.014	0.023	-4.984	1.167
5LB	0.018	0.019	-4.355	0.843	0.034	0.023	-3.566	0.619
6LB	0.018	0.019	-4.350	0.847	0.027	0.023	-3.865	0.724
7LB	0.028	0.013	-3.670	0.434	0.034	0.019	-3.521	0.527
8LB	0.003	0.007	-7.019	1.470	0.005	0.011	-6.266	1.359
9LB	0.000	0.000	-12.544	1.339	0.000	0.000	-10.788	1.438
1RB	0.026	0.020	-3.873	0.674	0.038	0.026	-3.464	0.622
2RB	0.002	0.007	-7.551	1.640	0.003	0.009	-7.028	1.542
3RB	0.016	0.019	-4.600	0.941	0.025	0.029	-4.124	0.925
4RB	0.004	0.012	-6.728	1.526	0.002	0.009	-7.612	1.719
5RB	0.018	0.016	-4.333	0.778	0.023	0.018	-3.995	0.695
6RB	0.017	0.016	-4.426	0.810	0.016	0.021	-4.623	1.004
7RB	0.028	0.015	-3.674	0.482	0.034	0.018	-3.485	0.484
8RB	0.003	0.009	-6.705	1.428	0.007	0.013	-5.768	1.232
9RB	0.000	0.000	-12.423	1.384	0.001	0.009	-8.463	1.935

0.000 means value less than $1x10^{-6}$

Table 5.9 – Probability Distribution Parameters for 9-story SC-CBF Braces

Brace	9 story SC-CBF							
	DBE				MCE			
	Normal mean (μ)	Normal std. dev. (σ)	Lognormal mean (λ)	Lognormal std. dev. (ζ)	Normal mean (μ)	Normal std. dev. (σ)	Lognormal mean (λ)	Lognormal std. dev. (ζ)
1LB	0.000	0.000	-11.966	0.281	0.000	0.000	-12.419	1.496
2LB	0.000	0.000	-10.981	0.251	0.000	0.000	-11.394	1.363
3LB	0.000	0.000	-10.531	0.323	0.000	0.000	-11.117	1.565
4LB	0.000	0.000	-9.986	0.313	0.000	0.000	-9.982	0.506
5LB	0.000	0.001	-9.037	1.514	0.003	0.010	-6.839	1.498
6LB	0.006	0.010	-5.751	1.136	0.017	0.016	-4.392	0.808
7LB	0.005	0.008	-5.856	1.116	0.016	0.016	-4.525	0.858
8LB	0.000	0.000	-8.057	0.328	0.001	0.001	-7.622	0.969
9LB	0.000	0.000	-8.057	0.328	0.005	0.014	-6.230	1.415
1RB	0.000	0.000	-12.033	0.284	0.000	0.000	-12.159	1.686
2RB	0.000	0.000	-10.929	0.246	0.000	0.000	-11.511	1.387
3RB	0.000	0.000	-10.606	0.327	0.000	0.000	-10.822	1.100
4RB	0.000	0.000	-9.942	0.319	0.000	0.000	-10.128	1.463
5RB	0.000	0.000	-9.490	1.018	0.001	0.003	-7.649	1.430
6RB	0.006	0.009	-5.769	1.122	0.017	0.016	-4.372	0.784
7RB	0.006	0.009	-5.799	1.120	0.016	0.014	-4.426	0.749
8RB	0.000	0.000	-8.070	0.359	0.001	0.001	-7.741	0.982
9RB	0.001	0.000	-7.071	0.170	0.002	0.007	-7.498	1.587

0.000 means value less than $1x10^{-6}$

Table 5.10 – Damage state probabilities for braces in 4-story model buildings

Brace	EQ Level	P(B1 or worse)		P(DS≥DS$_1$)		P(Y5 or worse)		P(DS≥DS$_2$)	
		SCBF	SC-CBF	SCBF	SC-CBF	SCBF	SC-CBF	SCBF	SC-CBF
1LB	DBE	0.633	0.000	0.840	0.000	0.120	0.000	0.323	0.000
	MCE	0.923	0.000	0.984	0.000	0.383	0.000	0.684	0.000
2LB	DBE	0.003	0.000	0.008	0.000	4.05E-04	0.000	0.001	0.000
	MCE	0.069	0.000	0.115	0.000	0.016	0.000	0.035	0.000
3LB	DBE	0.007	0.000	0.012	0.000	0.001	0.000	0.003	0.000
	MCE	0.011	0.000	0.019	0.000	0.003	0.000	0.006	0.000
4LB	DBE	0.130	0.000	0.260	0.000	0.013	0.000	0.046	0.000
	MCE	0.186	0.000	0.342	0.000	0.023	0.000	0.073	0.000
1RB	DBE	0.603	0.000	0.814	0.000	0.116	0.000	0.308	0.000
	MCE	0.923	0.000	0.985	0.000	0.365	0.000	0.675	0.000
2RB	DBE	4.00E-04	0.000	0.001	0.000	2.63E-05	0.000	1.12E-04	0.000
	MCE	0.053	0.000	0.088	0.000	0.013	0.000	0.027	0.000
3RB	DBE	0.006	0.000	0.011	0.000	0.001	0.000	0.003	0.000
	MCE	0.022	0.000	0.038	0.000	0.005	0.000	0.011	0.000
4RB	DBE	0.087	0.000	0.167	0.000	0.012	0.000	0.035	0.000
	MCE	0.242	0.000	0.424	0.000	0.032	0.000	0.099	0.000

0.000 means value less than $1x10^{-6}$

Table 5.11 – Damage state probabilities for braces in 9-story model buildings

Brace	EQ Level	P(B1 or worse)		$P(DS \geq DS_1)$		P(Y5)		$P(DS \geq DS_2)$	
		SCBF	SC-CBF	SCBF	SC-CBF	SCBF	SC-CBF	SCBF	SC-CBF
1LB	DBE	0.584	0.000	0.788	0.000	0.125	0.000	0.308	0.000
	MCE	0.964	0.000	0.995	0.000	0.484	0.000	0.780	0.000
2LB	DBE	0.004	0.000	0.009	0.000	6.95E-04	0.000	0.002	0.000
	MCE	0.157	0.000	0.238	0.000	0.045	0.000	0.087	0.000
3LB	DBE	0.383	0.000	0.565	0.000	0.085	0.000	0.197	0.000
	MCE	0.802	0.000	0.921	1.83E-05	0.311	0.000	0.552	0.000
4LB	DBE	0.023	0.000	0.039	0.000	0.005	0.000	0.011	0.000
	MCE	0.254	0.000	0.374	0.000	0.072	0.000	0.141	0.000
5LB	DBE	0.429	7.69E-04	0.614	0.002	0.102	8.20E-05	0.229	2.66E-04
	MCE	0.835	0.040	0.945	0.070	0.308	0.009	0.572	0.020
6LB	DBE	0.432	0.089	0.615	0.160	0.104	0.016	0.231	0.040
	MCE	0.672	0.409	0.838	0.601	0.205	0.087	0.412	0.208
7LB	DBE	0.866	0.072	0.975	0.135	0.197	0.011	0.515	0.030
	MCE	0.886	0.356	0.973	0.536	0.310	0.076	0.610	0.179
8LB	DBE	0.029	0.000	0.052	0.000	0.006	0.000	0.013	0.000
	MCE	0.066	2.72E-04	0.113	0.001	0.014	0.000	0.032	5.30E-05
9LB	DBE	0.000	0.000	0.000	0.000	0.000	0.000	0.000	0.000
	MCE	0.000	0.078	1.03E-05	0.128	0.000	0.019	6.76E-07	0.040
1RB	DBE	0.679	0.000	0.851	0.000	0.188	0.000	0.402	0.000
	MCE	0.870	0.000	0.960	0.000	0.362	0.000	0.628	0.000
2RB	DBE	0.021	0.000	0.037	0.000	0.005	0.000	0.010	0.000
	MCE	0.035	0.000	0.060	0.000	0.008	0.000	0.017	0.000
3RB	DBE	0.339	0.000	0.502	0.000	0.081	0.000	0.178	0.000
	MCE	0.532	0.000	0.694	0.000	0.176	0.000	0.328	0.000
4RB	DBE	0.050	0.000	0.084	0.000	0.012	0.000	0.025	0.000
	MCE	0.024	2.98E-05	0.041	9.19E-05	0.006	0.000	0.012	0.000
5RB	DBE	0.434	0.000	0.633	0.000	0.091	0.000	0.220	0.000
	MCE	0.612	0.009	0.801	0.018	0.153	0.001	0.344	0.003
6RB	DBE	0.393	0.084	0.585	0.154	0.081	0.014	0.197	0.037
	MCE	0.340	0.416	0.493	0.613	0.090	0.085	0.187	0.208
7RB	DBE	0.843	0.080	0.963	0.147	0.212	0.013	0.511	0.035
	MCE	0.914	0.385	0.984	0.591	0.321	0.068	0.641	0.181
8RB	DBE	0.041	0.000	0.073	0.000	0.009	0.000	0.019	0.000
	MCE	0.104	2.05E-04	0.176	8.76E-04	0.022	5.34E-06	0.051	3.99E-05
9RB	DBE	0.000	0.000	0.000	0.000	0.000	0.000	0.000	0.000
	MCE	0.014	0.020	0.024	0.035	0.004	0.004	0.007	0.009

0.000 means value less than $1x10^{-6}$

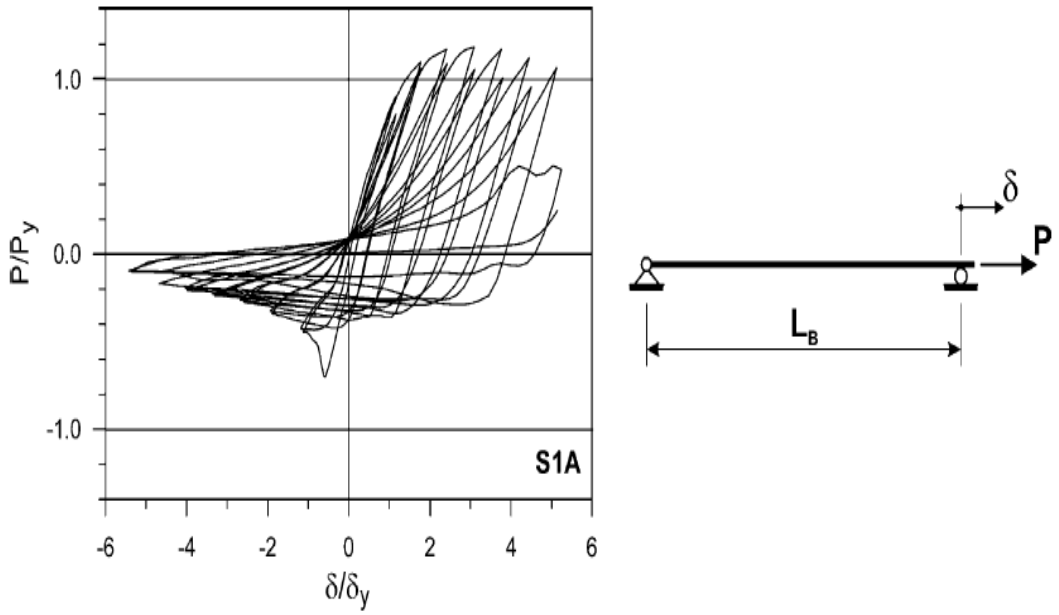

Figure 5.1 – Typical brace hysteresis curve under symmetric cyclic loading (Tremblay, 2002)

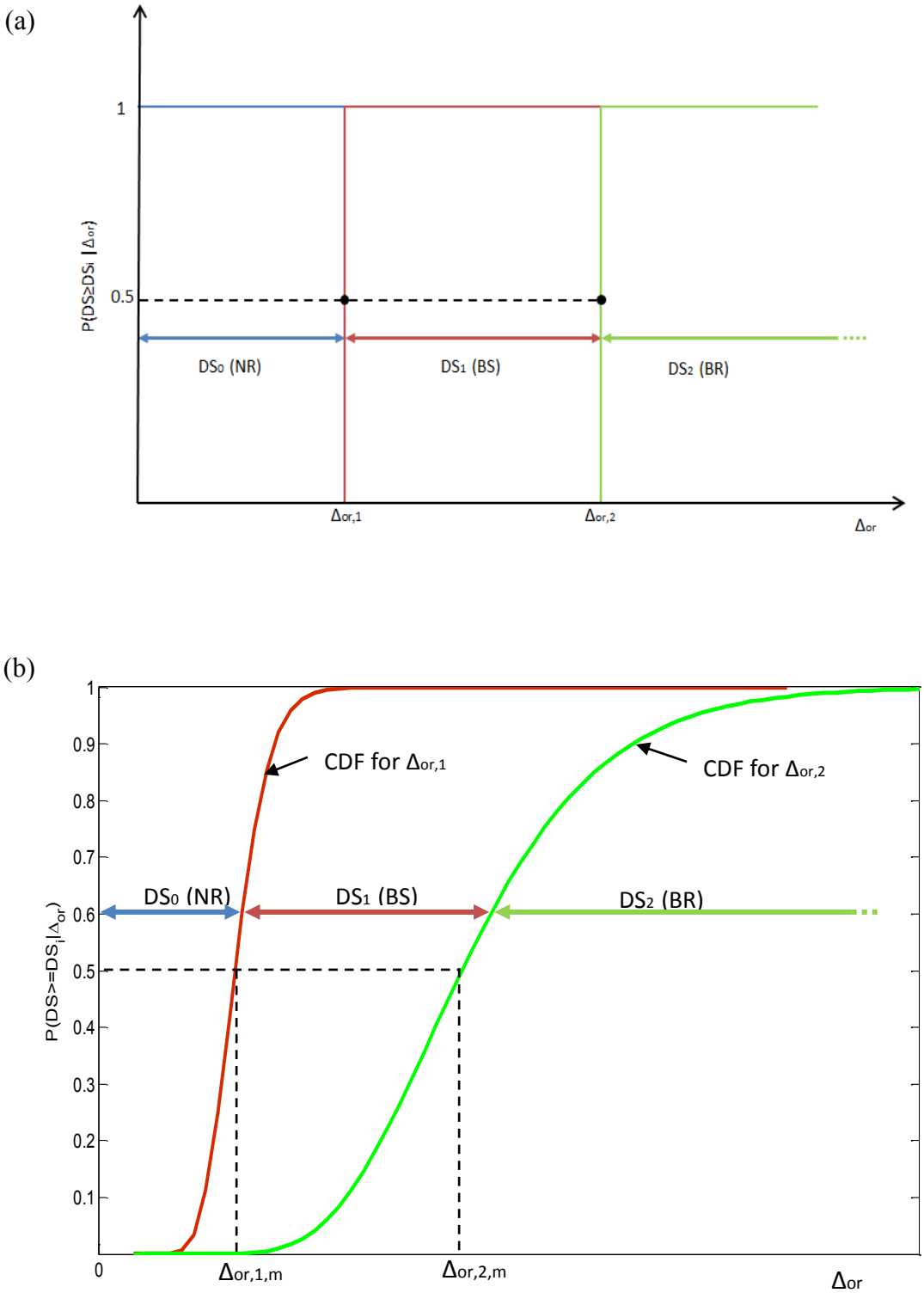

Figure 5.2 – (a) Brace damage fragility function with zero dispersion (β_i=0), (b) Brace damage fragility function with non-zero dispersion

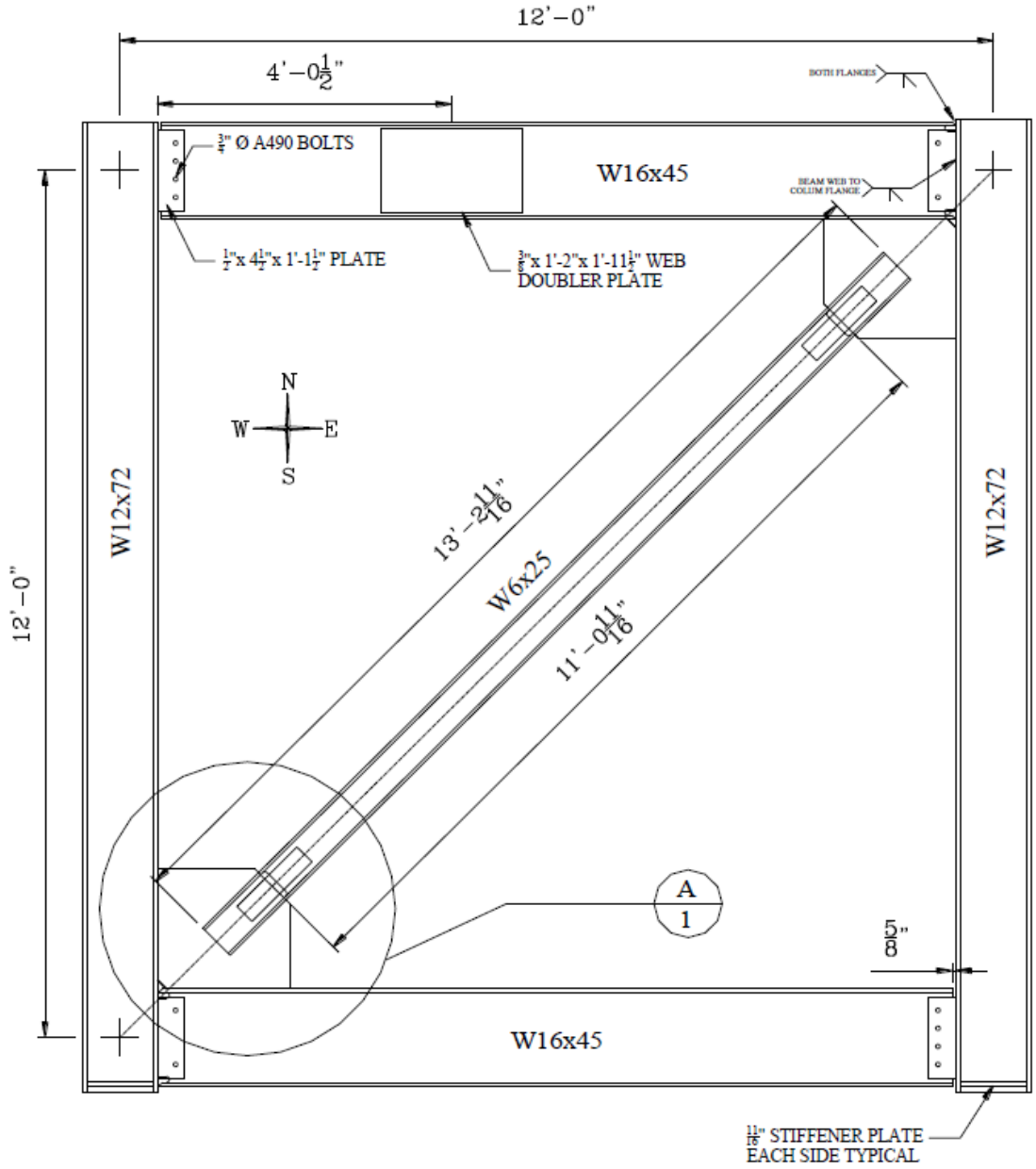

Figure 5.3 – Test specimen drawing (Powell, 2009)

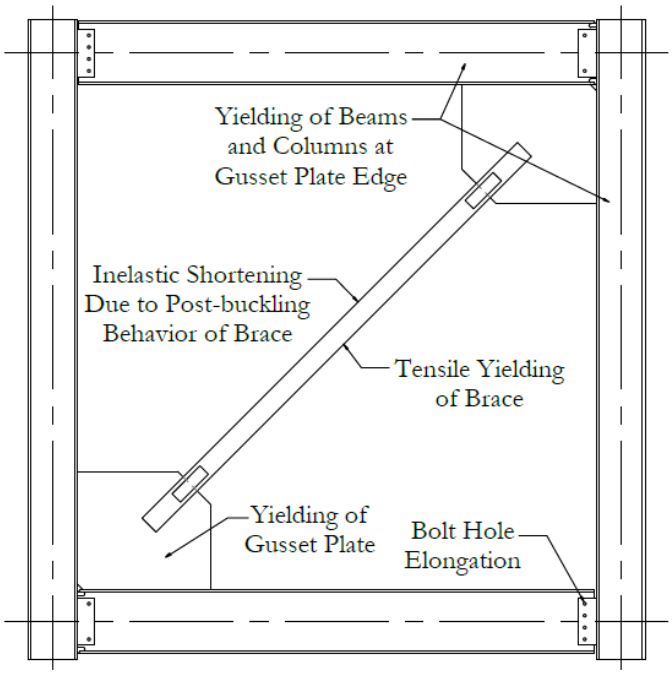

a) Yield Mechanisms

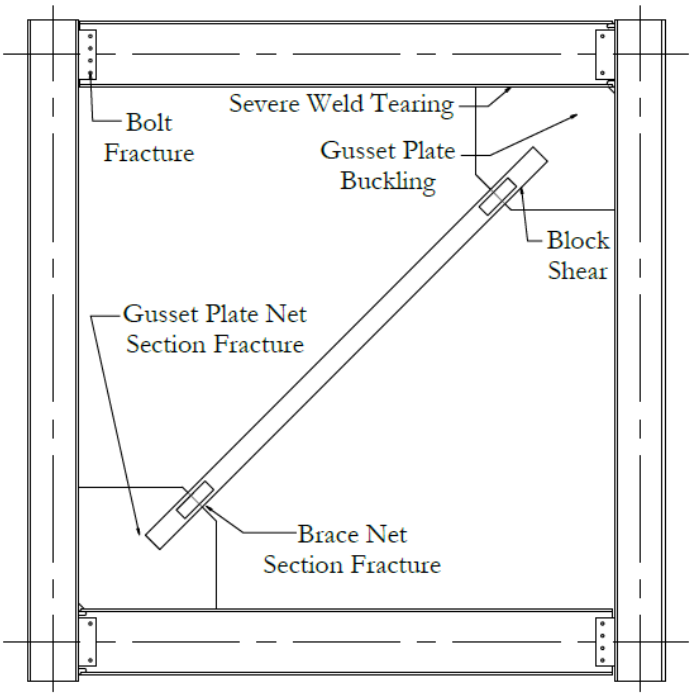

b) Failure Modes

Figure 5.4 – Yield mechanisms and failure modes for SCBFs (Powell, 2009)

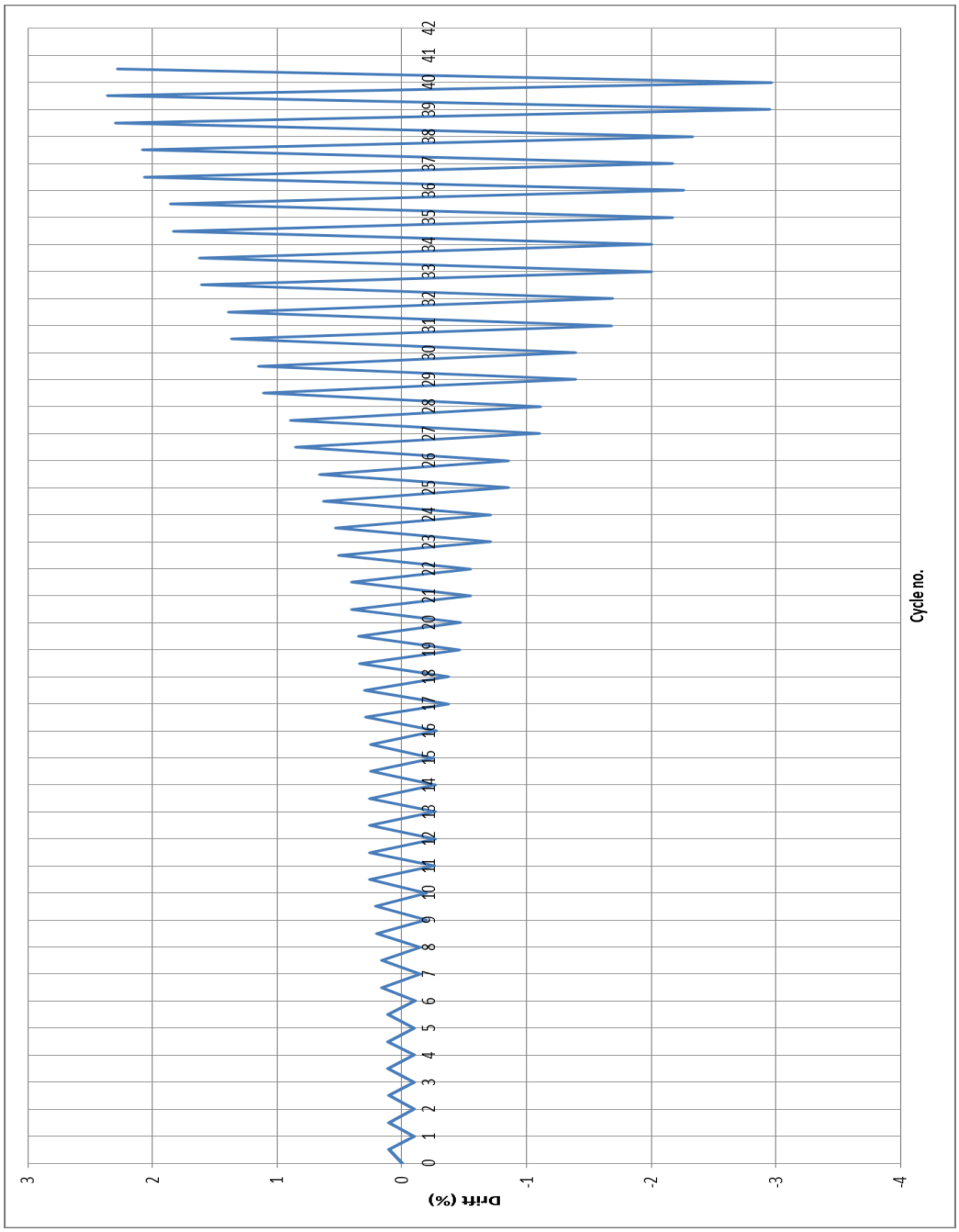

Figure 5.5 – Actual frame displacement vs. loading cycle of brace WF-23 test

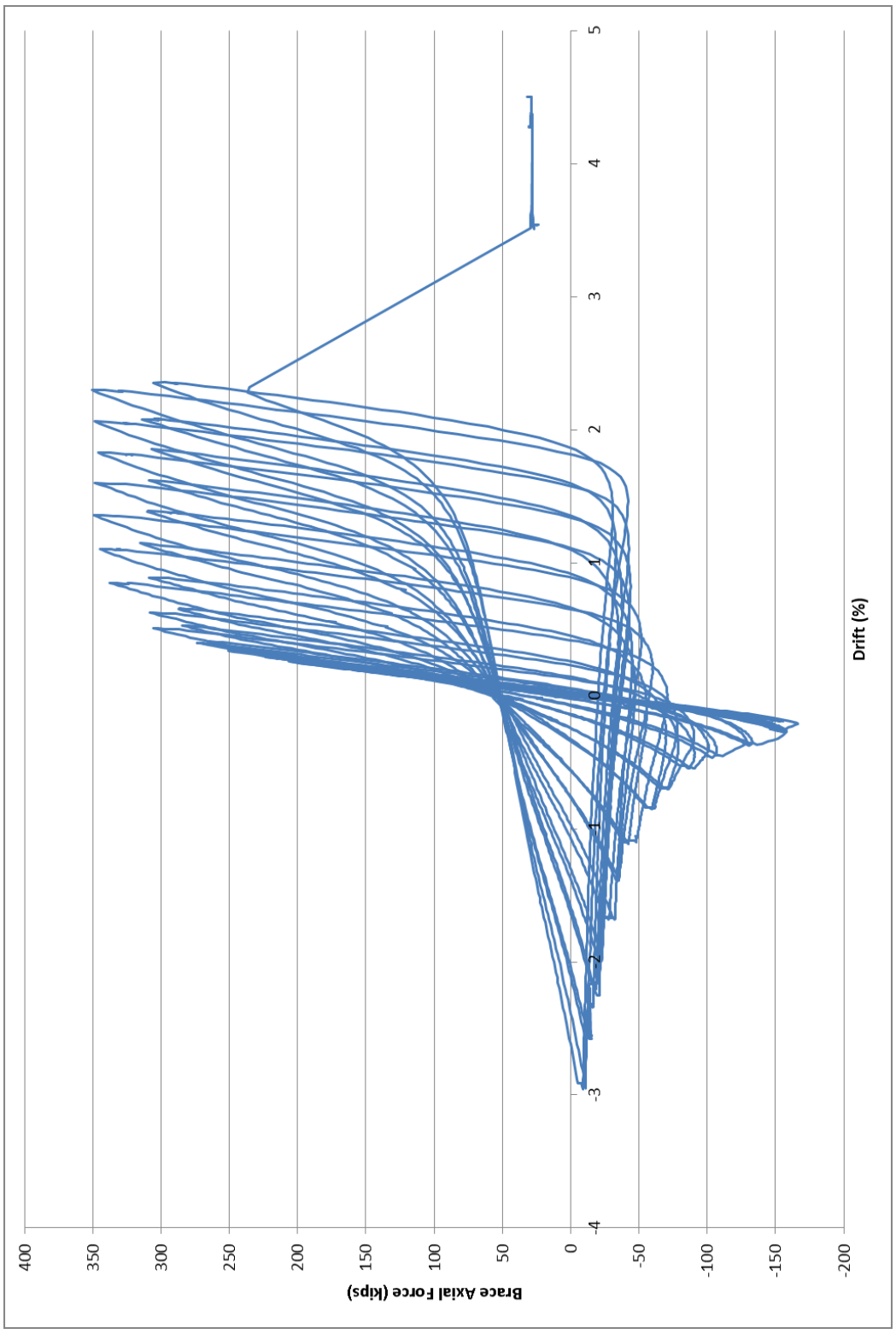

Figure 5.6 – Plot of test results: brace axial force vs. drift (brace hysteresis curve)

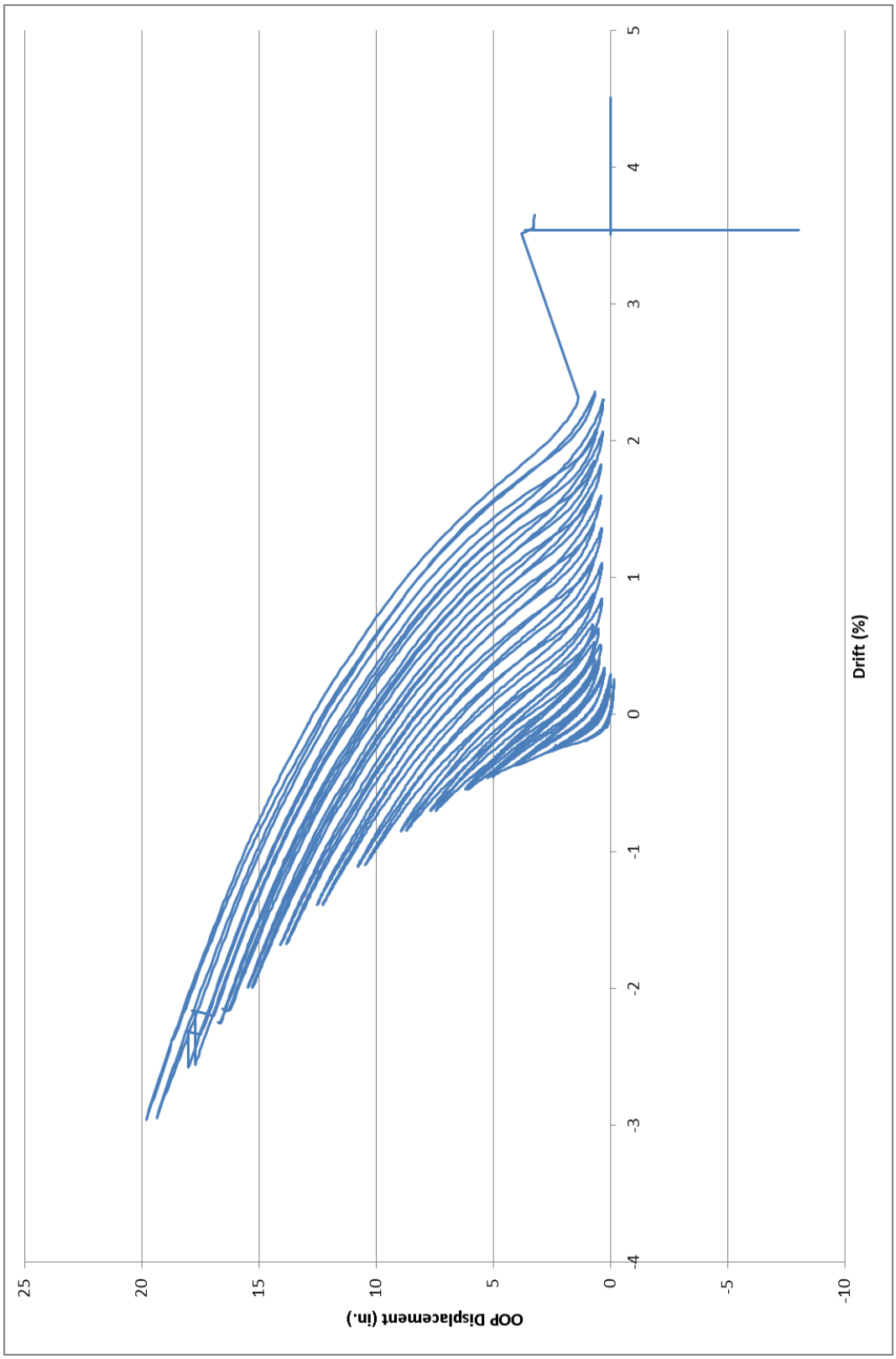

Figure 5.7 – Plot of test results: OOP displacement vs. drift

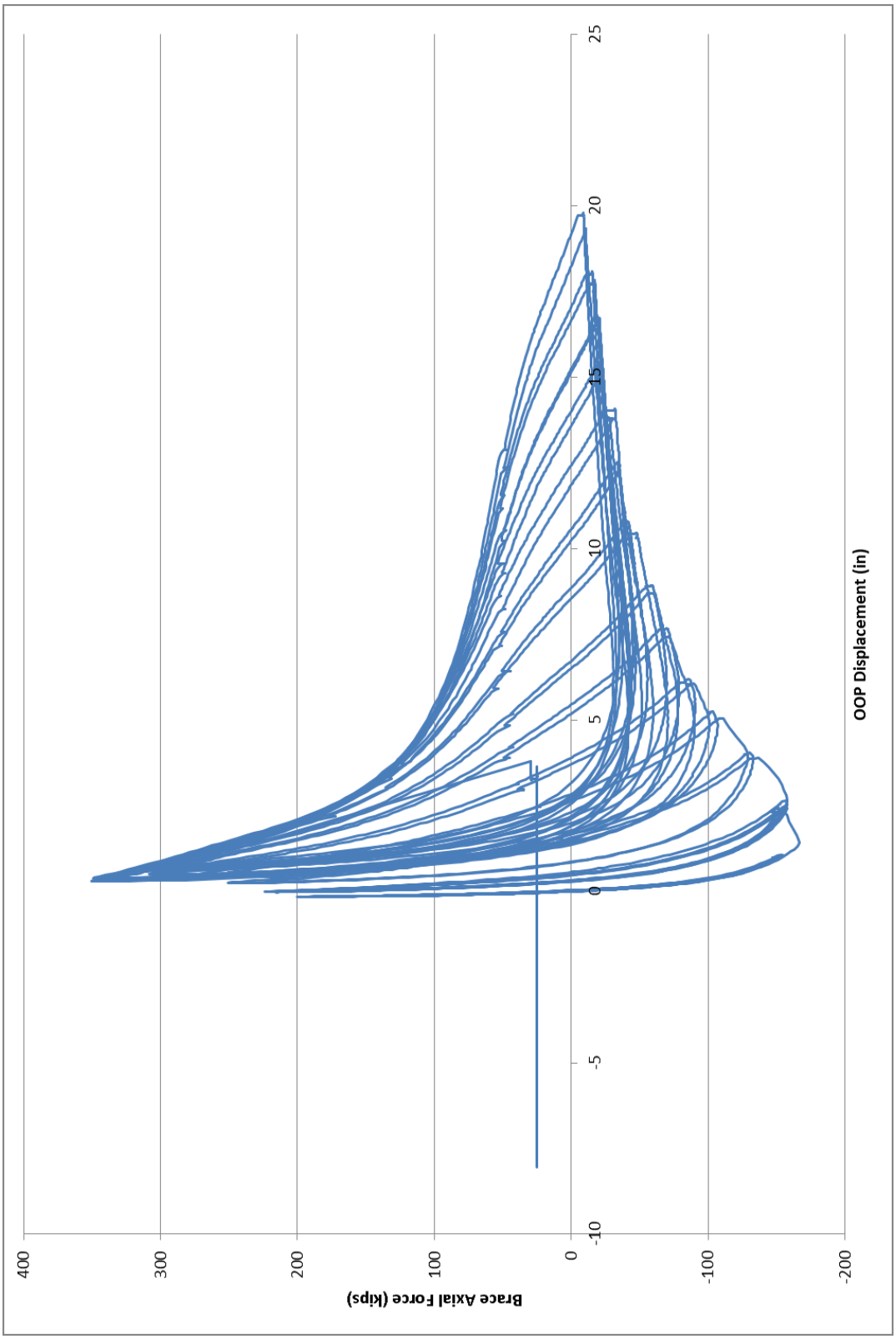

Figure 5.8 – Plot of test results: brace axial force vs. OOP displacement

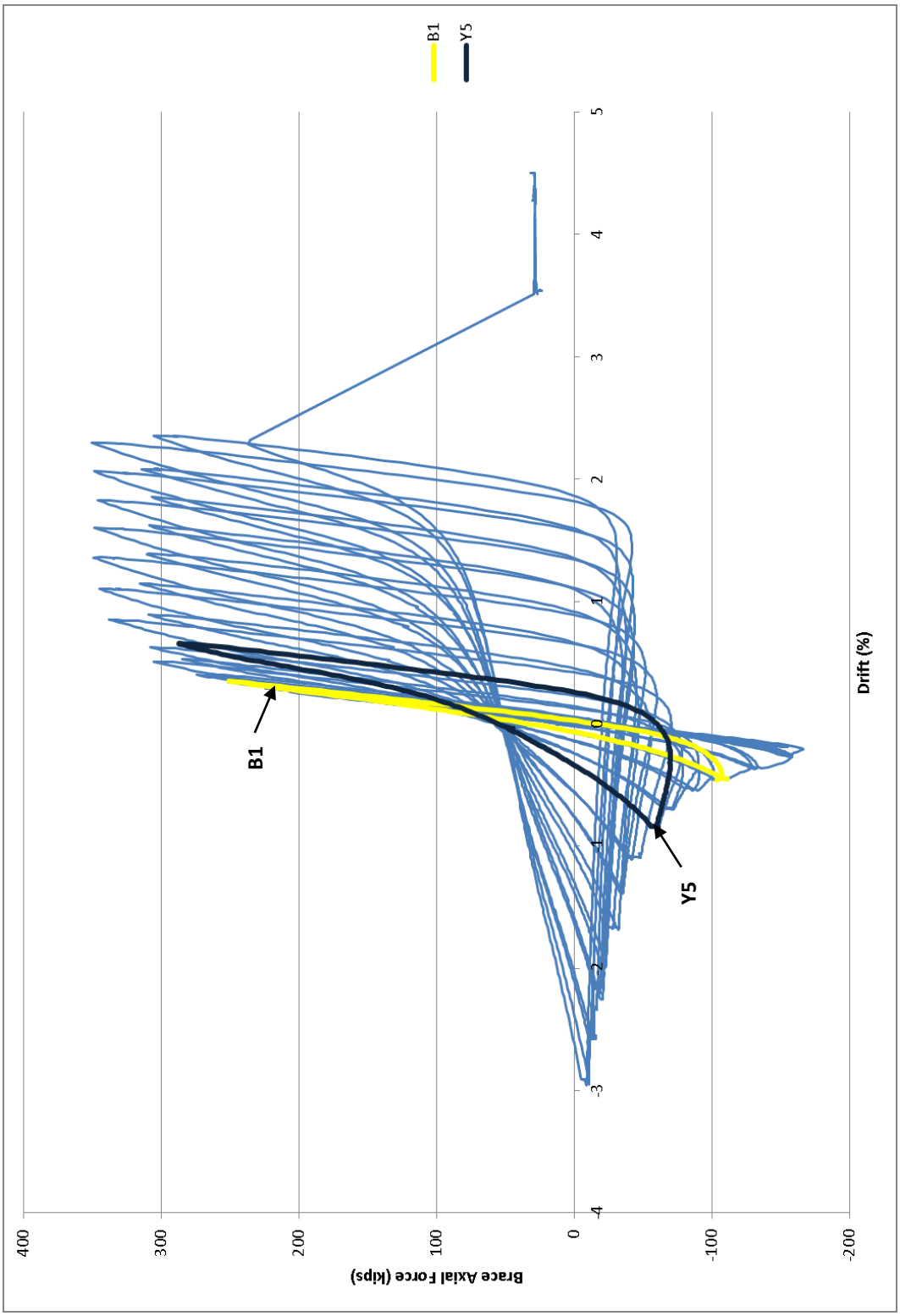

Figure 5.9 – Brace hysteresis curve with the emphasis on B1 and Y5 cycles

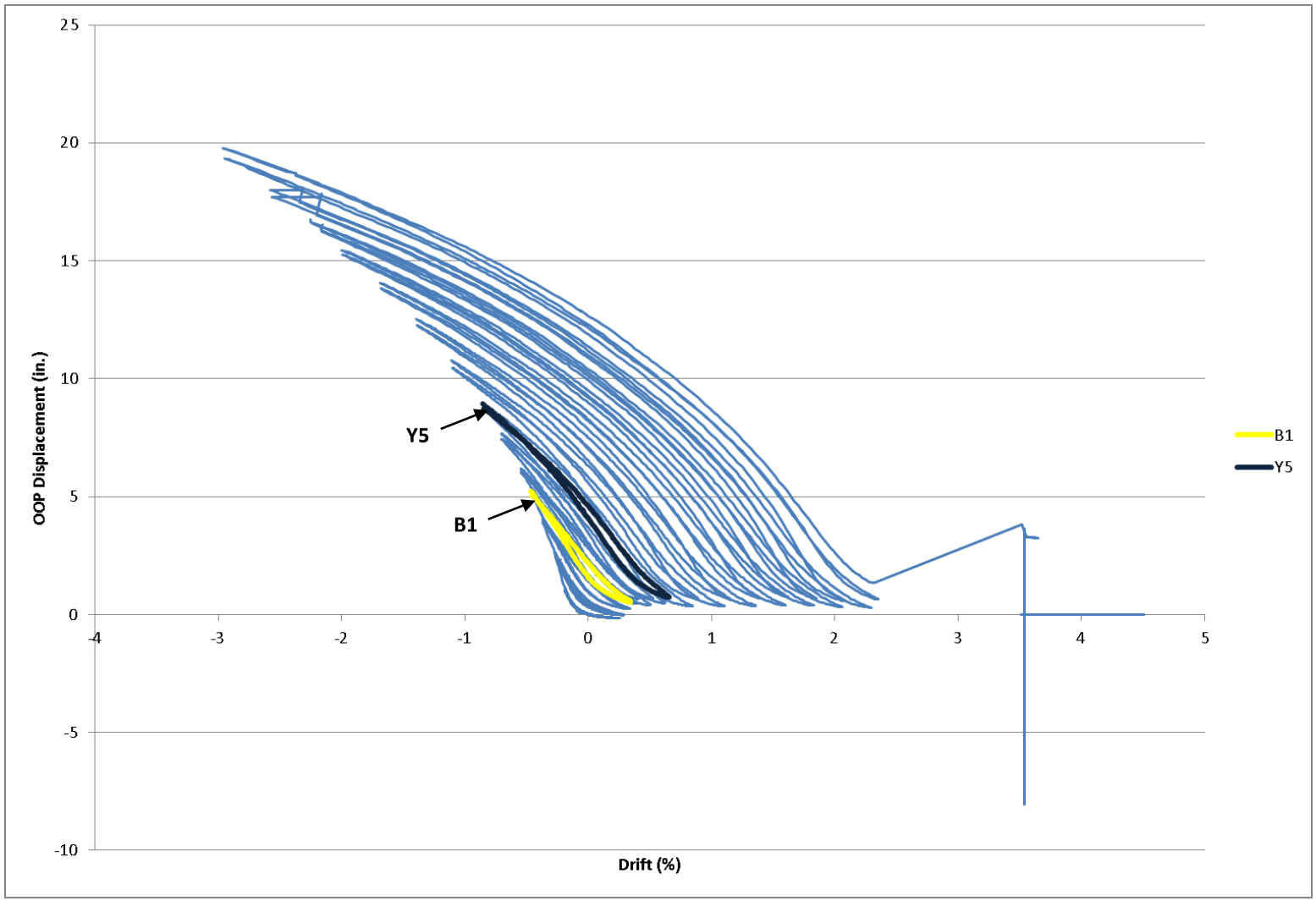

Figure 5.10 – OOP displacement vs. drift plot with the emphasis on B1 and Y5 cycles

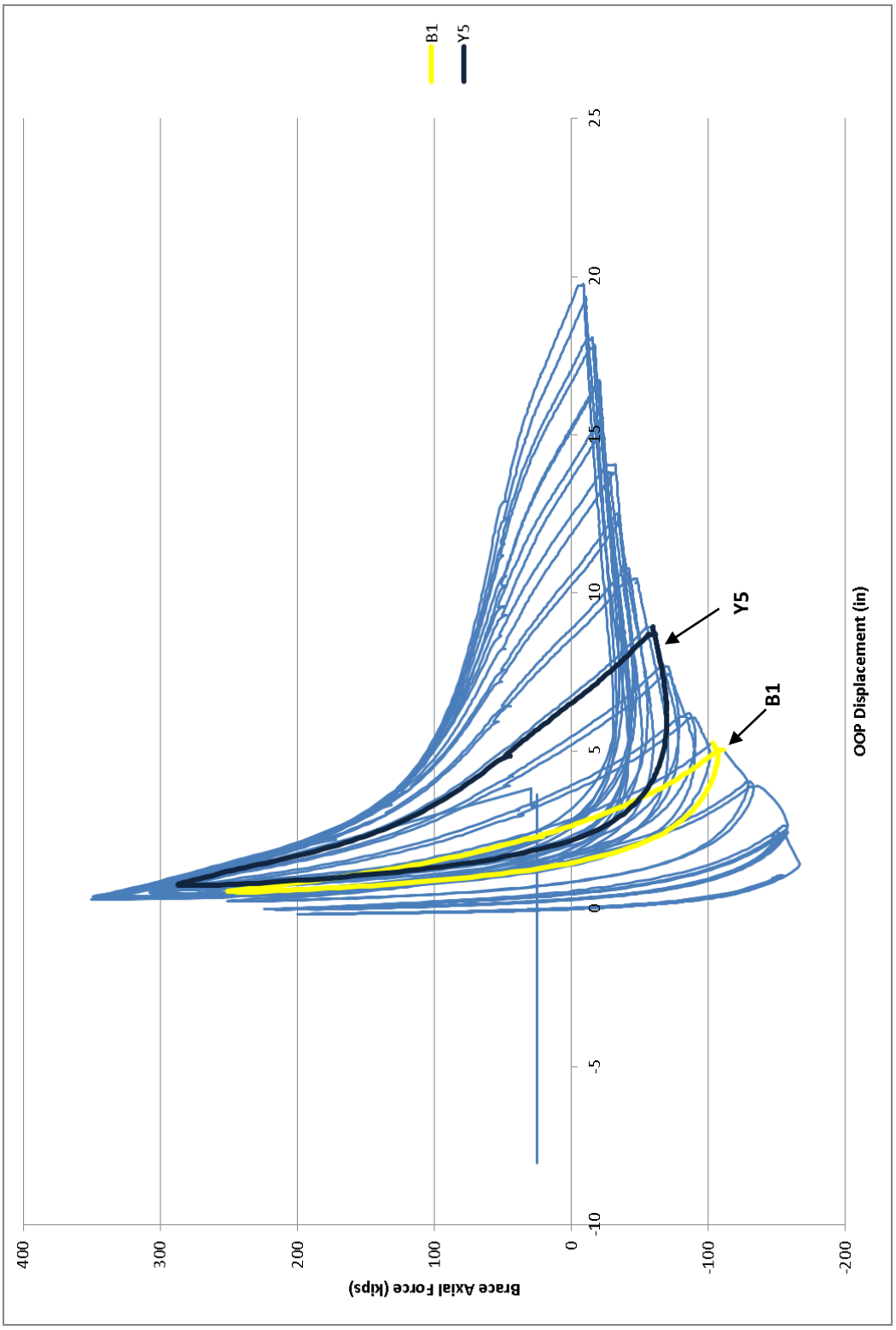

Figure 5.11 – Brace axial force vs. OOP displacement plot with the emphasis on B1 and Y5 cycles

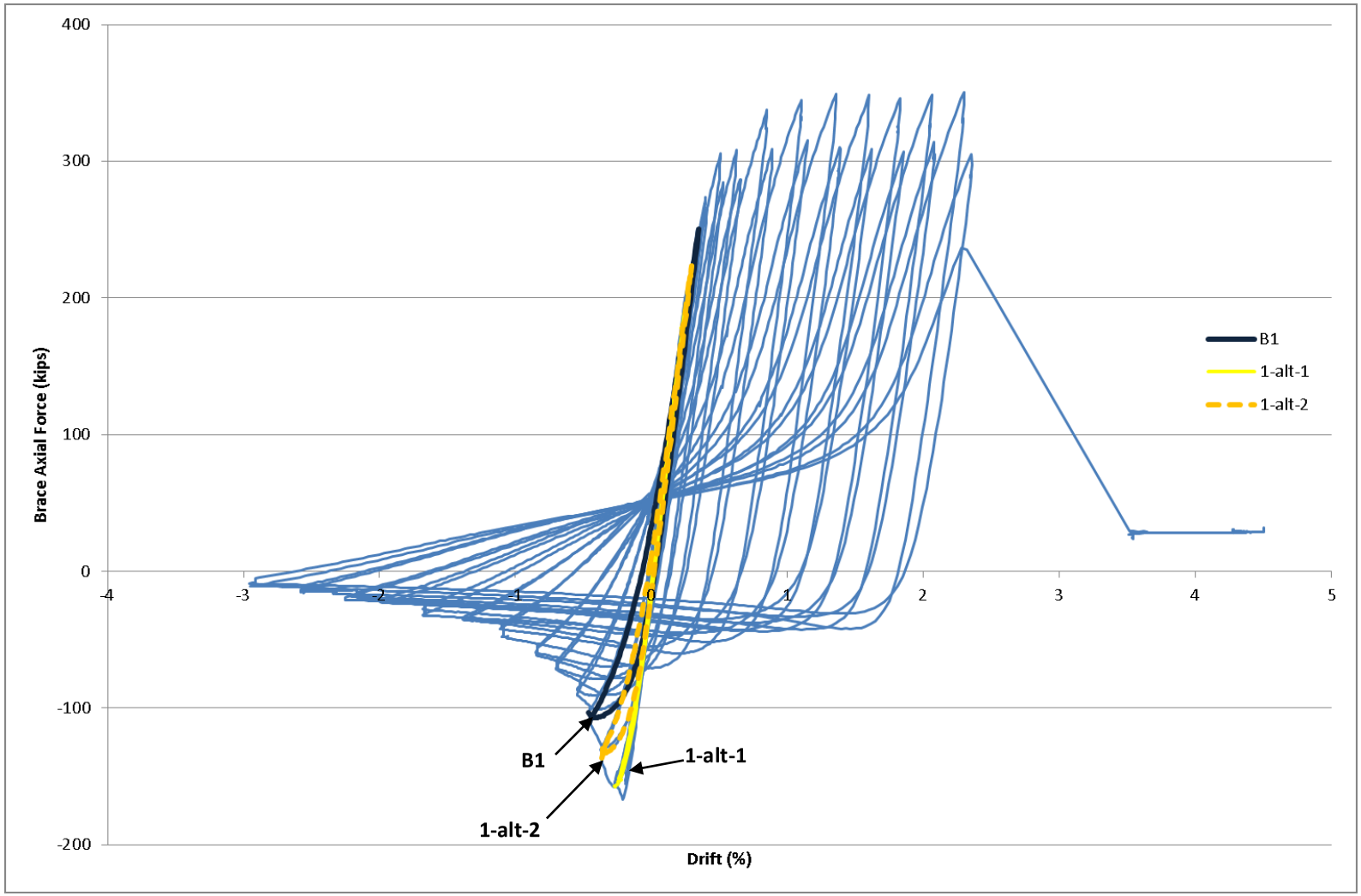

Figure 5.12 – Brace hysteresis curve with the emphasis on B1 cycle, cycle 1-alt-1 and cycle 1-alt-2

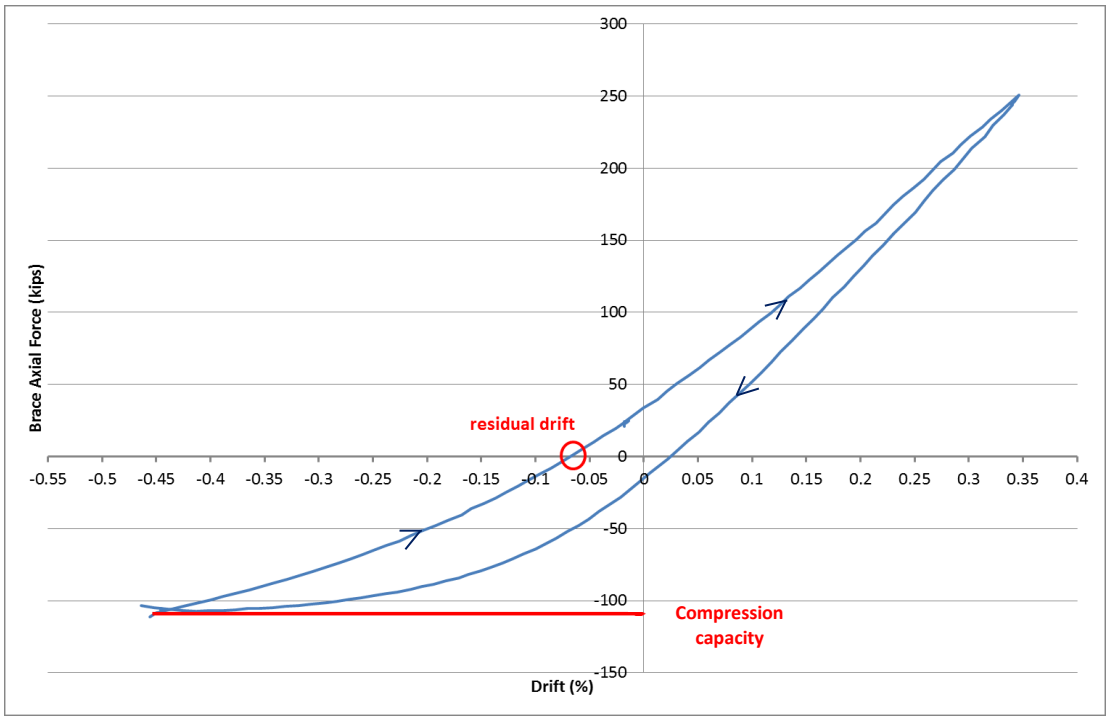

Figure 5.13 – Brace axial force vs. drift plot for cycle B1

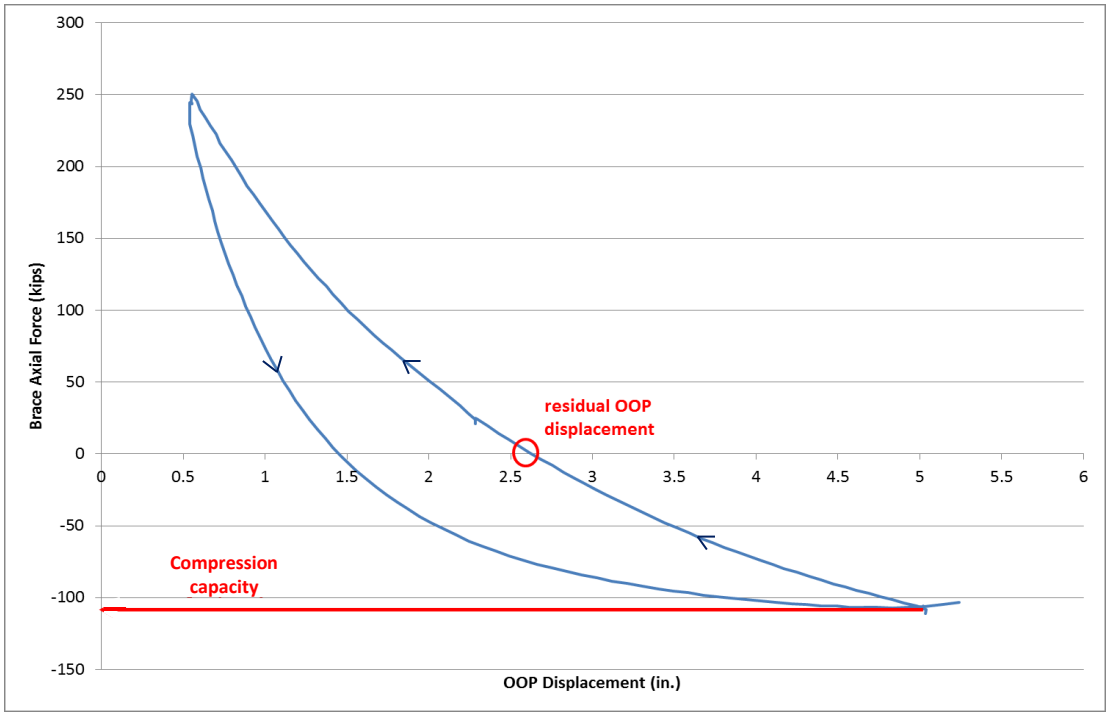

Figure 5.14 – Brace axial force vs. OOP displacement plot for cycle B1

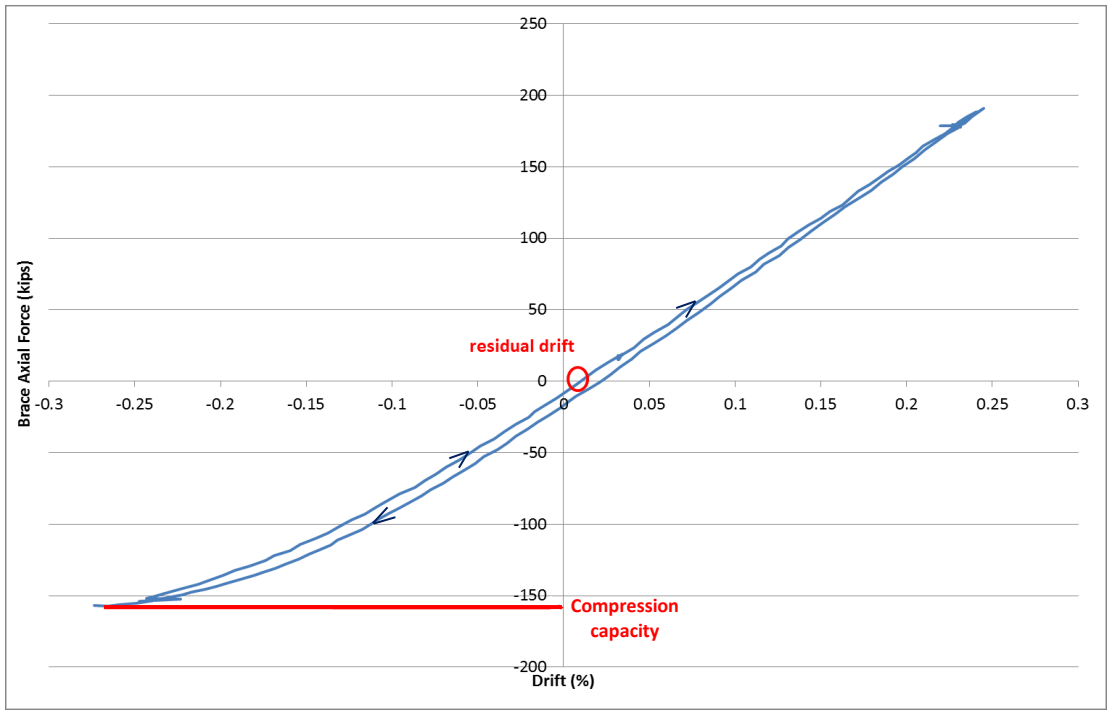

Figure 5.15 – Brace axial force vs. drift plot for cycle 1-alt-1

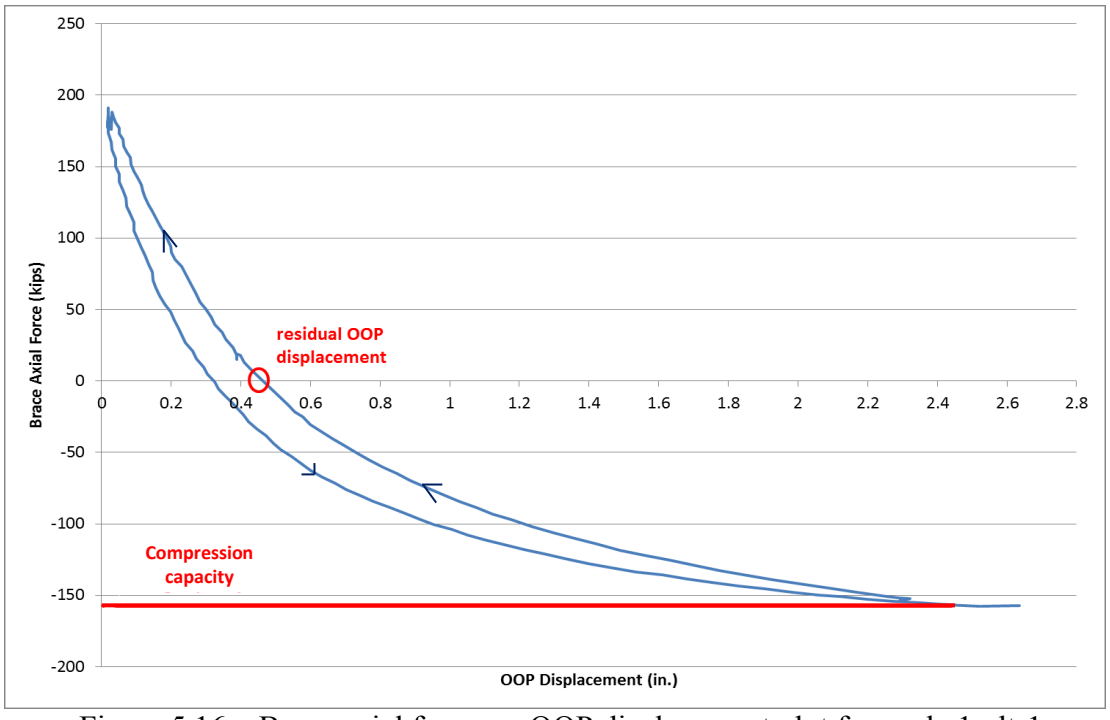

Figure 5.16 – Brace axial force vs. OOP displacement plot for cycle 1-alt-1

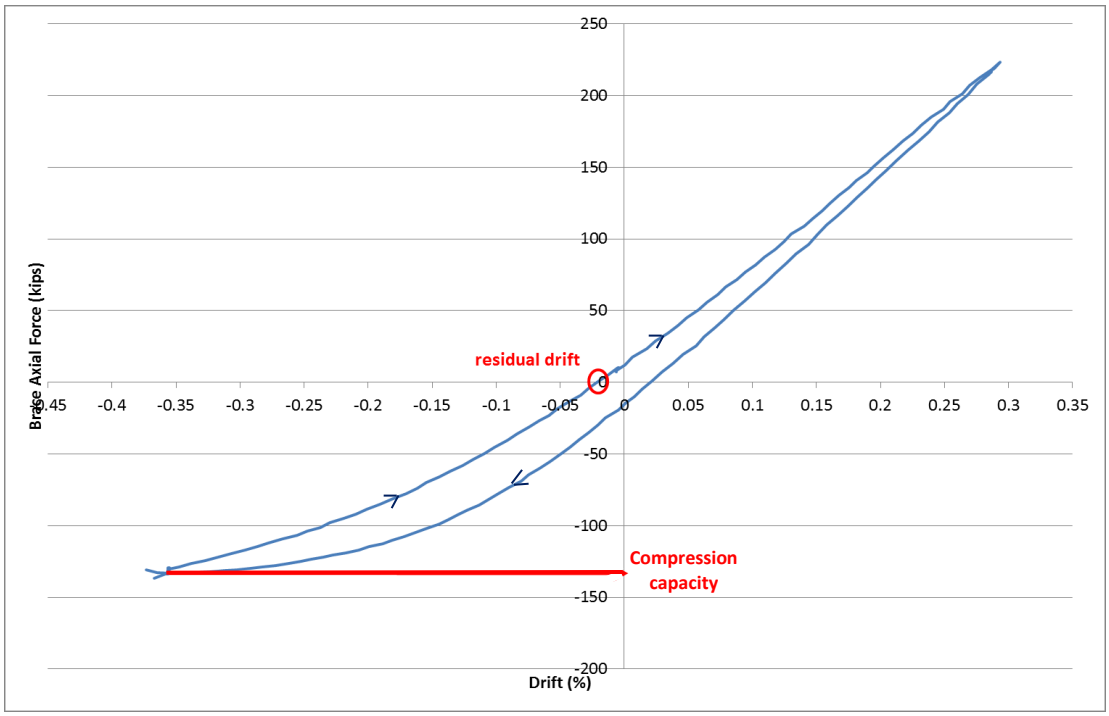

Figure 5.17 – Brace axial force vs. drift plot for cycle 1-alt-2

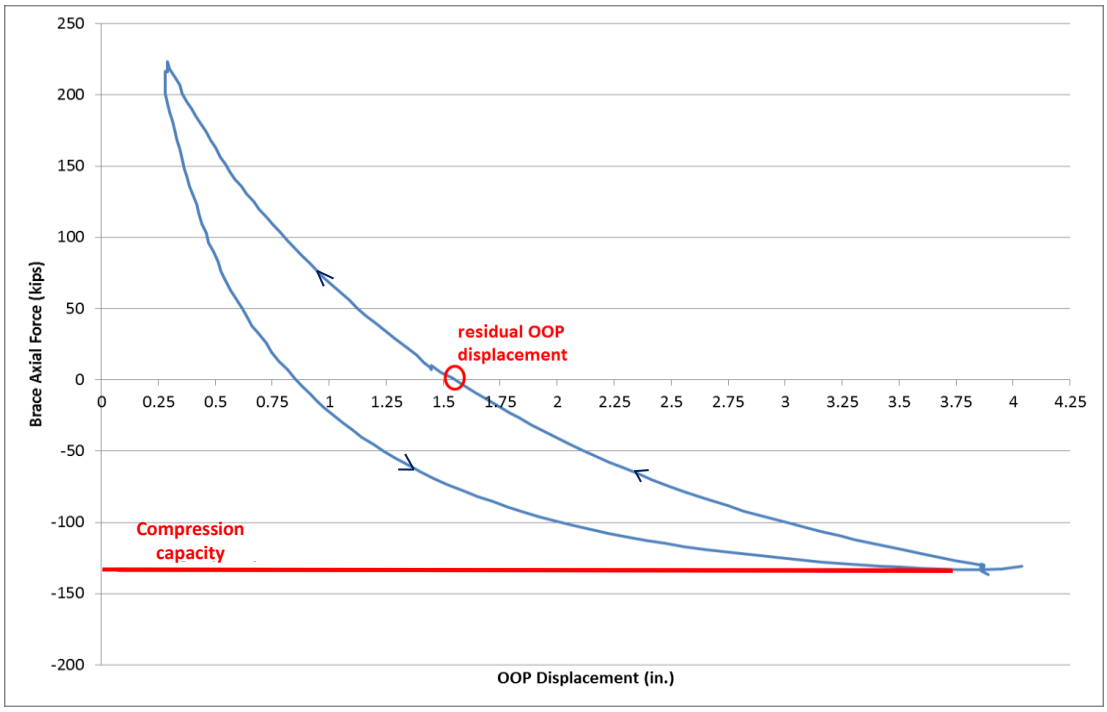

Figure 5.18 – Brace axial force vs. OOP displacement plot for cycle 1-alt-2

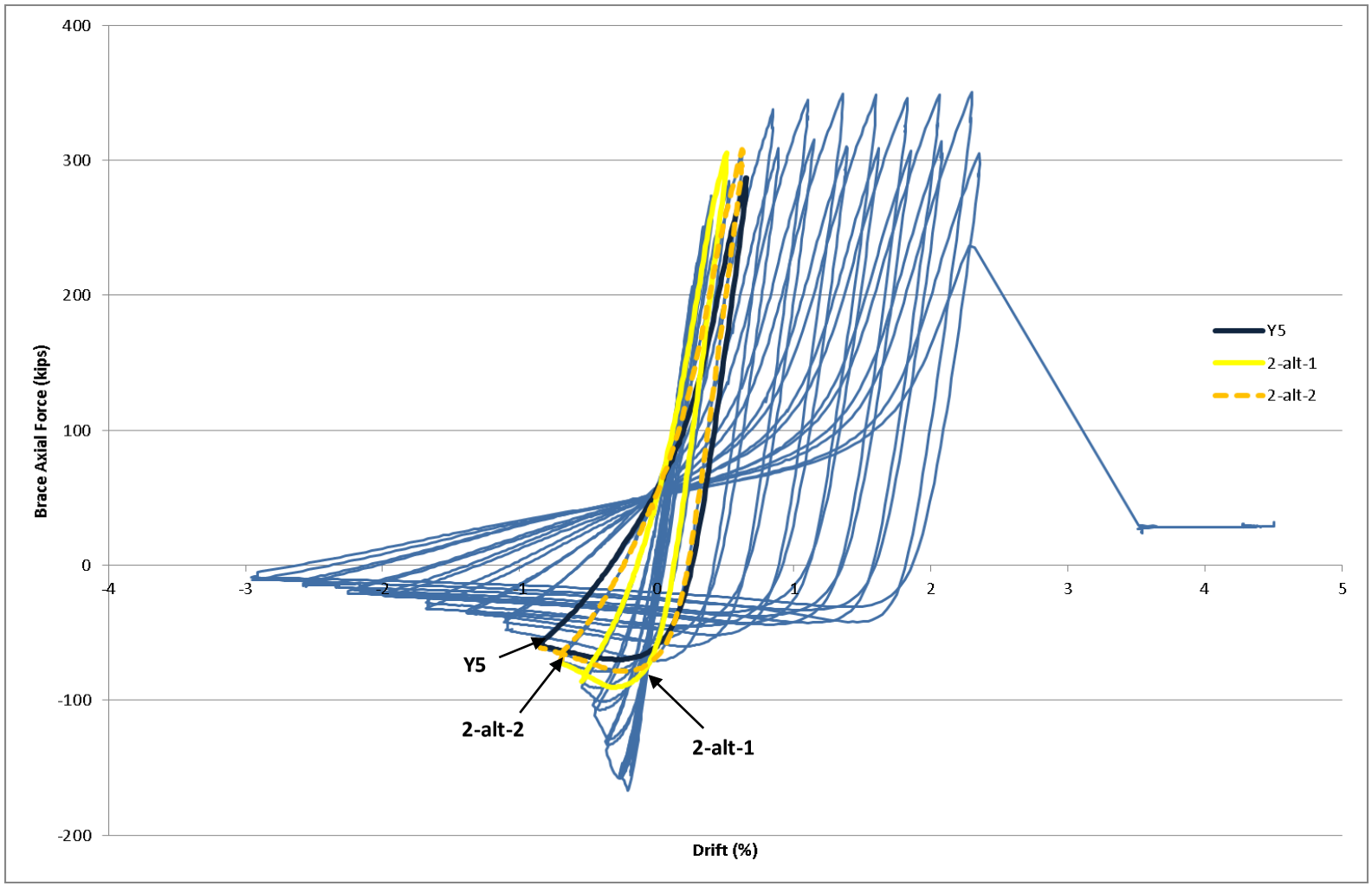

Figure 5.19 – Brace hysteresis curve with the emphasis on Y5 cycle, cycle 2-alt-1 and cycle 2-alt-2

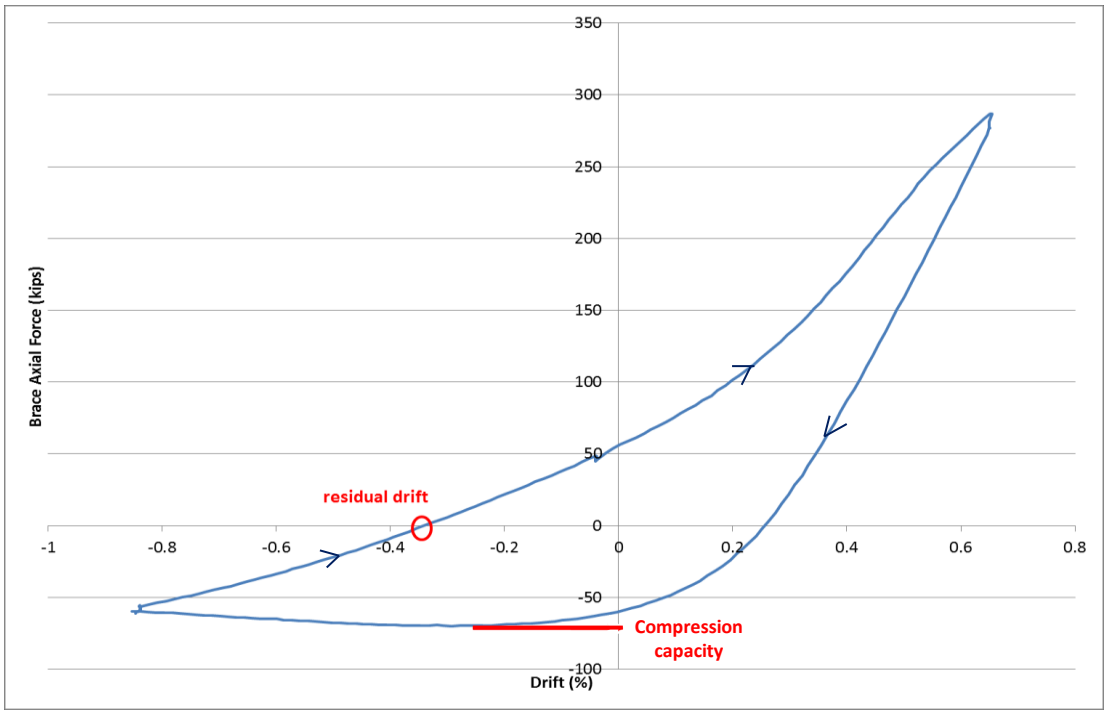

Figure 5.20 – Brace axial force vs. drift plot for cycle Y5

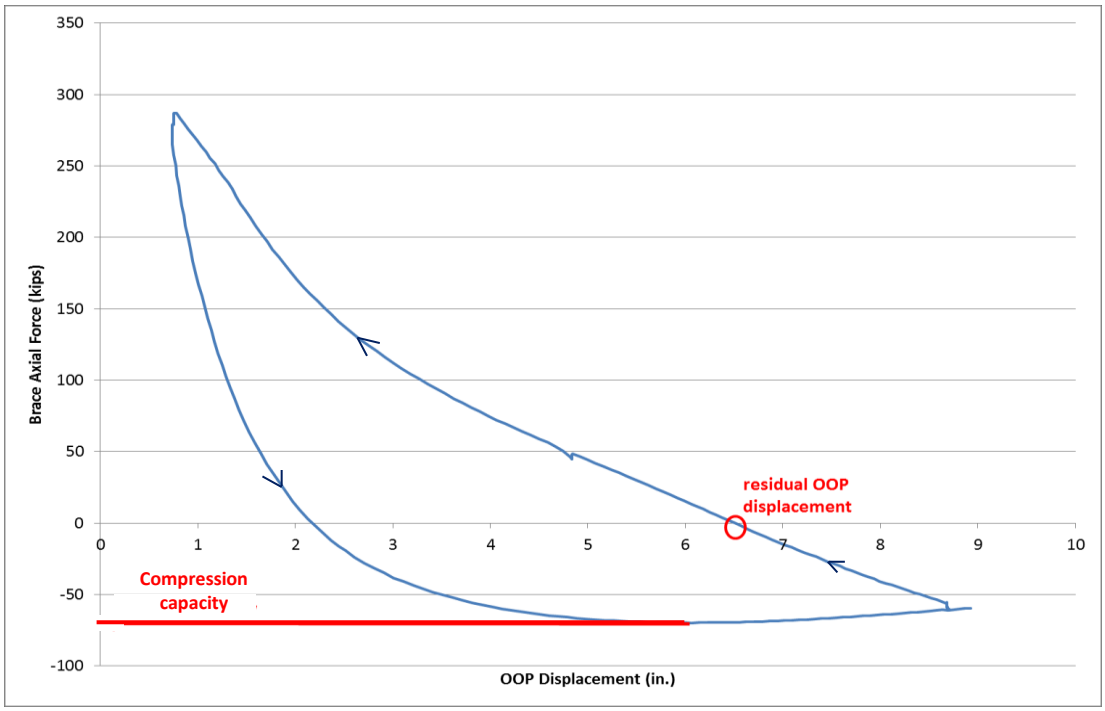

Figure 5.21 – Brace axial force vs. OOP displacement plot for cycle Y5

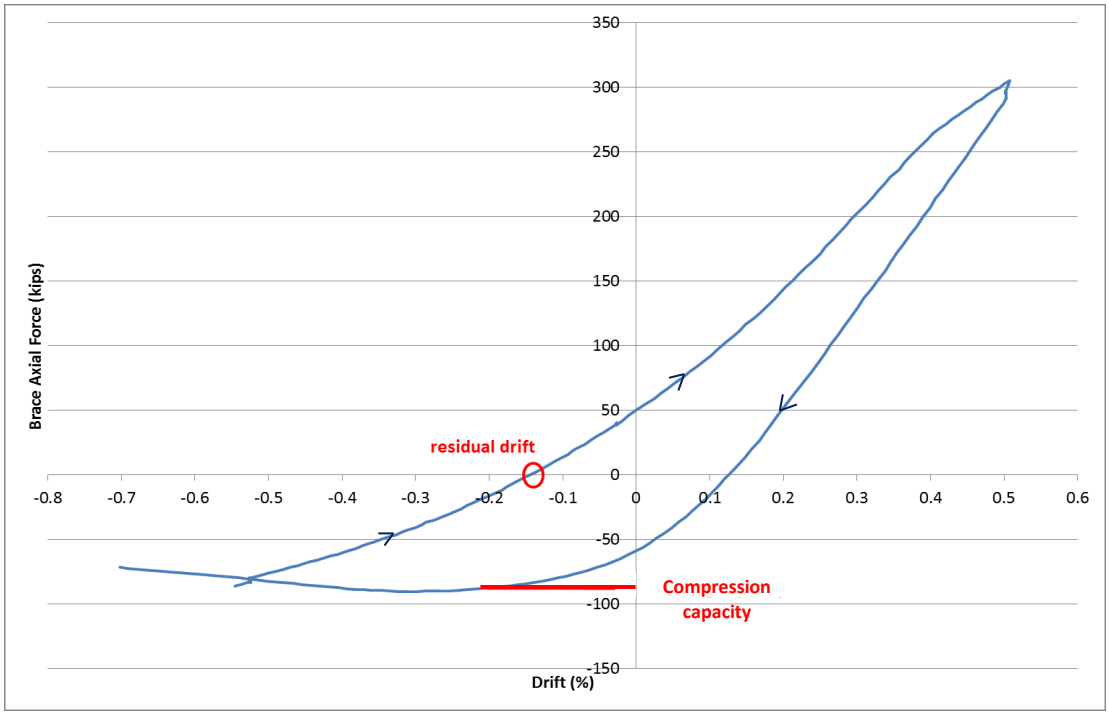

Figure 5.22 – Brace axial force vs. drift plot for cycle 2-alt-1

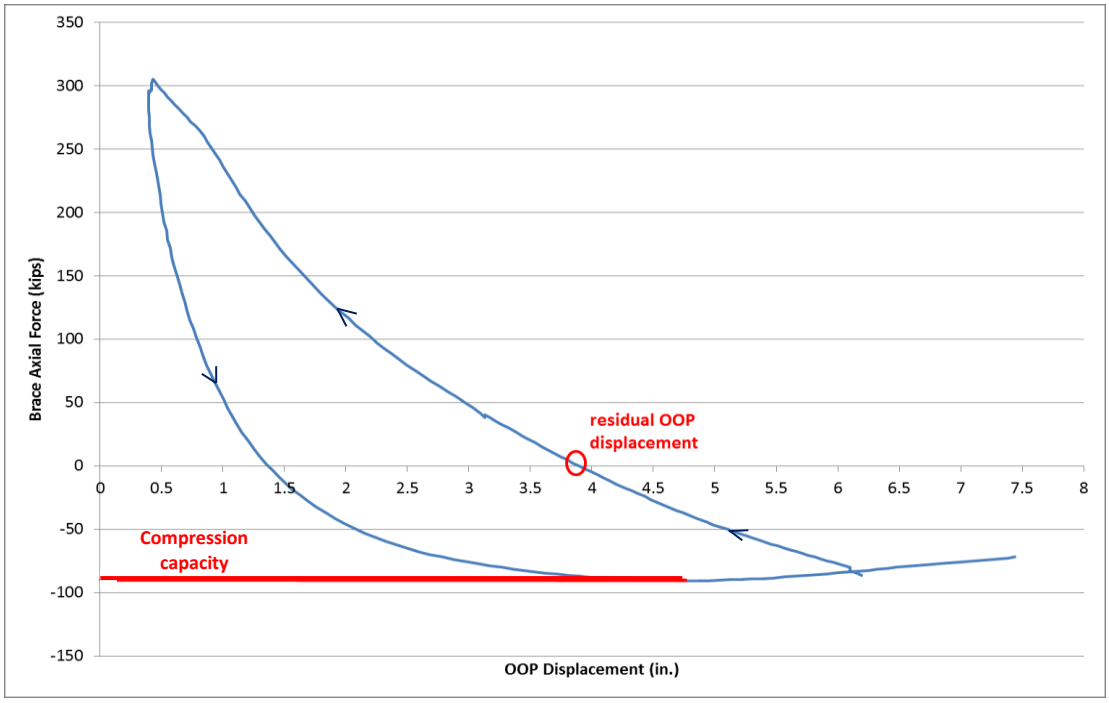

Figure 5.23 – Brace axial force vs. OOP displacement plot for cycle 2-alt-1

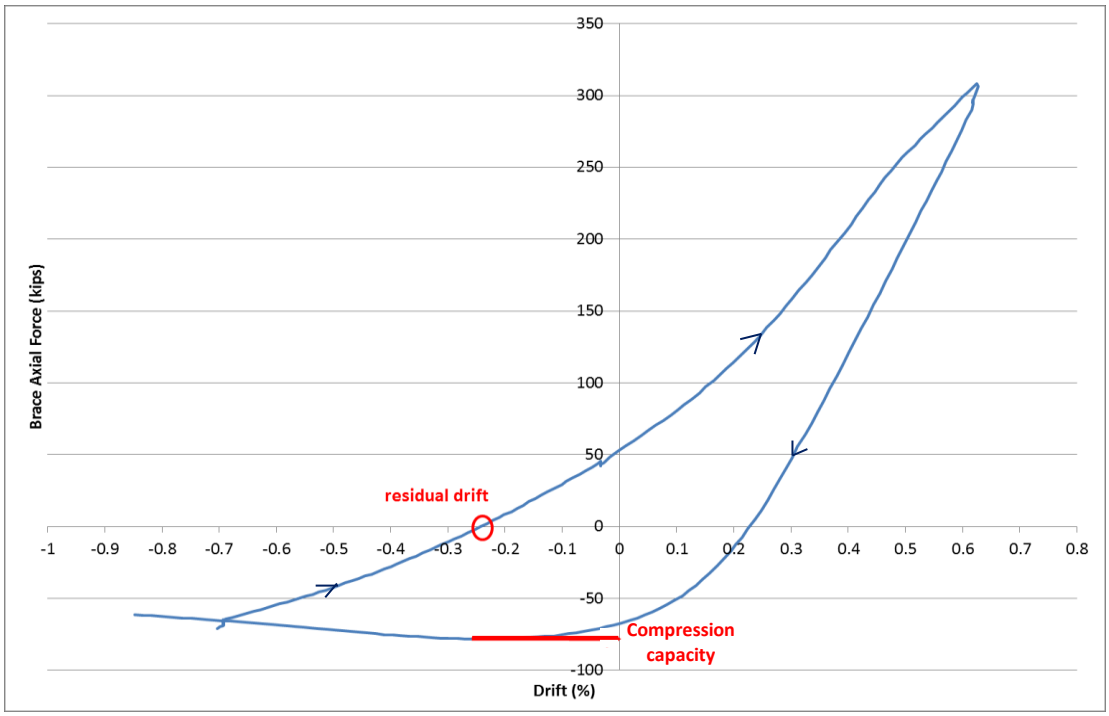

Figure 5.24 – Brace axial force vs. drift plot for cycle 2-alt-2

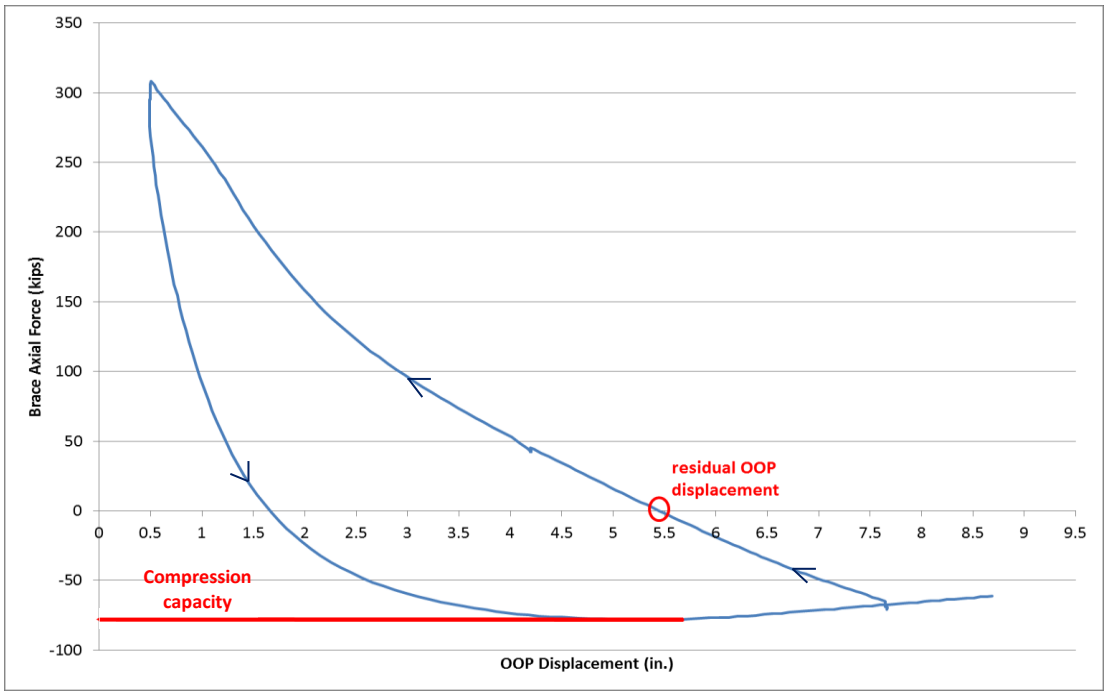

Figure 5.25 – Brace axial force vs. OOP displacement plot for cycle 2-alt-2

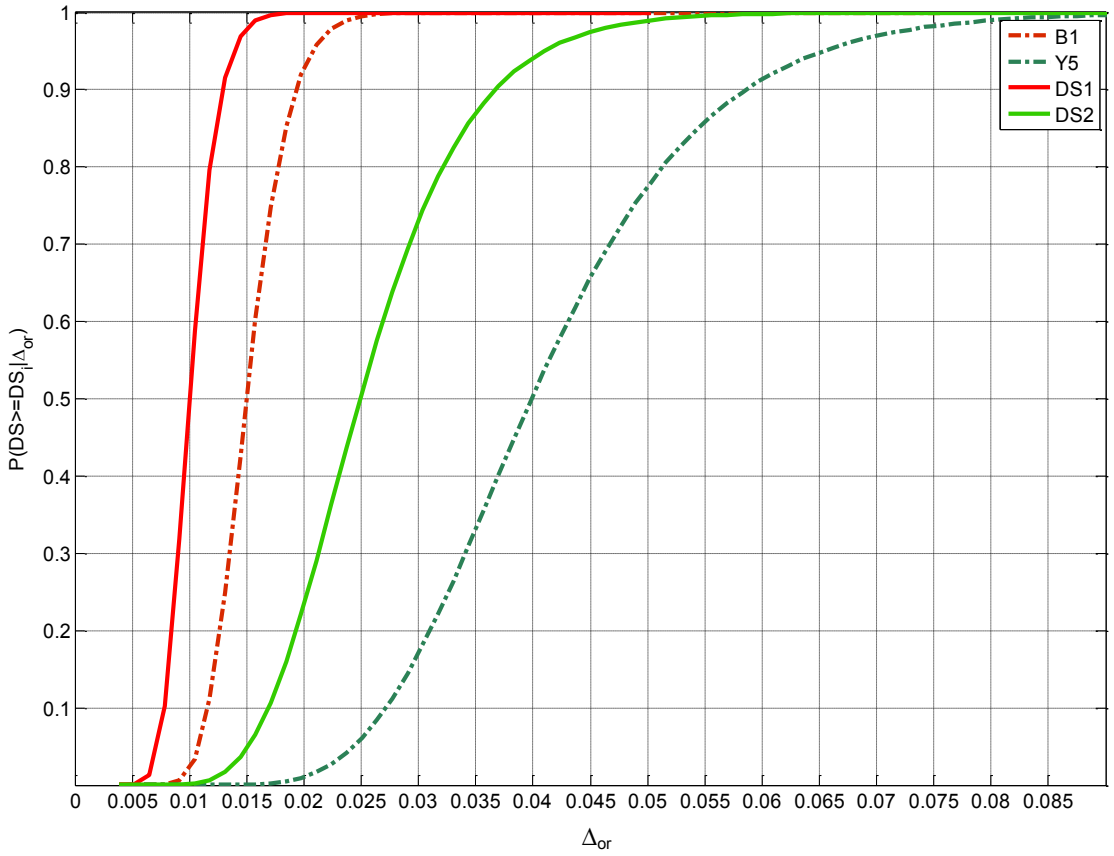

Figure 5.26 – Brace damage fragility functions for DS_1, DS_2, B1, and Y5

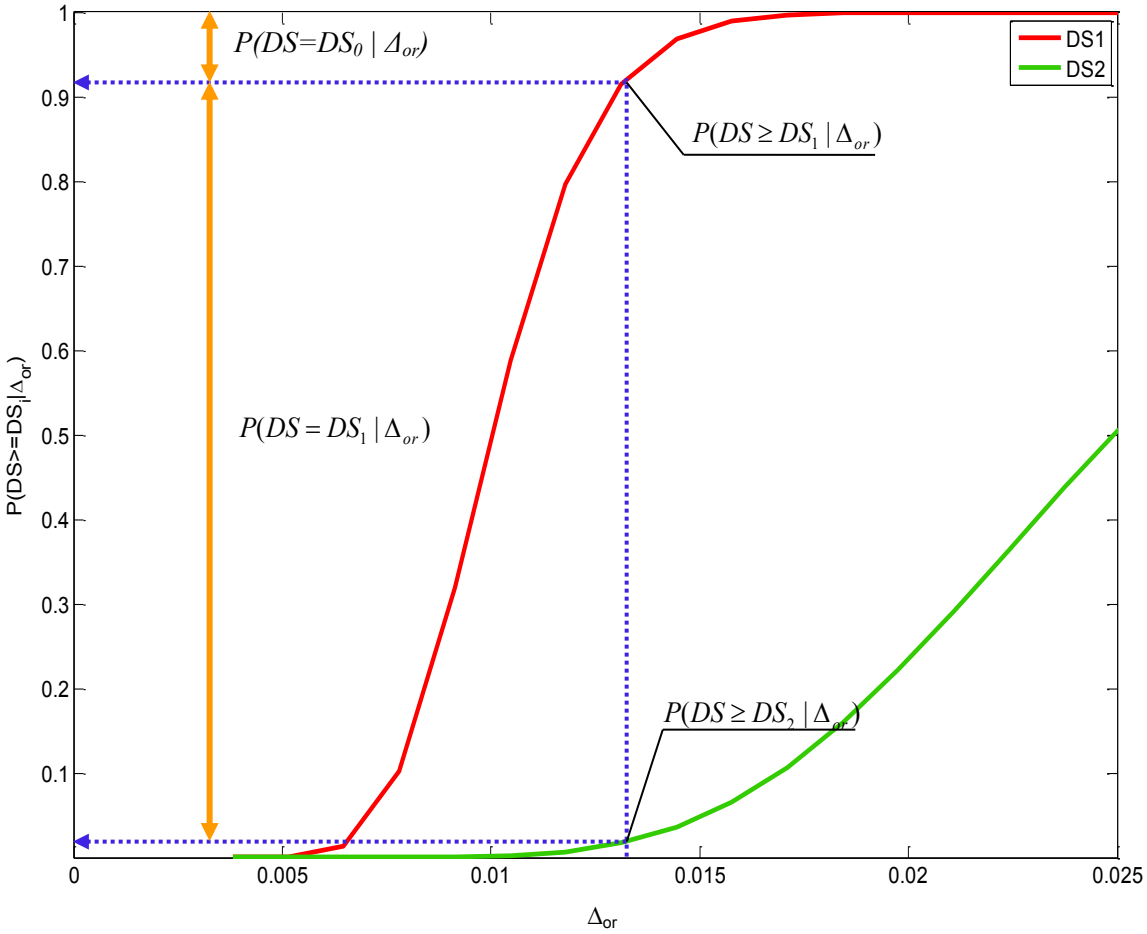

Figure 5.27 –Conditional individual damage state probabilities

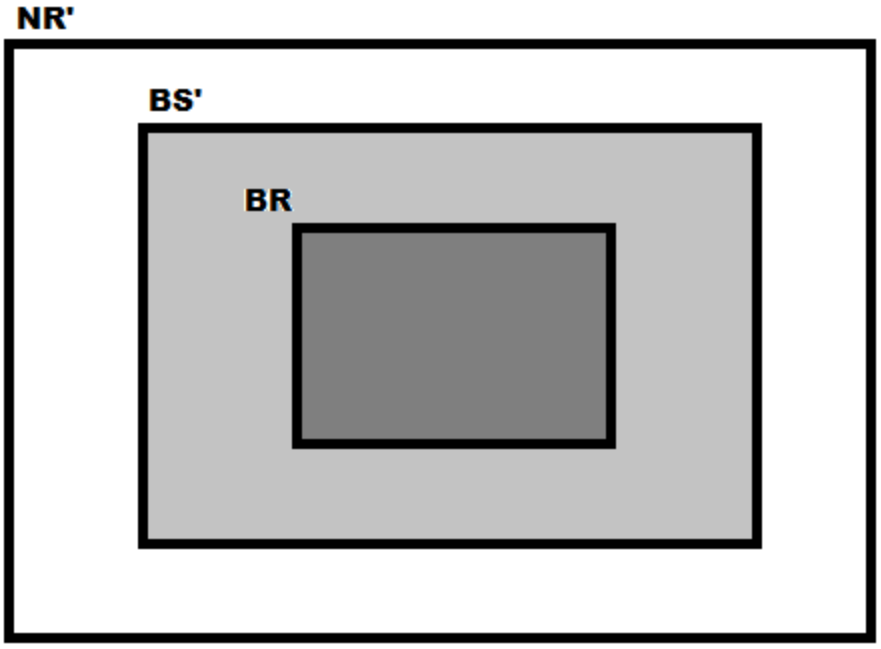

Figure 5.28 – Illustration of repair actions NR', BS' and BR with a Venn diagram

CHAPTER 6

PROBABILISTIC EARTHQUAKE STRUCTURAL DAMAGE ASSESSMENT

6.1 General

The assessment of building damage and the assessment of brace damage were explained in Chapter 4 and 5, treating these damage events as individual events. However, the structural damage in a building during earthquake loading should be assessed considering them as possibly correlated events. In this chapter, an event tree (ET) model is formed and used to understand the possible damage scenarios. A multi-event probabilistic assessment is made to estimate the probability of occurrence of each damage scenario.

The performance of the model buildings is assessed from the damage scenario probabilities. Results are obtained for all model buildings (4SCBF, 4SC-CBF, 9SCBF, and 9SC-CBF) under both the DBE and MCE level ground motion intensities. The results are compared for each damage scenario.

6.2 Event Tree Analysis

When an initiating event occurs, one or more adverse outcomes may occur. To consider all potential adverse outcomes of the initiating event, the possible sequences of subsequent events should be identified (Ang and Tang, 1984). Event tree analysis (ETA) is used to identify the possible sequences of subsequent events after the initiating event.

The objective of an ETA is to evaluate the probability of all possible outcomes of the initiating event (Ericson, 2005).

An event tree (ET) starts with the initiating event (IE) and proceeds with subsequent pivotal events (PE) until an end state is reached. Ericson (2005) defined the IE as an undesired event that triggers an undesired sequence; the IE is the earthquake loading of the building in this study. PEs were defined by Ericson (2005) as the intermediate events between the IE and the end state. The PEs are mutually exclusive events (Ang and Tang, 1984). In this study, each path in the ET represents a different damage scenario. Calculations of the probability of each event lead to an estimate of the probabilities of occurrence of the damage scenarios.

6.2.1 Event Tree Model

An ET model is created to help visualize the sequence of damage events in each damage scenario. The ET for this study is given in Figure 6.1. According to Figure 6.1, "Building subjected to DBE or MCE (DBE/MCE)" is the IE. There are 3 stages of PE in the ET, listed in their possible occurrence order: PE-1, PE-2 and PE-3. Collapse (C) and non-collapse (NC) events are PE-1 and represent building damage associated with the peak story drift, θ_m. C and NC are mutually exclusive events. Demolition (D) and no demolition (ND) events are PE-2 and represent building damage associated with the peak residual story drift, θ_r. D and ND are also mutually exclusive events. No brace repair (NR), brace straightening (BS) and brace replacement (BR) events are PE-3; these events

represent repair actions corresponding to the brace damage associated with the normalized brace residual out-of-plane displacement, Δ_{or}.

It should be noted that the occurrence of each PE in the ET depends on a different engineering demand parameter (EDP) as described in Chapters 4 and 5. To recall, θ_m is the EDP chosen for the C/NC event assessment, θ_r is the EDP chosen for the D/ND assessment, and Δ_{or} is the EDP chosen for the NR/BS/BR assessment.

6.2.2 Damage Scenarios

There are 5 paths in the ET. Each path represents a different damage scenario. The paths for each damage scenario are shown schematically in Figure 6.2. The damage scenarios are as follows:

Damage Scenario # 1 (D.S.#1): Building collapse occurs because of a large θ_m. There is no need for further damage assessment since collapse (C) causes a total loss of the building.

Damage Scenario # 2 (D.S.#2): The building does not collapse (NC) but the building is demolished. θ_m is not large enough to cause building collapse; however θ_r is large enough to make repair infeasible so that the decision is made to demolish the building. There is no need for further damage assessment since demolition (D) causes a total building loss.

Damage Scenario # 3 (D.S.#3): The building does not collapse (NC), and is not demolished (ND), and no repair (NR) is needed in the braces. θ_m and θ_r are not large enough for building collapse or building demolition. A component-based damage

assessment is performed for the braces. The normalized brace residual out-of-plane displacement, Δ_{or}, is not significant and corresponds to brace damage state DS_0 or NR.

Damage Scenario # 4 (D.S.#4): The building does not collapse (NC), and is not demolished (ND). Brace straightening (BS) is needed. θ_m and θ_r are not large enough for building collapse or building demolition. Δ_{or} is in the range corresponding to brace damage state DS_1 or BS.

Damage Scenario # 5 (D.S.#5): The building does not collapse (NC) and is not demolished (ND). Brace replacement (BR) is needed. θ_m and θ_r are not large enough for building collapse or building demolition. There is a significant Δ_{or} in the braces in the range corresponding to brace damage state DS_2 or BR.

It should be noted that D.S.#3, D.S.#4 and D.S.#5 are simplified. In fact many possible combinations of these scenarios could occur as the various brace components in the building can be in different damage states. Therefore, these damage scenarios are assessed for each individual brace in the model buildings.

6.3 Event Tree Probabilistic Assessment

The probabilities of building C/NC, building D/ND and brace damage (NR/BS/BR) were explained in detail in Chapters 4 and 5, treating each case as an individual damage event. Figure 6.3 shows these individual damage events using Venn diagrams. As seen in this figure, the individual events fill the sample space independent of the other event occurrences. However, in the study presented in this chapter, the damage scenario probabilities are based on a sequence of damage events as illustrated in Figure 6.1.

The multi-event system used in this study can be illustrated using the Venn diagram shown in Figure 6.4. According to this representation, the damage events share the same sample space. The damage events have independent occurrences, however the events depend on random variables (EDPs) which are correlated. The EDPs used in this study, namely θ_m, θ_r and Δ_{or}, represent different aspects of the structural response of the same building to earthquake loading. Therefore they are correlated with each other.

The probability of a particular damage scenario is the product of the probabilities of the events in the scenario path (Ang and Tang, 1984). For statistically independent events, the product of the probabilities of each event corresponds to the probability of the intersection of those events (Ang and Tang, 2007). The probability of the intersection denotes the probability that all events in the scenario path occur.

Using this approach, the probability of the damage scenarios defined in Section 6.2 can be obtained as follows:

$$P(D.S.\#1) = P(C) \tag{6.1}$$

$$P(D.S.\#2) = P(NC \cap D) = P(NC) \cdot P(D) \tag{6.2}$$

$$P(D.S.\#3) = P(NC \cap ND \cap NR) = P(NC) \cdot P(ND) \cdot P(NR) \tag{6.3}$$

$$P(D.S.\#4) = P(NC \cap ND \cap BS) = P(NC) \cdot P(ND) \cdot P(BS) \tag{6.4}$$

$$P(D.S.\#5) = P(NC \cap ND \cap BR) = P(NC) \cdot P(ND) \cdot P(BR) \tag{6.5}$$

where,

P(D.S.#1) = the probability of damage scenario # 1

P(D.S.#2) = the probability of damage scenario # 2

P(D.S.#3) = the probability of damage scenario # 3

P(D.S.#4) = the probability of damage scenario # 4

P(D.S.#5) = the probability of damage scenario # 5

P(C) = the probability of collapse

P(NC) = the probability of non-collapse

P(D) = the probability of demolition

P(ND) = the probability of no demolition

P(NR) = the probability of no brace repair

P(BS) = the probability of brace straightening

P(BR) = the probability of brace replacement

The event tree probabilistic assessment estimates the probability of occurrence of each damage scenario using Equations 6.1 through 6.5.

In the damage assessment presented in this chapter, the probability estimates presented in Chapter 4 and Chapter 5 are combined considering the ET, and considering the correlation of the EDPs to estimate the damage scenario probabilities. In Chapter 4, the building damage assessment was described in terms of the probabilities of C/NC and

D/ND. In Chapter 5, the damage assessment of the braces was described in terms of the probabilities of repair actions corresponding to damage states in the braces.

In the multi-event system, these individual events are combined. The damage scenarios of this multi-event system are shown schematically in Figure 6.5. In this figure, the median values of the EDP limits for each damage state are indicated. To illustrate the combined assessment simply, the dispersion in these limits is omitted. As shown in this figure, the probabilities of C/NC events are estimated. θ_m is the EDP for the C/NC event assessment. The median value of θ_m corresponding to collapse, $\theta_{m,c,m}$, is 10%. If θ_m is in the NC region, the probabilities of D/ND events are estimated. These probabilities are P(NC∩D) and P(NC∩ND). θ_r is the EDP for the D/ND event assessment. The median value of θ_r corresponding to demolition, $\theta_{r,d,m}$, is 1%. If θ_m is in the NC region and θ_r is in the ND region, the probabilities of NR/BS/BR events are estimated. These probabilities are P(NC∩ND∩NR), P(NC∩ND∩BS), and P(NC∩ND∩BR). Δ_{or} is the EDP for the NR/BS/BR event assessment. The median value of $\Delta_{or,1}$ corresponding to BS, $\Delta_{or,1,m}$, is 1%, and the median value of $\Delta_{or,2}$ corresponding to BR, $\Delta_{or,2,m}$, is 2.5%.

The probability estimate for each damage scenario is explained in the following sections. The probability estimates for D.S.#3, D.S.#4 and D.S.#5 are explained in one section since they are related to brace damage. The probability estimates for D.S.#1 and D.S.#2 are explained in separate sections.

6.3.1 Probability of D.S. #1

P(D.S.#1) is equivalent to P(C). The estimate of P(C) is explained in detail in Chapter 4, where P(C) is calculated as follows:

$$P(C) = \int_0^\infty P(C \mid \theta_m) \cdot f(\theta_m) \cdot d\theta_m \tag{6.6}$$

where,

P(C) = the probability of collapse

$P(C| \theta_m)$ = the probability of collapse for a given θ_m from the collapse fragility function (Chapter 4)

$f(\theta_m)$ = the probability density function (PDF) for θ_m

P(C) is also shown using a Venn diagram in Figure 6.6, where the shaded region represents P(C). Since C and NC are mutually exclusive events, P(NC) can be found as follows:

$$P(NC) = 1 - P(C) \tag{6.7}$$

6.3.2 Probability of D.S. #2

P(D.S.#2) is equivalent to P(NC∩D) which is the probability of NC and D events together. The following equation is used to calculate P(NC∩D) from the total probability theory:

$$P(NC \cap D) = \int_0^\infty \int_0^\infty P(NC \cap D \mid \theta_m, \theta_r) \cdot f(\theta_m, \theta_r) \cdot d\theta_m d\theta_r \quad (6.8)$$

where,

$P(NC \cap D)$ = the probability of NC and D

$P(NC \cap D \mid \theta_m, \theta_r)$ = the probability of NC and D for a given θ_m and θ_r

$f(\theta_m, \theta_r)$ = the joint probability density function (PDF) for θ_m and θ_r

NC and D are independent events since they have two different fragility functions, although they depend on correlated variables. Therefore, Equation 6.8 is simplified as follows:

$$P(NC \cap D) = \int_0^\infty \int_0^\infty \left[P(NC \mid \theta_m, \theta_r) \cdot P(D \mid \theta_m, \theta_r)\right] \cdot f(\theta_m, \theta_r) \cdot d\theta_m d\theta_r \quad (6.9)$$

NC depends on θ_m only and D depends on θ_r only, therefore Equation 6.9 can be simplified further as follows:

$$P(NC \cap D) = \int_0^\infty \int_0^\infty \left[P(NC \mid \theta_m) \cdot P(D \mid \theta_r)\right] \cdot f(\theta_m, \theta_r) \cdot d\theta_m d\theta_r \quad (6.10)$$

where,

$P(NC \mid \theta_m)$ = the probability of non-collapse for a given θ_m from the non-collapse fragility function (Chapter 4)

$P(D|\theta_r)$ = the probability of demolition for a given θ_r from the demolition fragility function (Chapter 4)

$f(\theta_m, \theta_r)$ = the joint probability density function (PDF) for θ_m and θ_r

Although the fragility functions of NC and D are independent, the underlying random variables, θ_m and θ_r, as noted above are correlated. The correlation coefficient ($\rho_{\theta m \theta r}$) is the measure of correlation between these two random variables. To consider this correlation between θ_m and θ_r, the joint PDF is used. The multivariate lognormal probability density function is used to formulate the joint PDF for θ_m and θ_r. Fletcher (2007) gives the multivariate lognormal probability density function as follows:

$$f(x_1,\cdots,x_k) = \frac{1}{(2\pi)^{\frac{k}{2}}|\sum|^{\frac{1}{2}}} \cdot \left(\prod_{i=1}^{k}\left(\frac{1}{x_i}\right)\right) \cdot \exp\left(-\frac{1}{2}(\ln \bar{x} - \bar{\lambda})^T \sum^{-1}\left(\ln \bar{x} - \bar{\lambda}\right)\right) \quad (6.11)$$

$$\ln \bar{x} = \begin{bmatrix} \ln x_1 \\ \vdots \\ \ln x_k \end{bmatrix} \quad (6.12)$$

$$\bar{\lambda} = \begin{bmatrix} \lambda_1 \\ \vdots \\ \lambda_k \end{bmatrix} \quad (6.13)$$

$$\sum = \begin{bmatrix} \zeta_1^2 & \cdots & \rho_{1k}\zeta_1\zeta_k \\ & \ddots & \\ & & \zeta_k^2 \end{bmatrix} \quad (6.14)$$

where,

$x_1,\ldots,x_k$ = the k random variables of the distribution

$\lambda_1, \ldots, \lambda_k$ = the lognormal mean values for the k random variables

$\zeta_1, \ldots, \zeta_k$ = the lognormal standard deviation values for the k random variables

k = the number of random variables

Σ = the covariance matrix

$$\rho_{ij} = \frac{Cov(I,J)}{\sigma_i \ \sigma_j} \tag{6.15}$$

where,

ρ_{ij} = the correlation coefficient between random variables i and j

Cov(I,J) = covariance of random variables i and j

σ_i = the standard deviation for random variable i

σ_j = the standard deviation for random variable j

For two random variables θ_m and θ_r, the multivariate lognormal probability density function given in Equation 6.11 is as follows:

$$f(\theta_m,\theta_r) = \frac{1}{(2\pi)|\sum|^{\frac{1}{2}}} \cdot \left(\frac{1}{\theta_m \cdot \theta_r}\right) \cdot \exp\left(-\frac{1}{2}(\ln \bar{x} - \bar{\lambda})^T \sum^{-1} \left(\ln \bar{x} - \bar{\lambda}\right)\right) \tag{6.16}$$

$$\ln \bar{x} = \begin{bmatrix} \ln \theta_m \\ \ln \theta_r \end{bmatrix} \tag{6.17}$$

$$\overline{\lambda} = \begin{bmatrix} \lambda_m \\ \lambda_r \end{bmatrix} \tag{6.18}$$

$$\Sigma = \begin{bmatrix} \zeta_m^2 & \rho_{\theta m,\theta r}\zeta_m\zeta_r \\ \rho_{\theta m,\theta r}\zeta_m\zeta_r & \zeta_r^2 \end{bmatrix} \tag{6.19}$$

where,

θ_m = the peak story drift

θ_r = the peak residual story drift

λ_m = the lognormal mean of θ_m

λ_r = the lognormal mean of θ_r

ζ_m = the lognormal standard deviation of θ_m

ζ_r = the lognormal standard deviation of θ_r

$\rho_{\theta m,\theta r}$ = the correlation coefficient between θ_m and θ_r

Equation 6.16 can also be written in the following scalar form, which is the lognormal bivariate probability density function (Ang and Tang, 2007):

$$f(\theta_m,\theta_r) = \frac{1}{(2\pi)\zeta_m\zeta_r\sqrt{1-\rho_{\theta m,\theta r}^2}}\cdot\left(\frac{1}{\theta_m\cdot\theta_r}\right)\cdot$$
$$\exp\left(-\frac{1}{2\left(1-\rho_{\theta m,\theta r}^2\right)}\left\{\left(\frac{\ln\theta_m-\lambda_m}{\zeta_m}\right)^2-2\rho_{\theta m,\theta r}\left(\frac{\ln\theta_m-\lambda_m}{\zeta_m}\right)\left(\frac{\ln\theta_r-\lambda_r}{\zeta_r}\right)+\left(\frac{\ln\theta_r-\lambda_r}{\zeta_r}\right)^2\right\}\right) \tag{6.20}$$

A Venn diagram is given in Figure 6.7 where P(NC∩D) is represented by the shaded region. As seen in this figure, the portion of D intersecting with NC is the region representing P(NC∩D). Although D has a portion intersecting with C, the probability of building demolition and building collapse is not of interest. As discussed earlier, C/NC depends on the θ_m response, and D/ND depends on the θ_r response. When a θ_m value obtained from nonlinear dynamic earthquake response analysis for a given ground motion is in the NC region, the θ_r value obtained for the same ground motion may be either in the D region or in the ND region. Therefore, the shaded region representing P(NC∩D) in Figure 6.7 represents the case when θ_m is in the NC region and θ_r is in the D region.

These relationships are shown mathematically with the following equations:

$$P(C) = P(C \cap D) + P(C \cap ND) \tag{6.21}$$

$$P(NC) = P(NC \cap D) + P(NC \cap ND) \tag{6.22}$$

or

$$P(D) = P(D \cap C) + P(D \cap NC) \tag{6.23}$$

$$P(ND) = P(ND \cap C) + P(ND \cap NC) \tag{6.24}$$

P(NC∩D) is calculated by using Equations 6.10 and 6.20 considering the correlation between θ_m and θ_r. As seen in Equation 6.10, the NC and D fragility functions developed in Chapter 4 are used to estimate P(NC∩D).

6.3.3 Probability of Brace Damage Scenarios (D.S.#3, D.S.#4, and D.S.#5)

If the building has not collapsed (NC) and will not be demolished (ND), a building component damage assessment is appropriate. In this study, a damage assessment of the braces was performed. The probabilities of the repair actions corresponding to different brace damage states are estimated for the case when NC and ND events occur. Three brace damage scenarios are considered in this study, namely D.S.#3, D.S.#4 and D.S.#5 which were described in Section 6.2.2. According to these definitions, P(D.S.#3) is equivalent to P(NC∩ND∩NR); P(D.S.#4) is equivalent to P(NC∩ND∩BS); and P(D.S.#5) is equivalent to P(NC∩ND∩BR).

The following equations are used to calculate the probabilities of brace damage scenarios 4 and 5 by using total probability theorem:

$$P(NC \cap ND \cap BS) = \int_0^\infty \int_0^\infty \int_0^\infty P(NC \cap ND \cap BS \mid \theta_m, \theta_r, \Delta_{or}) \cdot f(\theta_m, \theta_r, \Delta_{or}) \cdot d\theta_m d\theta_r d\Delta_{or} \tag{6.25}$$

$$P(NC \cap ND \cap BR) = \int_0^\infty \int_0^\infty \int_0^\infty P(NC \cap ND \cap BR \mid \theta_m, \theta_r, \Delta_{or}) \cdot f(\theta_m, \theta_r, \Delta_{or}) \cdot d\theta_m d\theta_r d\Delta_{or} \tag{6.26}$$

where,

P(NC∩ND∩BS) = the probability of NC and ND and BS

P(NC∩ND∩BR) = the probability of NC and ND and BS

$P(NC \cap ND \cap BS \mid \theta_m, \theta_r, \Delta_{or})$ = the probability of NC and ND and BS for a given θ_m , θ_r and Δ_{or}

$P(NC \cap ND \cap BR \mid \theta_m, \theta_r, \Delta_{or})$ = probability of NC and ND and BR for a given θ_m , θ_r and Δ_{or}

$f(\theta_m, \theta_r, \Delta_{or})$ = the joint probability density function (PDF) for θ_m, θ_r, and Δ_{or}

Events in the damage scenarios are considered as independent events, Equations 6.25 and 6.26 can be simplified as follows:

$$P(NC \cap ND \cap BS) = \int_0^\infty \int_0^\infty \int_0^\infty P(NC \mid \theta_m, \theta_r, \Delta_{or}) \cdot P(ND \mid \theta_m, \theta_r, \Delta_{or}) \cdot P(BS \mid \theta_m, \theta_r, \Delta_{or}) \cdot f(\theta_m, \theta_r, \Delta_{or}) \cdot d\theta_m d\theta_r d\Delta_{or} \quad (6.27)$$

$$P(NC \cap ND \cap BR) = \int_0^\infty \int_0^\infty \int_0^\infty P(NC \mid \theta_m, \theta_r, \Delta_{or}) \cdot P(ND \mid \theta_m, \theta_r, \Delta_{or}) \cdot P(BR \mid \theta_m, \theta_r, \Delta_{or}) \cdot f(\theta_m, \theta_r, \Delta_{or}) \cdot d\theta_m d\theta_r d\Delta_{or} \quad (6.28)$$

NC depends on θ_m only, ND depends on θ_r only, and BS and BR depend on Δ_{or} only; therefore Equations 6.27 and 6.28 can be simplified further as follows:

$$P(NC \cap ND \cap BS) = \int_0^\infty \int_0^\infty \int_0^\infty P(NC \mid \theta_m) \cdot P(ND \mid \theta_r) \cdot P(BS \mid \Delta_{or}) \cdot f(\theta_m, \theta_r, \Delta_{or}) \cdot d\theta_m d\theta_r d\Delta_{or} \quad (6.29)$$

$$P(NC \cap ND \cap BR) = \int_0^\infty \int_0^\infty \int_0^\infty P(NC \mid \theta_m) \cdot P(ND \mid \theta_r) \cdot P(BR \mid \Delta_{or}) \cdot f(\theta_m, \theta_r, \Delta_{or}) \cdot d\theta_m d\theta_r d\Delta_{or} \quad (6.30)$$

where,

$P(NC|\ \theta_m)$ = the probability of non-collapse for a given θ_m from the non-collapse fragility function (Chapter 4)

$P(ND|\ \theta_r)$ = the probability of no demolition for a given θ_r from the no demolition fragility function (Chapter 4)

$P(BS|\ \Delta_{or})$ = the probability of brace straightening for a given Δ_{or} from the brace damage fragility function (i.e., $P(DS=DS_1|\Delta_{or})$ from Equation 5.4)

$P(BR|\ \Delta_{or})$ = the probability of brace replacement for a given Δ_{or} from the brace damage fragility function (i.e., $P(DS=DS_2|\Delta_{or})$ from Equation 5.5)

Although the events in the damage scenarios are independent, the random variables are correlated. To consider the correlation between θ_m, θ_r and Δ_{or} the joint PDF for these three variables is used. The multivariate lognormal probability density function (Equation 6.11) is used to formulate this joint PDF as follows for these three random variables:

$$f(\theta_m,\theta_r,\Delta_{or}) = \frac{1}{(2\pi)^{\frac{3}{2}}|\sum|^{\frac{1}{2}}}\cdot\left(\frac{1}{\theta_m\cdot\theta_r\cdot\Delta_{or}}\right)\cdot\exp\left(-\frac{1}{2}(\ln\bar{x}-\bar{\lambda})^T\sum^{-1}\left(\ln\bar{x}-\bar{\lambda}\right)\right) \tag{6.31}$$

$$\ln\bar{x} = \begin{bmatrix}\ln\theta_m\\ \ln\theta_r\\ \ln\Delta_{or}\end{bmatrix} \tag{6.32}$$

$$\overline{\lambda} = \begin{bmatrix} \lambda_m \\ \lambda_r \\ \lambda_{or} \end{bmatrix} \tag{6.33}$$

$$\Sigma = \begin{bmatrix} \zeta_m^2 & \rho_{\theta m,\theta r}\zeta_m\zeta_r & \rho_{\theta m,\Delta or}\zeta_m\zeta_{or} \\ \rho_{\theta m,\theta r}\zeta_m\zeta_r & \zeta_r^2 & \rho_{\theta r,\Delta or}\zeta_r\zeta_{or} \\ \rho_{\theta m,\Delta or}\zeta_m\zeta_{or} & \rho_{\theta r,\Delta or}\zeta_r\zeta_{or} & \zeta_{or}^2 \end{bmatrix} \tag{6.34}$$

where,

θ_m = the peak story drift

θ_r = the peak residual story drift

Δ_{or} = the residual out of plane displacement at brace mid-length normalized by the brace length

λ_m = the lognormal mean of θ_m

λ_r = the lognormal mean of θ_r

λ_{or} = the lognormal mean of Δ_{or}

ζ_m = the lognormal standard deviation of θ_m

ζ_r = the lognormal standard deviation of θ_r

ζ_{or} = the lognormal standard deviation of Δ_{or}

$\rho_{\theta m,\theta r}$ = the correlation coefficient between θ_m and θ_r

$\rho_{\theta m,\Delta or}$ = the correlation coefficient between θ_m and Δ_{or}

$\rho_{\theta r,\Delta or}$ = the correlation coefficient between θ_r and Δ_{or}

The probability calculations given in Equations 6.29 and 6.30 are used to find the probability of a specific brace damage state when the building is in the NC and ND states. This multi-event probability concept is similar to the single event probability concept explained in Chapter 5, except in a multi-event system there is more than a single event that contributes to the probability.

A Venn diagram illustration of the brace damage scenarios is given in Figure 6.8. A different shaded region represents each damage scenario in the figure. The portion of ND intersecting with NC is the region where brace damage states and subsequent brace repair events are of interest. Since a total building loss occurs from the D and C events, brace repair is not of interest.

The dark grey region in Figure 6.8 represents P(NC∩ND∩BR). P(NC∩ND∩BR) is the probability of being in a brace damage state DS_2 that requires brace replacement (BR) when the building is neither collapsed nor demolished. Here, $\Delta_{or}>\Delta_{or,2}$.

The medium grey region in Figure 6.8 represents P(NC∩ND∩BS), which is the probability of being in brace damage state DS_1 that requires brace straightening (BS) when the building is neither collapsed nor demolished. Here, $\Delta_{or,1}\leq\Delta_{or}<\Delta_{or,2}$.

Similarly, the light grey region in Figure 6.8 represents P(NC∩ND∩NR), which is the probability of being in brace damage state DS_0 that requires no repair (NR) when the building is neither collapsed nor demolished. Here, $\Delta_{or}<\Delta_{or,1}$. P(NC∩ND∩NR) is obtained as follows:

$$P(NC \cap ND \cap NR) = P(NC \cap ND) - P(NC \cap ND \cap BS) - P(NC \cap ND \cap BR) \quad (6.35)$$

Probability of Brace Damage Scenarios – Simplified Methodology

The θ_r values obtained from dynamic analysis for some of the model buildings are very low (see Chapter 4 for details). P(D) is zero (i.e., P(ND) is one) for those buildings since there is no significant θ_r leading to building demolition. The estimate of the probability of the brace damage scenarios can be simplified for the buildings that have very low values of θ_r, which can be treated as θ_r=0.

When P(ND| θ_r) is equal to one, Equations 6.29 and 6.30 can be simplified as follows:

$$P(NC \cap BS \mid ND) = \int_0^\infty \int_0^\infty P(NC \mid \theta_m) \cdot P(BS \mid \Delta_{or}) \cdot f(\theta_m, \Delta_{or}) \cdot d\theta_m d\Delta_{or} \quad (6.36)$$

$$P(NC \cap BR \mid ND) = \int_0^\infty \int_0^\infty P(NC \mid \theta_m) \cdot P(BR \mid \Delta_{or}) \cdot f(\theta_m, \Delta_{or}) \cdot d\theta_m d\Delta_{or} \quad (6.37)$$

where,

P(NC∩BS|ND) = the probability of NC and BS given that building is not demolished

P(NC∩BR|ND) = the probability of NC and BR given that building is not demolished

$$f(\theta_m, \Delta_{or}) = \frac{1}{(2\pi)|\Sigma|^{\frac{1}{2}}} \cdot \left(\frac{1}{\theta_m \cdot \Delta_{or}} \right) \cdot \exp\left(-\frac{1}{2} (\ln \bar{x} - \bar{\lambda})^T \Sigma^{-1} \left(\ln \bar{x} - \bar{\lambda} \right) \right) \quad (6.38)$$

$$\ln \bar{x} = \begin{bmatrix} \ln \theta_m \\ \ln \Delta_{or} \end{bmatrix} \quad (6.39)$$

$$\bar{\lambda} = \begin{bmatrix} \lambda_m \\ \lambda_{or} \end{bmatrix} \quad (6.40)$$

$$\Sigma = \begin{bmatrix} \zeta_m^2 & \rho_{\theta m, \Delta or} \zeta_m \zeta_{or} \\ \rho_{\theta m, \Delta or} \zeta_m \zeta_{or} & \zeta_{or}^2 \end{bmatrix} \quad (6.41)$$

Since θ_r=0, there is no need to consider the correlation of θ_r with θ_m and Δ_{or}. For this reason, the joint PDF for θ_m and Δ_{or} is used in Equations 6.36 and 6.37 which is given by Equation 6.38.

This simplified case is shown by the Venn diagram in Figure 6.9. As seen in this figure, the ND event fills the sample space which means P(ND) is equal to one.

6.4 Event Tree Probability Results

The probabilities of the damage scenarios are estimated as explained in Section 6.3 for the model buildings analyzed in this study. Calculations are performed for both the DBE and MCE intensity levels and reported accordingly for each model building.

6.4.1 Probability of D.S. #1

Equation 6.6 is used to estimate P(D.S.#1), which equals P(C). As mentioned in Chapter 4, the PDF for θ_m in Equation 6.6 is obtained from dynamic earthquake response analysis results, with one value of θ_m for each ground motion at each intensity level. The probability distribution parameters for θ_m were tabulated in Chapter 4 and can be seen in Tables 4.2, 4.3, 4.5 and 4.6 for all model buildings. P(NC) is calculated using Equation 6.7.

Results obtained from the calculations of P(C) and P(NC) for each model building are given in Table 6.1. These results are the same as those shown in Table 4.6. The probability values given in this table are rounded off in order to equate the summation of P(C) and P(NC) to one, since C and NC are mutually exclusive events.

Results given in Table 6.1 show that for all model buildings the P(C) values are very low. The P(NC) values are much larger and very close to 1. This means that collapse is not likely to occur for the model buildings under both the DBE and MCE. There are slight differences observed in the results because of the different CBF systems, number of stories and intensity levels.

For the 4-story model buildings, the 4SCBF building has a slightly larger P(C) than the 4SC-CBF building under both the DBE and MCE. For 9-story model buildings, the situation is opposite; the 9SC-CBF building has a larger P(C) than the 9SCBF building under both the DBE and MCE.

The 9-story model buildings have larger P(C) values than the 4-story model buildings under both ground motion intensity levels. As expected, a larger ground motion intensity, MCE, results in larger P(C) values.

6.4.2 Probability of D.S. #2

Equation 6.10 is used to estimate P(D.S.#2). As seen in Equation 6.10 and discussed in Section 6.3.2, the joint PDF for θ_m and θ_r is used to calculate P(NC∩D) together with the NC and D fragility curves. The joint PDF considers the correlation between the random variables θ_m and θ_r. Dynamic earthquake response analysis results mentioned in Chapter 4 provide the data points needed to develop the PDF (Equation 6.20). Correlation coefficients between θ_m and θ_r data points ($\rho_{\theta m,\theta r}$) for each model building under the DBE and MCE are listed in Table 6.2. According to Table 6.2, there is correlation between θ_m and θ_r since $\rho_{\theta m,\theta r}$ values are non-zero. $\rho_{\theta m,\theta r}$ closer to 1 (or -1) indicates higher correlation between the random variables. Table 6.2 shows that θ_m and θ_r for the 4SCBF have the highest correlation. θ_m and θ_r obtained for the 4SC-CBF under the DBE have the lowest correlation.

The relationship given in Equation 6.22 is solved to determine P(NC∩ND), where P(NC) is from Equation 6.7.

P(NC∩D) and P(NC∩ND) results are obtained from a program coded in MatLab and are given in Table 6.3. The probability values given in this table are rounded off in order to equate the summation of P(NC∩D) and P(NC∩ND) to P(NC) according to Equation 6.22 and Figure 6.7. Results in Table 6.3 show that the P(NC∩D) values are very low

compared to the P(NC∩ND) values for all model buildings both under the DBE and MCE. Results vary for the different CBF systems, number of stories and intensity levels.

For the 4-story model buildings, the 4SCBF has a larger P(NC∩D) than the 4SC-CBF. P(NC∩D) is zero for the 4SC-CBF under both the DBE and MCE, since it has very low θ_r. For 9-story model buildings, the same difference is observed between the 9SCBF and the 9SC-CBF. The 9SCBF has a larger P(NC∩D) than the 9SC-CBF. For the DBE, P(NC∩D) is about 3% for the 9SCBF, but P(NC∩D) is very small ($1x10^{-4}$) for the 9SC-CBF. For the MCE, P(NC∩D) for the 9SCBF is about 26%, while P(NC∩D) is about 10% for the 9SC-CBF. This is an expected result because the rocking behavior of SC-CBFs nearly eliminates residual deformations.

When the results are compared in terms of the number of stories, it is seen that taller buildings have larger P(NC∩D) than the shorter buildings. Unlike the 4SC-CBF, P(NC∩D) is not zero for the 9SC-CBF.

The MCE causes more residual deformations than the DBE, resulting in larger P(NC∩D) under the MCE than under the DBE.

6.4.3 Probability of Brace Damage Scenarios

Equation 6.29 is used to estimate P(D.S.#4), and Equation 6.30 is used to estimate P(D.S.#5). P(D.S.#3) is obtained from the relationship given in Equation 6.35. Calculations are performed for each brace of each model building.

As given in Equations 6.29 and 6.30, the joint PDF for θ_m, θ_r and Δ_{or} is used to calculate P(NC∩ND∩BS) and P(NC∩ND∩BR) together with the NC, ND and BS/BR fragility curves. θ_m, θ_r and Δ_{or} results from the dynamic analyses are used to develop the lognormal trivariate joint PDF (Equation 6.31) for each brace of each model building. In addition to $\rho_{\theta m,\theta r}$ obtained for the building, correlation coefficients between θ_m and Δ_{or} ($\rho_{\theta m,\Delta or}$), and between θ_r and Δ_{or} ($\rho_{\theta r,\Delta or}$) are obtained for each brace in the building from the analysis results. $\rho_{\theta m,\Delta or}$ and $\rho_{\theta r,\Delta or}$ values for each brace of each model building under both the DBE and MCE are given in Table 6.4 for 4-story model buildings and in Table 6.5 for 9-story model buildings. According to the values in Tables 6.4 and 6.6, both θ_m and Δ_{or} and θ_r and Δ_{or} are correlated since the $\rho_{\theta m,\Delta or}$ and $\rho_{\theta r,\Delta or}$ values are non-zero.

P(NC∩ND∩NR), P(NC∩ND∩BS) and P(NC∩ND∩BR) results are obtained from a program coded in MatLab and are given in Table 6.6 for the braces of the 4-story model buildings and in Table 6.7 for the braces of the 9-story model buildings. The probability values given in these tables are rounded off in order to equate the summation of P(NC∩ND∩NR), P(NC∩ND∩BS) and P(NC∩ND∩BR) to P(NC∩ND) according to Equation 6.35 and Figure 6.8.

The results for the 4-story model buildings given in Table 6.6 indicate that the brace damage probabilities (i.e., P(NC∩ND∩BS) and P(NC∩ND∩BR)) for the 4SC-CBF are zero for all braces. The very low Δ_{or} (in the range of 10^{-6} to 10^{-7}) for the braces of the 4SC-CBF is the reason for the zero brace damage probability. For the 4SCBF, Δ_{or} in the braces leads to higher brace repair probabilities. Table 6.6 shows that the highest repair probabilities are obtained for the 1st story braces of the 4SCBF. P(NC∩ND∩BS) for the

1st story braces is larger than P(NC∩ND∩BR) under the DBE. This makes BS is the most probable repair action for the 1st story braces of 4SCBF under the DBE with a probability of about 52%. The probability of BR is about 32%, and the probability of needing some type of brace repair is 84%. Under the MCE, BR is the most probable repair action for the 1st story braces of the 4SCBF. The probability of BR is about 65% and the probability of BS is about 29%. The probability of needing some type of brace repair is about 94%. There is some probability of needing repair of 4th story braces of the 4SCBF; however it is not as high as the probability of repair for the 1st story braces. These results show that there is a high probability of reparable brace damage in the 4SCBF.

The results for the 9-story model buildings in Table 6.7 show that the brace repair probabilities are higher than those for the 4-story buildings. The 9SC-CBF has brace repair probabilities much larger than zero under the MCE. For the DBE, the brace repair probabilities are very low. Damage is concentrated in upper story braces of the 9SC-CBF, mainly in the 5th, 6th and 7th story braces. P(NC∩ND∩BS) is higher than P(NC∩ND∩BR) for these braces of the 9SC-CBF both under the DBE and MCE. Under the DBE, the probability of BS is about 8% and the probability of BR is about 3% for the 6th and 7th story braces of 9SC-CBF. The probability of needing some type of brace repair is about 11% for these braces under the DBE. Under the MCE, the probability of BS is about 36% and the probability of BR is about 19% for the 6th story braces of the 9SC-CBF. For the 7th story braces of the 9SC-CBF under the MCE, the probability of BS is 37% and the probability of BR is about 16%. The probability of needing some type of brace repair is about 55% for 6th and 7th story braces under the MCE.

Results show that the 9SCBF has more uniformly distributed brace repair probabilities. Brace damage is not concentrated in a specific story of the 9SCBF but the highest repair probability is in the 1st story. The probability of BS is about 45% and the probability of BR is about 35% under the DBE which gives about 80% probability of needing some type of brace repair. Under the MCE, the probability of BR is larger than the probability of BS for the 1st braces of 9SCBF with about 70% probability of needing some type of brace repair. For many braces of the 9SCBF, the probability of needing some type of brace repair is about 80% under the DBE and about 70% under the MCE. Note that the probability of brace repair under the MCE is less than under the DBE because the probability of demolition is greater. Overall, it is observed that BS is the most probable repair action under the DBE. However, under the MCE, with increased brace damage, BR is the most probable repair action.

6.4.4 Summary of Results

The probability of collapse (i.e., P(C)) is very low for the model buildings both under the DBE and MCE. The probability of demolition when the building does not collapse, i.e., P(NC∩D), is also low for the model buildings except for the 9SCBF. P(NC∩D) is about 26% for the 9SCBF under the MCE.

The SC-CBF model buildings have less brace damage with lower brace repair probabilities than the SCBF model buildings. The braces of 4SC-CBF are damage free both under the DBE and MCE. The braces of 9SC-CBF are mainly undamaged under the DBE with braces in the 6th and 7th stories having about 10% probability of needing some

type of brace repair. Braces of the 4SCBF have large repair probabilities in the 1st and 4th story braces. Braces of the 9SCBF are damaged more uniformly over the building height and have probabilities of needing some type of brace repair up to 80% under the DBE, and up to 70% under the MCE. The reason of this reduction in the brace repair probability is the larger probability of demolition (P(NC∩D)) for the 9SCBF under the MCE. As the demolition probability of the building increases, brace repair probability decreases since there is no need for brace repair when the building is demolished. Under the DBE, 9SCBF has about 83% probability of needing brace repair or being demolished. Under the MCE, the 9SCBF has about 96% probability of needing some type of brace repair or being demolished.

Table 6.1 – P(C) and P(NC) results for model buildings

Frame	Hazard	P(C)	P(NC)
4SCBF	DBE	3.00E-06	9.99997E-01
	MCE	5.60E-04	9.9944E-01
4SC-CBF	DBE	1.50E-06	9.999985E-01
	MCE	1.70E-04	9.9983E-01
9SCBF	DBE	4.50E-05	9.99955E-01
	MCE	6.70E-04	9.9933E-01
9SC-CBF	DBE	2.00E-04	9.998E-01
	MCE	5.60E-03	9.944E-01

Table 6.2 – Correlation coefficients between θ_m and θ_r ($\rho_{\theta m,\theta r}$) for model buildings

	SCBF		SC-CBF	
$\rho_{\theta m,\theta r}$	DBE	MCE	DBE	MCE
4-story	0.823	0.712	0.039	0.359
9-story	0.563	0.479	0.104	0.631

Table 6.3 – P(ND∩NC) and P(D∩NC) results for model buildings

Frame	Hazard	P(NC∩ND)	P(NC∩D)
4SCBF	DBE	9.9946E-01	5.36E-04
	MCE	9.638E-01	3.56E-02
4SC-CBF	DBE	9.999985E-01	0.00
	MCE	9.9983E-01	0.00
9SCBF	DBE	9.6856E-01	3.1395E-02
	MCE	7.435E-01	2.5583E-01
9SC-CBF	DBE	9.997E-01	1.00E-04
	MCE	8.946E-01	9.98E-02

Table 6.4 – Correlation coefficients between θ_m and Δ_{or} ($\rho_{\theta m,\Delta or}$) and between θ_r and Δ_{or} ($\rho_{\theta r,\Delta or}$) for each brace in 4-story model buildings

		SCBF		SC-CBF	
		DBE	MCE	DBE	MCE
1LB	$\rho_{\theta m,\Delta or}$	0.859	0.888	-0.778	-0.634
	$\rho_{\theta r,\Delta or}$	0.690	0.566	0.091	-0.047
2LB	$\rho_{\theta m,\Delta or}$	0.101	0.464	-0.783	-0.928
	$\rho_{\theta r,\Delta or}$	0.203	0.360	0.069	-0.272
3LB	$\rho_{\theta m,\Delta or}$	0.064	0.125	-0.785	-0.923
	$\rho_{\theta r,\Delta or}$	0.151	0.264	0.071	-0.289
4LB	$\rho_{\theta m,\Delta or}$	0.319	0.346	-0.781	-0.932
	$\rho_{\theta r,\Delta or}$	0.170	0.230	0.065	-0.307
1RB	$\rho_{\theta m,\Delta or}$	0.929	0.782	-0.776	-0.895
	$\rho_{\theta r,\Delta or}$	0.724	0.424	0.085	-0.179
2RB	$\rho_{\theta m,\Delta or}$	0.563	0.395	-0.782	-0.925
	$\rho_{\theta r,\Delta or}$	0.645	0.413	0.069	-0.240
3RB	$\rho_{\theta m,\Delta or}$	0.091	-0.088	-0.785	-0.890
	$\rho_{\theta r,\Delta or}$	-0.023	-0.087	0.072	-0.289
4RB	$\rho_{\theta m,\Delta or}$	0.475	0.305	-0.781	-0.930
	$\rho_{\theta r,\Delta or}$	0.230	0.079	0.065	-0.286

Table 6.5 – Correlation coefficients between θ_m and Δ_{or} ($\rho_{\theta m,\Delta or}$) and between θ_r and Δ_{or} ($\rho_{\theta r,\Delta or}$) for each brace in 9-story model buildings

		SCBF		SC-CBF	
		DBE	MCE	DBE	MCE
1LB	$\rho_{\theta m,\Delta or}$	0.236	0.385	-0.268	-0.241
	$\rho_{\theta r,\Delta or}$	0.228	0.458	0.070	0.046
2LB	$\rho_{\theta m,\Delta or}$	0.086	0.103	-0.358	-0.291
	$\rho_{\theta r,\Delta or}$	0.214	0.221	-0.070	0.024
3LB	$\rho_{\theta m,\Delta or}$	0.251	0.333	-0.269	-0.311
	$\rho_{\theta r,\Delta or}$	0.458	0.464	0.132	-0.066
4LB	$\rho_{\theta m,\Delta or}$	0.123	0.138	-0.286	-0.273
	$\rho_{\theta r,\Delta or}$	0.075	0.064	0.116	0.210
5LB	$\rho_{\theta m,\Delta or}$	0.473	0.402	0.157	0.042
	$\rho_{\theta r,\Delta or}$	0.382	0.405	0.278	-0.034
6LB	$\rho_{\theta m,\Delta or}$	0.636	0.586	0.029	-0.031
	$\rho_{\theta r,\Delta or}$	0.248	0.086	0.554	-0.095
7LB	$\rho_{\theta m,\Delta or}$	0.626	0.503	0.229	0.124
	$\rho_{\theta r,\Delta or}$	-0.052	0.046	0.539	0.021
8LB	$\rho_{\theta m,\Delta or}$	0.197	0.244	-0.107	-0.037
	$\rho_{\theta r,\Delta or}$	-0.159	0.271	0.654	0.097
9LB	$\rho_{\theta m,\Delta or}$	0.196	-0.175	-0.107	-0.010
	$\rho_{\theta r,\Delta or}$	0.509	0.344	0.654	0.113
1RB	$\rho_{\theta m,\Delta or}$	0.209	0.307	-0.292	-0.255
	$\rho_{\theta r,\Delta or}$	0.403	0.157	-0.059	0.017
2RB	$\rho_{\theta m,\Delta or}$	-0.028	-0.073	-0.367	-0.337
	$\rho_{\theta r,\Delta or}$	-0.021	-0.086	0.016	-0.090
3RB	$\rho_{\theta m,\Delta or}$	0.255	0.280	-0.245	-0.320
	$\rho_{\theta r,\Delta or}$	0.465	0.432	0.047	0.029
4RB	$\rho_{\theta m,\Delta or}$	0.264	0.013	-0.296	-0.291
	$\rho_{\theta r,\Delta or}$	0.296	0.143	0.089	-0.065
5RB	$\rho_{\theta m,\Delta or}$	0.516	0.316	0.127	-0.109
	$\rho_{\theta r,\Delta or}$	0.396	0.021	0.141	0.014
6RB	$\rho_{\theta m,\Delta or}$	0.519	0.495	0.264	0.069
	$\rho_{\theta r,\Delta or}$	0.009	-0.172	0.587	-0.031
7RB	$\rho_{\theta m,\Delta or}$	0.741	0.619	-0.020	-0.085
	$\rho_{\theta r,\Delta or}$	0.228	0.058	0.559	-0.067
8RB	$\rho_{\theta m,\Delta or}$	0.142	0.168	-0.138	-0.228
	$\rho_{\theta r,\Delta or}$	0.034	0.097	0.699	-0.036
9RB	$\rho_{\theta m,\Delta or}$	0.146	0.048	-0.537	0.106
	$\rho_{\theta r,\Delta or}$	0.476	-0.037	0.449	0.014

Table 6.6 – Probabilities of brace damage states for 4-story model buildings

		P(NC∩ND∩NR)		P(NC∩ND∩BS)		P(NC∩ND∩BR)	
		SCBF	SC-CBF	SCBF	SC-CBF	SCBF	SC-CBF
1LB	DBE	0.159	9.999985E-01	0.517	0.000	0.323	0.000
	MCE	0.026	9.9983E-01	0.293	0.000	0.646	0.000
2LB	DBE	0.992	9.999985E-01	0.006	0.000	0.001	0.000
	MCE	0.861	9.9983E-01	0.074	0.000	0.029	0.000
3LB	DBE	0.987	9.999985E-01	0.009	0.000	0.003	0.000
	MCE	0.946	9.9983E-01	0.013	0.000	0.005	0.000
4LB	DBE	0.740	9.999985E-01	0.213	0.000	0.046	0.000
	MCE	0.638	9.9983E-01	0.258	0.000	0.068	0.000
1RB	DBE	0.186	9.999985E-01	0.506	0.000	0.308	0.000
	MCE	0.024	9.9983E-01	0.301	0.000	0.639	0.000
2RB	DBE	0.998	9.999985E-01	0.001	0.000	1.123E-04	0.000
	MCE	0.886	9.9983E-01	0.057	0.000	0.021	0.000
3RB	DBE	0.988	9.999985E-01	0.008	0.000	0.003	0.000
	MCE	0.960	9.9983E-01	0.006	0.000	0.010	0.000
4RB	DBE	0.832	9.999985E-01	0.133	0.000	0.035	0.000
	MCE	0.556	9.9983E-01	0.314	0.000	0.094	0.000

0.000 means value less than $1x10^{-6}$

Table 6.7 – Probabilities of brace damage states for 9-story model buildings

		P(NC∩ND∩NR)		P(NC∩ND∩BS)		P(NC∩ND∩BR)	
		SCBF	SC-CBF	SCBF	SC-CBF	SCBF	SC-CBF
1LB	DBE	0.215	9.997E-01	0.463	0.000	0.290	0.000
	MCE	0.014	8.946E-01	0.191	0.000	0.539	0.000
2LB	DBE	0.961	9.997E-01	0.006	0.000	0.002	0.000
	MCE	0.592	8.946E-01	0.103	0.000	0.049	0.000
3LB	DBE	0.431	9.997E-01	0.360	0.000	0.177	0.000
	MCE	0.084	8.946E-01	0.310	0.000	0.350	0.000
4LB	DBE	0.932	9.997E-01	0.027	0.000	0.010	0.000
	MCE	0.479	8.946E-01	0.171	0.000	0.094	0.000
5LB	DBE	0.385	9.983E-01	0.375	0.001	0.208	2.030E-05
	MCE	0.058	8.482E-01	0.311	0.034	0.375	0.013
6LB	DBE	0.385	8.865E-01	0.371	0.080	0.212	0.033
	MCE	0.160	3.576E-01	0.314	0.351	0.269	0.186
7LB	DBE	0.034	9.027E-01	0.441	0.072	0.493	0.026
	MCE	0.027	5.323E-01	0.275	0.244	0.442	0.119
8LB	DBE	0.920	9.997E-01	0.037	0.000	0.012	0.000
	MCE	0.677	8.938E-01	0.050	7.730E-04	0.017	3.700E-05
9LB	DBE	0.969	9.997E-01	0.000	0.000	0.000	0.000
	MCE	0.744	8.081E-01	0.000	0.061	0.000	0.026
1RB	DBE	0.156	9.997E-01	0.439	0.000	0.374	0.000
	MCE	0.052	8.946E-01	0.259	0.000	0.432	0.000
2RB	DBE	0.933	9.997E-01	0.026	0.000	0.009	0.000
	MCE	0.697	8.946E-01	0.034	0.000	0.013	0.000
3RB	DBE	0.535	9.997E-01	0.276	0.000	0.158	0.000
	MCE	0.278	8.946E-01	0.279	0.000	0.187	0.000
4RB	DBE	0.893	9.997E-01	0.055	0.000	0.021	0.000
	MCE	0.718	8.946E-01	0.019	0.000	0.007	0.000
5RB	DBE	0.364	9.997E-01	0.402	0.000	0.202	0.000
	MCE	0.154	8.827E-01	0.341	0.010	0.248	0.002
6RB	DBE	0.412	8.858E-01	0.372	0.082	0.185	0.032
	MCE	0.365	3.466E-01	0.236	0.362	0.143	0.186
7RB	DBE	0.046	8.933E-01	0.435	0.077	0.488	0.029
	MCE	0.016	3.666E-01	0.261	0.366	0.467	0.162
8RB	DBE	0.900	9.997E-01	0.051	0.000	0.018	0.000
	MCE	0.622	8.940E-01	0.089	5.686E-04	0.033	2.710E-05
9RB	DBE	0.969	9.997E-01	0.000	0.000	0.000	0.000
	MCE	0.726	8.709E-01	0.013	0.018	0.005	0.006

0.000 means value less than $1x10^{-6}$

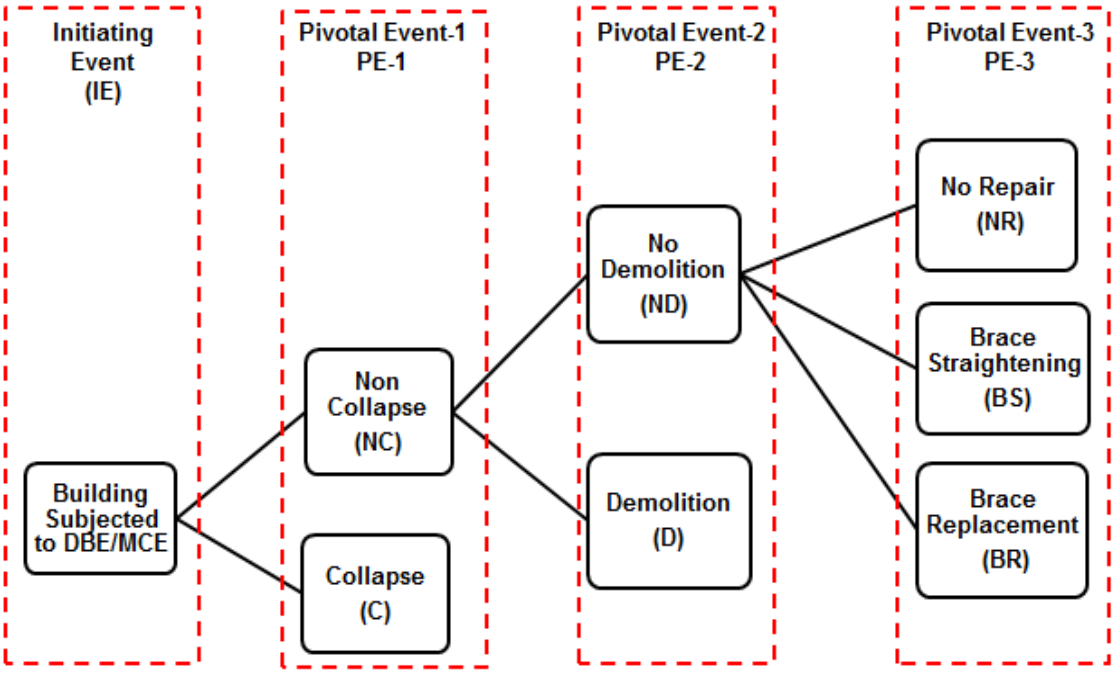

Figure 6.1 – Event tree (ET) used in this study

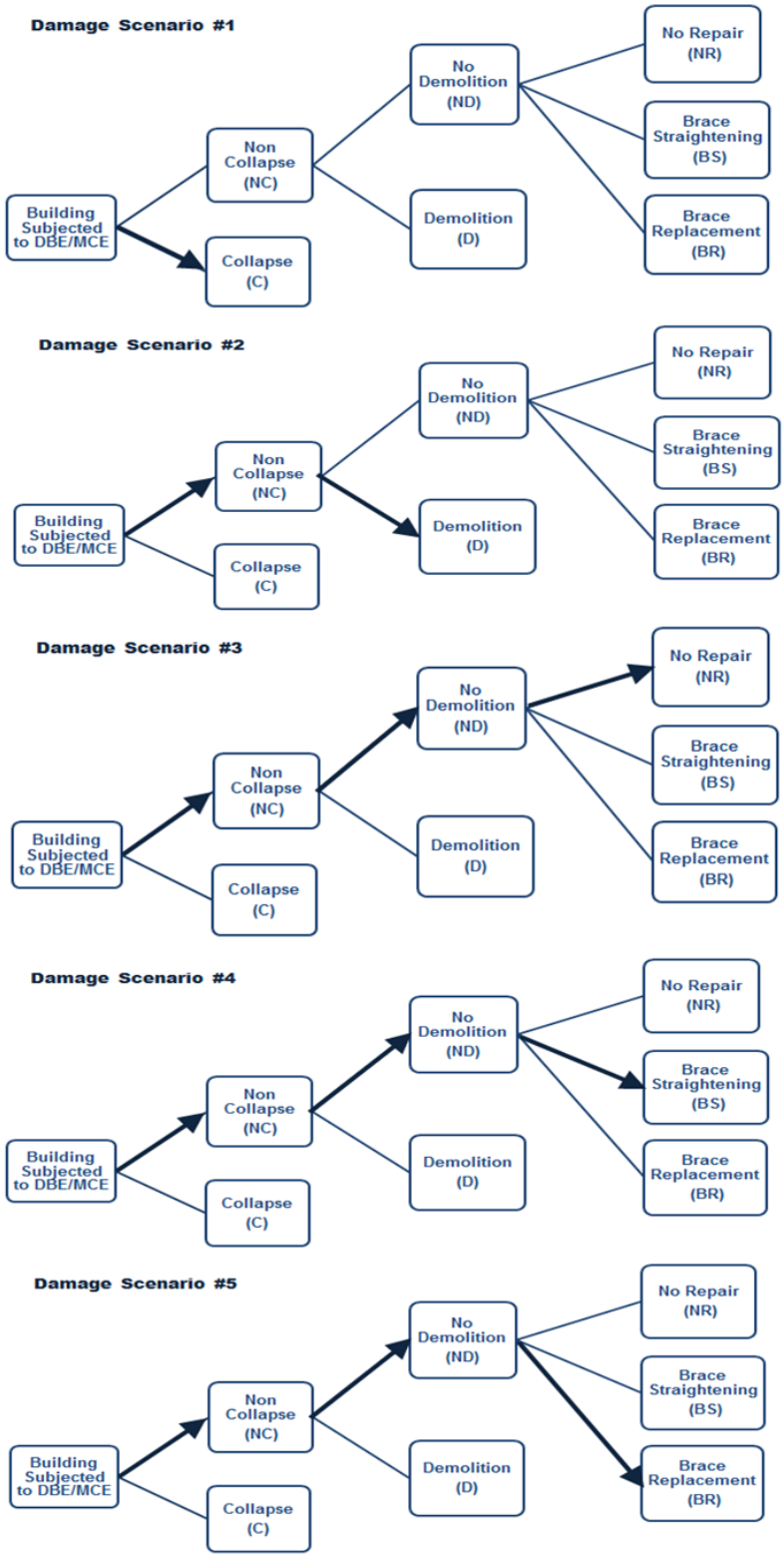

Figure 6.2 –Damage scenarios' paths

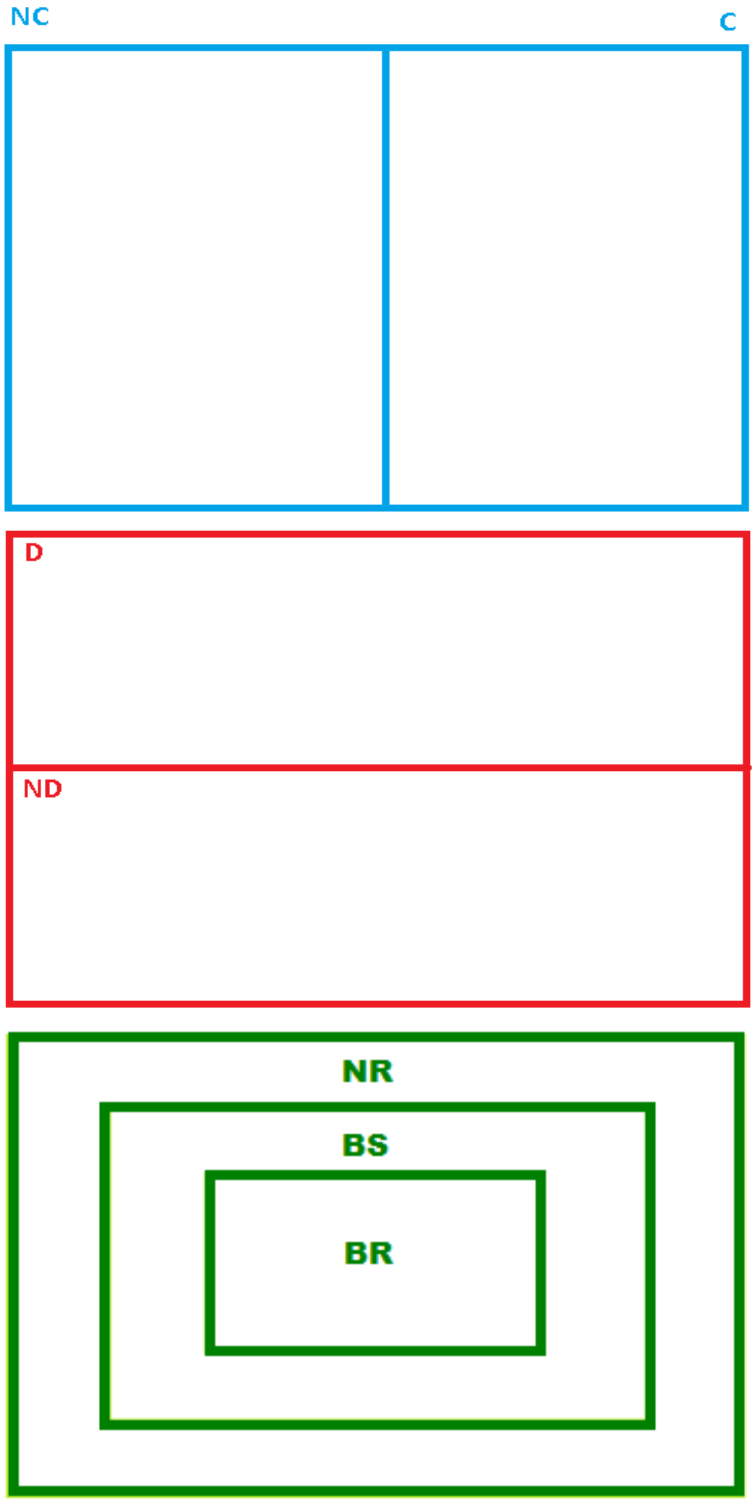

Figure 6.3 – Venn diagrams for individual damage events

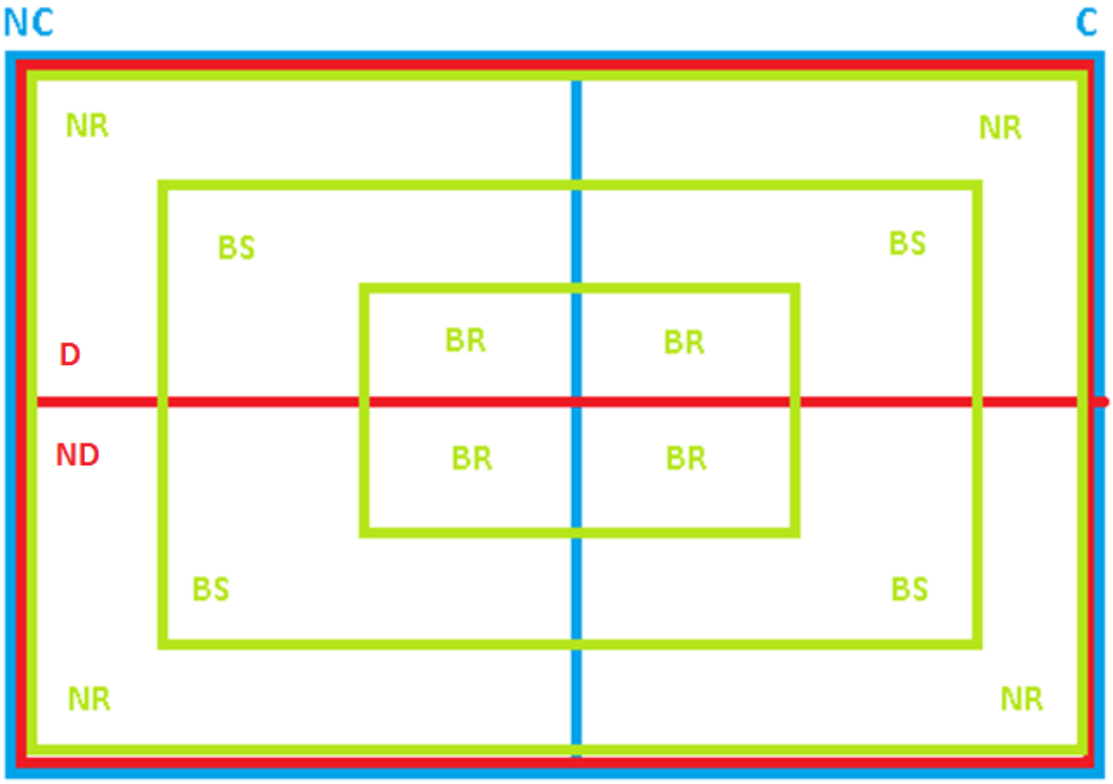

Figure 6.4 – Venn diagram for the multi-event system

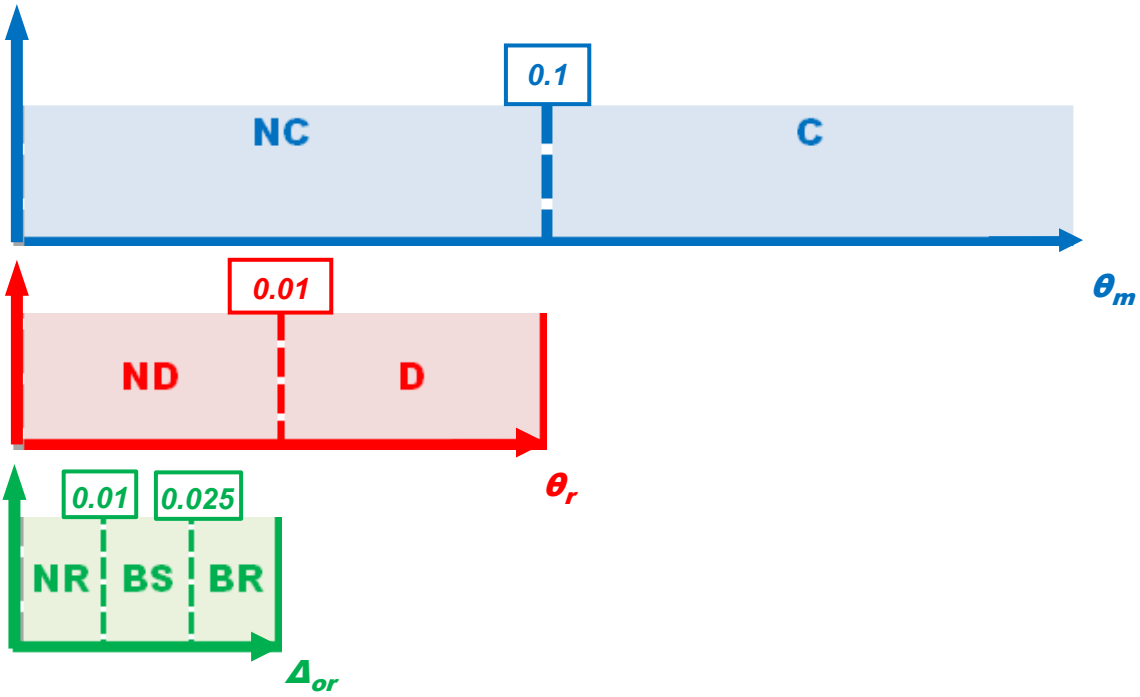

Figure 6.5 – Schematic representation of damage scenarios indicating median EDP limit values of each individual event

Figure 6.6 – Venn diagram representing P(C)

Figure 6.7 – Venn diagram representing P(NC∩D)

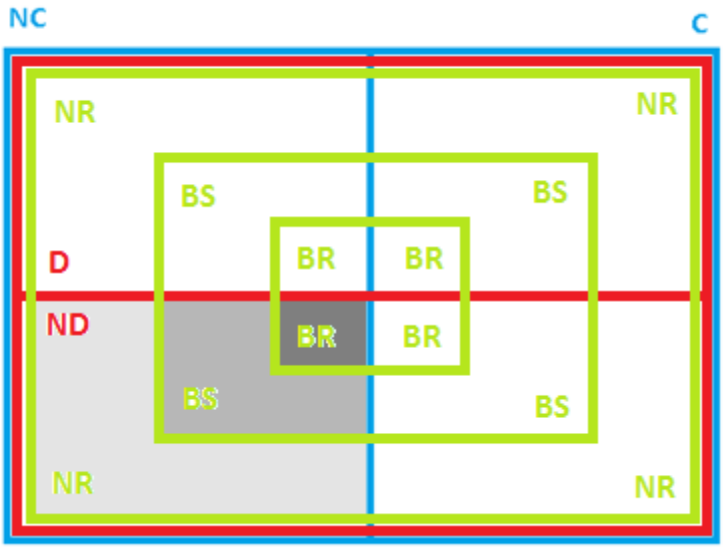

Figure 6.8 – Venn diagram representing brace damage state (brace repair) probabilities

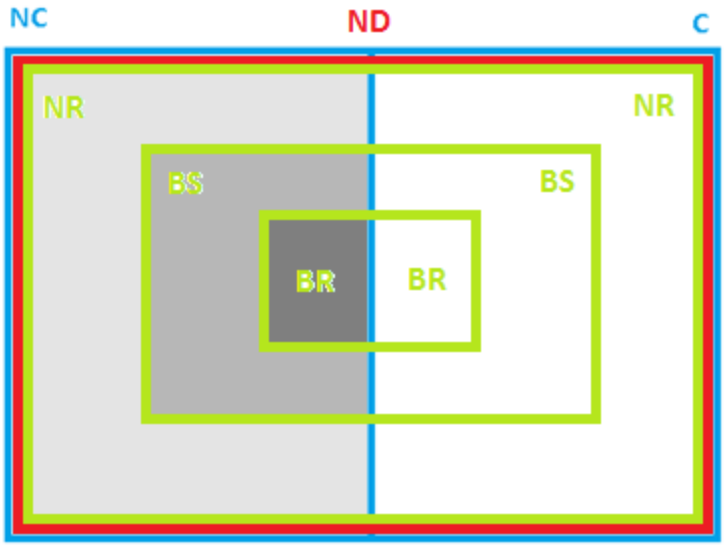

Figure 6.9 – Venn diagram representing brace damage state (brace repair) probabilities for the simplified methodology

CHAPTER 7

SUMMARY, CONCLUSIONS AND FUTURE WORK

7.1 Summary

A probabilistic earthquake structural damage assessment of SCBFs and SC-CBFs was presented in this thesis. The objective is to develop a better understanding of the earthquake performance of SC-CBFs by comparing this performance with that of SCBFs. An SC-CBF is designed to rock on its foundation, and the rocking action increases the lateral drift capacity of the system. SC-CBFs exhibit a capability to soften with little structural damage and residual drift. Therefore, the earthquake performance of an SC-CBF is expected to be better than the earthquake performance of an SCBF because an SC-CBF has greater lateral drift capacity before damage of individual members begins.

This thesis summarizes the seismic design procedures for SCBFs and SC-CBFs. Structural response parameters (EDPs) obtained from nonlinear dynamic earthquake response analyses of model SCBF and SC-CBF buildings performed by Chancellor (2013) and Tahmasebi (2014) are summarized. A probabilistic building damage assessment of the model buildings, and a detailed discussion of brace damage and the probabilistic brace damage assessment for the model buildings are presented. Comparisons of the damage assessment for the SCBF and SC-CBF model buildings are given.

First, the designs of 4- and 9-story SCBF buildings (4SCBF and 9SCBF, respectively) were presented to permit comparisons with the 4- and 9-story SC-CBF model buildings (4SC-CBF and 9SC-CBF, respectively) designed previously by Chancellor (2013). The nonlinear dynamic earthquake response analyses of these model buildings were performed in OpenSees by Tahmasebi (2014) and Chancellor (2013) under DBE and MCE ground motion intensities. Forty-four ground motion records, known as the Far-Field record set (FEMA, 2009), were used in these analyses. Structural response data (values of the engineering demand parameters, EDPs) necessary for the damage assessment were obtained from the dynamic analysis results. The peak story drift (θ_m), the peak residual story drift (θ_r) and the normalized residual brace OOP displacement (Δ_{or}) were extracted from the dynamic analysis results. These EDPs were taken as random variables in the probabilistic damage assessment.

Second, the building damage assessment was performed. The probability of collapse/non-collapse (C/NC) and the probability of demolition/no demolition (D/ND) were used to quantify the building damage. θ_m was used as the EDP for the collapse assessment and θ_r was used as the EDP for the demolition assessment. To obtain these probabilities, C/NC and D/ND fragility functions were developed. Probabilities of (C/NC) and (D/ND) were obtained for each model building under both the DBE and MCE and the results were compared.

Third, the damage assessment of the braces was performed. Brace damage states (DS_0, DS_1 and DS_2) and the repair actions corresponding to each damage state (NR, BS, and BR) were specified. Probabilities of DS_0, DS_1 and DS_2 (or NR, BS, and BR) were used to

quantify the damage in the braces. Δ_{or} was used as the EDP for the brace damage assessment. Results of a previous experimental study were used to determine the damage state limit values of Δ_{or}. Using the damage state limit values of $\Delta_{or,}$ fragility functions for each damage state were developed. When Δ_{or} from the dynamic earthquake response analysis equaled or exceeded the limit values, the building was considered to be in the corresponding damage state. The probability of being in each damage state was obtained for each brace of each model building under both the DBE and MCE and the results were compared.

Finally, the building damage assessment and the brace damage assessment were combined into a multi-event damage assessment of each model building. The multi-event damage assessment was based on damage scenarios, where each scenario was a sequence of individual events. Damage scenarios were described as sequences of the individual building and brace damage events, and shown schematically using an event tree (ET) model. The probability of each damage scenario was obtained from the fragility functions and data developed previously, using an event tree analysis (ETA). The probability of each damage scenario was estimated for each model building under both the DBE and MCE. Results were compared and discussed.

7.2 Findings

The following findings are obtained from the work reported in this thesis:

- The earthquake design procedure for SC-CBF buildings resulted in SC-CBFs that are heavier than corresponding SCBFs for both the 4- and 9-story buildings, even

though the CBFs are designed for the same seismic mass and seismic conditions. The reason for this difference is the modified RSA used in the SC-CBF design procedure in which the higher mode spectral acceleration values are scaled up by a factor of 2, rather than scaled down by R/I.

- All model buildings have a very low collapse probability (P(C)) under both the DBE and MCE. However, some slight differences were observed in the results. P(C) for the 4SC-CBF is slightly lower than the P(C) of the 4SCBF; but, P(C) of the 9SC-CBF is slightly higher than the P(C) of the 9SCBF.
- The mean values of θ_m for the SCBF and SC-CBF buildings are very similar for buildings with same number of stories and under the same ground motion intensity. The difference in the standard deviations for θ_m between the different model buildings caused the differences in the P(C).
- The probability of demolition ($P(NC \cap D)$) is much lower than the probability of no demolition ($P(NC \cap ND)$) for all model buildings (when collapse has not occurred). The SC-CBF model buildings have a lower $P(NC \cap D)$ than the SCBF buildings. Specifically, $P(NC \cap D)$ for the 4SC-CBF is essentially zero under both the DBE and MCE. $P(NC \cap D)$ for the 9SCBF is about 26% under the MCE.
- Similar to $P(NC \cap D)$, θ_r is also lower in the SC-CBF buildings than in the SCBF buildings. This is expected since the demolition probability depends on θ_r.
- The braces of the SC-CBF model buildings have a lower probability of brace repair than the SCBF model buildings.

- The 4SC-CBF has zero probability of brace repair, therefore the braces of 4SC-CBF are considered to be damage free both under the DBE and MCE. On the other hand, the 4SCBF has brace damage concentrated in the 1st story braces under both the DBE and MCE. The 4th story braces of the 4SCBF also experienced some damage, but not as much as the braces in the 1st story.
- Brace damage was concentrated in the 6th and 7th story braces of the 9SC-CBF; the probability of some type of brace damage is about 11% under the DBE and about 55% under the MCE. The braces of the first 4 stories of the 9SC-CBF had zero probability of brace repair. The 8th and 9th story braces had low probabilities of brace repair under both the DBE and MCE.
- In the 9SCBF, the brace damage was more uniformly distributed over the building height. For many braces of the 9SCBF, the probability of some type of brace repair is about 80% under the DBE, and about 70% under the MCE. The probability of brace damage under the MCE is lower because of the higher probability of demolition under the MCE.
- Brace straightening (corresponding to minor damage) is the most probable brace repair action under the DBE. The most probable repair action is brace replacement (corresponding to major damage) under the MCE, except for the 9SC-CBF. Brace straightening is the most probable brace repair action under both the DBE and MCE for 9SC-CBF.
- Δ_{or} values for the braces are closely related to the brace repair probability results, therefore, the discussion of the brace repair probabilities are applicable to the Δ_{or}.

- In all model buildings, structural damage increased with increasing building height and with increasing ground motion intensity.

7.3 Conclusions

The following conclusions are developed from the findings of this study:

- The SC-CBF buildings have better earthquake performance than the SCBF buildings both under the DBE and MCE ground motion intensities.
- Both systems achieved collapse prevention with low probability of collapse.
- The SC-CBF buildings have a lower probability of demolition, because the residual drift is reduced with the self-centering capability.
- The probabilities of brace damage for the SC-CBF buildings are lower than for the SCBF buildings, because the brace buckling is delayed in the SC-CBF buildings.
- It is noteworthy that the taller SCBF model building (i.e., 9SCBF) had a very large probability of damage under the MCE. It had a 96% probability of needing some type of brace repair or being demolished under the MCE.

7.4 Future Work

The following recommendations are made for further research work:

- The design procedure for SC-CBFs should be modified for a more optimum design.

- The applications of SC-CBF buildings with different numbers of stories should be studied to observe the effect of building height on the earthquake performance extensively, since this study considered only 4- and 9-story SCBF and SC-CBF buildings.
- The lack of data on building damage and associated repair actions and repair costs is one of the most challenging aspects of the structural damage assessment. A damage database is needed which collects all available earthquake damage and repair data.
- A building damage assessment should consider the non-structural components because the damage to non-structural components are the main contributor to the earthquake related losses.
- The only brace configuration considered in this study is multi-story X-bracing. Other brace configurations, such as chevron bracing, should be studied to understand the effect of brace configuration on the earthquake performance of CBF buildings.
- Comparative studies on SCBF and SC-CBF structures with hollow steel structural sections for diagonal bracing should be pursued. Hollow steel structural sections are prone to low-cycle fatigue and fracture, which can have an effect on the on the probability of collapse and damage from an earthquake.
- Data from dynamic earthquake response analyses using a wide variety of ground motion intensities should be developed so the present study can be extended to other ground motion intensity levels.

- The results of building damage assessments should be considered in terms of economic losses which are more meaningful to decision-makers. To accomplish this, a comprehensive cost inventory should be prepared including initial material costs, building construction costs, demolition costs, and repair costs.

REFERENCES

AISC (2010a). *Code of Standard Practice for Steel Buildings and Bridges*. American Institute of Steel Construction, Chicago, IL.

AISC (2010b). *Seismic Provisions for Structural Steel Buildings*. American Institute of Steel Construction, Chicago, IL.

Ang, A.H-S., Tang, W.H. (2007), *Probability Concepts in Engineering – Emphasis on Applications to Civil and Environmental Engineering*, 2nd ed., John Wiley & Sons, Inc., Hoboken, NJ.

Ang, A.H-S., Tang, W.H. (1984*), Probability Concepts in Engineering Planning and Design. Volume II – decision, risk and reliability*, John Wiley & Sons, Inc., New York.

ASCE (2007). *Seismic Rehabilitation of Existing Buildings, ASCE 41-06.* American Society of Civil Engineers (ASCE), Reston, VA.

ASCE (2010). *Minimum Design Loads for Buildings and Other Structures*, *ASCE7-10*. American Society of Civil Engineers (ASCE), Reston, VA.

Aslani, H.; and Miranda, E. (2005). "Probabilistic Earthquake Loss Estimation and Loss Disaggregation in Buildings", Report No. 157. Stanford, CA: John A. Blume Earthquake Engineering Center, Stanford University, Palo Alto, CA.

ATC (2011). *Seismic Performance Assessment of Buildings, Volume 1-Methodology, ATC-58-1 75% Draft*. Applied Technology Council (ATC), Redwood City, CA.

Avent, R.R.; Mukai, D.J. (2001). "What You Should Know About Heat Straightening Repair of Damaged Steel," *Engineering Journal*, 38(1), pp 27-49.

Baker, J.W. (2008). "Introducing correlation among fragility functions for multiple components," *The 14th World Conference on Earthquake Engineering*, Beijing, China, October 12-17.

Chancellor, N.B. (2013). "Design and Seismic Performance of Self-Centering Concentrically-Braced Frames."Ph.D. Dissertation (in progress), Department of Civil and Environmental Engineering, Lehigh University, Bethlehem, PA.

Chancellor, N.B.; Akbas, G.; Sause, R.; Ricles, J.M.; Tahmasebi, E. (2012). "Evaluation of Performance-Based Design Methodology for Steel Self-Centering Braced Frame," *STESSA 2012, Proceedings of the 7th International Conference on Behavior of Steel Structures in Seismic Areas*, Santiago, Chile, January 9-11.

Cornell, C.A.; Jalayer, F.; Hamburger, R.O.; Foutch, D.A. (2002). "Probabilistic basis for 2000 SAC/FEMA steel moment frame guidelines," *ASCE Journal of Civil Engineering*, 128(4), pp 526-533.

Cornell, C.A.; Krawinkler, H. (2000). "Progress and challenges in seismic performance assessment," *PEER News*, April 2000, 3(2).

Deierlein, G.G.; Krawinkler, H.; and Cornell, C.A. (2003). "A Framework for Performance-Based Earthquake Engineering," *2003 Pacific Conference on Earthquake Engineering*, Christchurch, New Zealand, Paper Number 140.

Ericson, C.A. (2005), *Hazard Analysis Techniques for System Safety*, John Wiley & Sons, Inc., Hoboken, NJ.

FEMA (2003). *NEHRP Recommended Provisions and Commentary for Seismic Regulations for New Buildings and Other Structures, FEMA 450.* Federal Management Agency (FEMA), Washington, D.C.

FEMA (2009). *Quantification of Building Seismic Performance Factors, FEMA P695*. Federal Management Agency (FEMA), Washington, D.C.

Fletcher, S. (2007), "Non-Gaussian Data Assimilation," *Lecture for the Workshop on Applications of Remotely Sensed Observations in Data Assimilation*, University of Maryland, College Park, MD, August 3.

Kowalkowski, K.; Varma, A.H. (2007). "Effects of Multiple Damage-Heat Straightening Repairs on Steel Beams." *Transportation Research Record: Journal of the Transportation Research Board,* Volume 2028/2007, pp 67-77.

Krawinkler, H.; Miranda, E. (2004). "Performance-based earthquake engineering," *Earthquake Engineering: From Engineering Seismology to Performance-Based Engineering. Chapter 9*, CRC Press LLC, Boca Raton, FL, pp 9.1-9.59.

Krawinkler, H.; Zareian, F.; Lignos, D.G.; Ibarra, L.F. (2009). "Prediction of Collapse of Structures Under Earthquake Excitations," *COMPDYN 2009, ECCOMAS Thematic Conference on Computational Methods in Structural Dynamics and Earthquake Engineering*, Rhodes, Greece, June 22-24.

Lumpkin, E.J. (2009). "Enhanced Seismic Performance of Multi-Story Special Concentrically Brace Frames using a Balanced Design Procedure." M.S. Thesis, Department of Civil and Environmental Engineering, University of Washington, Seattle, WA.

Miranda, E. (2010). "Enhanced Building-Specific Seismic Performance Assessment," *Advances in Performance-Based Earthquake Engineering. Chapter 17*, Springer, Netherlands, pp 183-191.

Miranda, E.; Aslani, H. (2003). "Building Specific Loss Estimation for Performance Based Design," *2003 Pacific Conference on Earthquake Engineering*, Christchurch, New Zealand, Paper Number 140.

Miranda, E.; Aslani, H.; and Taghavi, S. (2004). "Assessment of Seismic Performance in terms of Economic Losses." *Proceedings of an International Workshop on Performance-Based Seismic Design: Concepts and Implementation* (pp. 149-160), Bled, Slovenia.

Mitrani-Reiser, J. (2007). "An Ounce of Prevention: Probabilistic Loss Estimation for Performance-Based Earthquake Engineering," Department of Civil Engineering and Applied Mechanics, California Institute of Technology, Pasadena, CA.

Moehle,J.; and Deierlein, G.G. (2004). "A Framework Methodology for Performance-Based Earthquake Engineering,"*13th World Conference on Earthquake Engineering*, Vancouver, B.C., Canada, Paper No. 679.

NEEShub. "International Hybrid Simulation of Tomorrow's Braced Frame Systems." *NEES Project Warehouse, Project no.NEES-2008-0605*, <http://nees.org/warehouse/experiment/1118/project/605> (July 18, 2012).

Porter, K.A. (2003). "An Overview of PEER's Performance-Based Earthquake Engineering Methodology," *Proceedings of the 9th International Conference on Application of Statistics and Probability in Civil Engineering (ICASP9)*, San Francisco, July 6-9 2003.

Porter, K.A.; Hamburger, R.; and Kennedy R. (2007). "Practical Development and Application of Fragility Functions," *Proceedings of the SEI Structures Congress*, Long Beach, CA, May 16-19.

Powell, J.A. (2009). "Evaluation of Special Concentrically Braced Frames for Improved Seismic Performance and Constructability." M.S. Thesis, Department of Civil and Environmental Engineering, University of Washington, Seattle, WA.

Ramirez, C.M.; Miranda, E. (2009). "Building-Specific Loss Estimation Methods and Tools for Simplified Performance-Based Earthquake Engineering," Report No. 171, Stanford, CA: John A. Blume Earthquake Engineering Center, Stanford University.

Roeder, C.W.; Lehman, D.E., and Yoo, J.H. (2004). "Performance-Based Seismic Design of Braced-Frame Gusset Plate Connections," *Connections in Steel Structures V*, Amsterdam, Netherlands, June 3-4 2004.

Roke, D.; Sause, R.; Ricles, J.M.; Seo, C.-Y.; and Lee, K.-S. (2006). "Self-Centering Seismic-Resistant Steel Concentrically-Braced Frames," *Proceedings of the 8th U.S. National Conference on Earthquake Engineering,* EERI, San Francisco, April 18-22.

Roke, D.; Sause, R.; Ricles, J.M.; and Chancellor, N.B. (2010). “Damage-Free Seismic Resistant Self-Centering Concentrically-Braced Frames.” *ATLSS Report 10-09,* Lehigh University, Bethlehem, PA.

Seo, C.-Y. (2005). “Influence of Ground Motion Characteristics and Structural Parameters on Seismic Responses of SDOF Systems.” Ph.D. Dissertation, Department of Civil and Environmental Engineering, Lehigh University, Bethlehem, PA.

Seo, C.-Y.; and Sause, R. (2005). “Ductility Demand on Self-Centering Systems Under Earthquake Loading,” *ACI Structural Journal*, 102(2), pp 275-285.

Tahmasebi, E. (2014). “Collapse Performance of Self-Centering Steel Concentrically-Braced Frame Systems Under Seismic Conditions.” Ph.D. Dissertation (in progress), Department of Civil and Environmental Engineering, Lehigh University, Bethlehem, PA.

Tremblay R. (2002). "Inelastic seismic response of steel bracing members," *Journal of Constructional Steel Research*, 58, pp 665-701.

Uriz, P; and Mahin, S.A. (2008). “Toward Earthquake-Resistant Design of Concentrically Braced Steel-Frame Structures.” PEER Report 2008/08, Pacific Earthquake Engineering Research Center, University of California, Berkeley, CA.

Vamvatsikos, D.; Cornell, C.A. (2002). “Incremental dynamic analysis,” *Journal of Earthquake Engineering and Structural Dynamics*, 31, pp 491-514.

Whittaker, A., Hamburger, R., Comartin, C., Mahoney, M., Bachman, R., and Rojahn, C. (2003). “Performance-Based Engineering of Buildings and Infrastructure for Extreme Loadings,” *Proceedings of AISC-SINY Symposium on Resisting Blast and Progressive Collapse*, American Institute of Steel Construction, New York.

Zareian, F. and Krawinkler, H. (2006). “Simplified Performance-based Earthquake Engineering,” Report No. 169, Stanford, CA: John A. Blume Earthquake Engineering Center, Stanford University.

VITA

Gulce Akbas, the daughter of Halit Levent and Gulsun Akbas, was born on May 26, 1987 in Ankara, Turkey. In June 2009, Gulce earned a Bachelor of Science in Environmental Engineering and a Minor degree in Civil Engineering-Structural Analysis and Design from Middle East Technical University (METU) in Ankara, Turkey, where she graduated with honors. Gulce began graduate studies in the Department of Civil and Environmental Engineering at Lehigh University in Bethlehem, PA in August 2010. She will receive a Master of Science in Structural Engineering in September 2012.